8-2006

Characterizing Monolithic Lean NOx Trap Catalysts Using A Bench-Flow Reactor

Hakyong Kim
University of Tennessee - Knoxville

To the Graduate Council:

I am submitting herewith a thesis written by Hakyong Kim entitled "Characterizing Monolithic Lean NOx Trap Catalysts Using A Bench-Flow Reactor." I have examined the final electronic copy of this thesis for form and content and recommend that it be accepted in partial fulfillment of the requirements for the degree of Master of Science, with a major in Mechanical Engineering.

Ke Nguyen, Major Professor

We have read this thesis and recommend its acceptance:

David K. Irick, J. Roger Parson

Accepted for the Council:
Carolyn R. Hodges

Vice Provost and Dean of the Graduate School

(Original signatures are on file with official student records.)

To the Graduate Council:

I am submitting herewith a thesis written by Hakyong Kim entitled "Characterizing Monolithic Lean NO_x Trap Catalysts Using A Bench-Flow Reactor." I have examined the final electronic copy of this thesis for form and content and recommend that it be accepted in partial fulfillment of the requirements for the degree of Master of Science, with a major in Mechanical Engineering.

Ke Nguyen
Major Professor

We have read this thesis
and recommend its acceptance:

David K. Irick

J. Roger Parson

Accepted for the Council:

Anne Mayhew
Vice Chancellor and
Dean of Graduate Studies

(Original signatures are on file with official student records.)

CHARACTERIZING MONOLITHIC LEAN NO_x TRAP CATALYSTS USING A BENCH-FLOW REACTOR

A

Thesis

Presented for the

Master of Science Degree

The University of Tennessee, Knoxville

Hakyong Kim

August 2006

DEDICATION

This thesis is dedicated to my parents

Their genuine prayer and endless love have provided the deep inspiration to complete this study.

ACKNOWLEDGEMENTS

I would like to express my deep gratitude to my advisor, Dr. Nguyen, who has taught me not only the knowledge but also responsibility to be a professional engineer through the past three years. I will never forget his guidance which becomes a milestone of my life. I would also like to thank my graduate committee members, Dr. David K. Irick and Dr. J. Roger Parson.

I would like show my deep appreciation to Danny Graham, Gary Hatmaker, and Dennis Higdon for their endless help and support to finish my project. I would like to thank my laboratory colleagues, Scott Eaton, Scott Smith, Vitaly Prikhodko, Adam Youngquist, Barath Kumar, and Ajit Gopinath for their encouragement and friendship throughout my project. I would like to thank EmeraChem for providing the catalyst samples used in this project. I would like to thank the U.S. Department of Energy and the Advanced Reciprocating Engine Systems (ARES) program for their financial support and to Dr. Ming Zheng for obtaining funding for this project.

Abstract

The performance of EmeraChem Lean NO_x Trap (LNT) catalysts with company proprietary washcoat formulation has been investigated using a bench-flow reactor (BFR). The washcoat composition consists of Pt, the precious metal component (PM), and two NO_x storage media of Ba and K, supported on γ-Al_2O_3 washcoat.

A series of isothermal absorption experiments was carried out at different temperatures and gas hourly space velocities (GHSVs) in order to investigate the effect of temperature and GHSV on the nitrogen oxides (NO_x) trapping capacity of EmeraChem LNT catalysts. The NO_x storage capacity exhibits a "volcano-type" dependence on the temperature, with a maximum storage capacity of catalyst occurring at 350°C. On the other hand the NO_x storage capacity of the LNT decreases as the GHSV increases.

The effects of lean and rich duration and type of reductants on the regeneration of the LNT catalyst are investigated at an optimum operating temperature of 350°C and a gas hourly space velocity of 50,000 hr^{-1}. The experiments are performed for two different cases. In the first case, the time durations of the lean and rich phases are varied at a fixed concentration of the reductants: carbon monoxide (CO) and hydrogen (H_2). In the second case, the reductant concentrations − CO and H_2 − are varied at constant time duration of the lean and the rich phases. For the first case, a lean/rich cycle of 100s lean and 5s rich is found to be optimum since this cycle would offer the highest NO_x conversion as well as the best fuel efficiency in regenerating the LNT catalysts. For the second case, H_2 is a slightly better reductant in reducing NO_x than CO.

Two separate direct fuel injection (DFI) experiments are carried out: DFI with and without O_2 in the simulated exhaust gases. The results from DFI without O_2 show that the amount of NO_x slip and NO_x excursion decreases and reaches a steady value as the concentration of the reductant increases. The results from DFI with O_2 show that the average NO_x conversion decreases significantly in the presence of O_2 in the regeneration phase. The results suggest that some of the reductant is consumed by directly reacting with oxygen, and thus less is available to participate in the reduction reactions.

Contents

LIST OF TABLES

TABLE **PAGE**

LIST OF FIGURES

FIGURE **PAGE**

APPENDIX FIGURES

FIGURE **PAGE**

LIST OF SYMBOLS

A/F……air/fuel ratio

Ba……..…...…….barium

bar.....barometric pressure

$BaCO_3$……..….barium carbonate

$Ba(OH)_2$……....barium hydroxide

BaO……..……...….barium oxide

$Ba(NO_2)_2$……...…….barium nitrite

$Ba(NO_3)_2$……..……...……barium nitrate

BFR……...…….bench-flow reactor

C……...…….……carbon atom

^oC……...……..…….degrees Celsius

cc/min……..cubic centimeters per minute

CO……..……carbon monoxide

CO_2……...……..carbon dioxide

cpsi……..……..cells per square inch

DAS…….……data acquisition system

DC…….…….……..direct current

DFI……..….direct fuel injection

γ-Al_2O_3…….……....gamma alumina

gmol.....gram mole

g/ft^3……grams per cubic foot

GHSV……gas hourly space velocity

HC…….…….……hydrocarbon

H_2…….……...…….hydrogen molecule

H_2O……..……...…water vapor

hr^{-1}…….……per hour

I.D…….…..inner diameter

K……Potassium

KNO_3…….Potassium Nitrate

L/min……...liters per minute

LNC……..…….lean NO_x catalyst

LNT……..…lean NO_x trap

MFC……..…mass flow controller

mL/min……milliliter per minute

ms……...……millisecond

N_2……..…nitrogen molecule

Nm……..…….nano meter

N_2O……..……..nitrous oxide

NO_x…….……..oxides of nitrogen

NH_3…….……...….ammonia

O……..…….……...…oxygen atom

O^*……oxygen atom stored in Pt site

O.D…….outer diameter

Pd……..…….……palladium

PGM…….precious group metal

PM……...…particular matter

ppm……..parts per million

psia……..……pounds per square inch (absolute)

Pt…….platinum

PtO……..…platinum oxide

Rh…….rhodium

SO_2……..……..……sulfur oxides

SCR…….……..…….. .selective catalytic reduction

STP……..……..……..standard temperature and pressure

T……..……..…..temperature

t……...…….……time

TM……...…….…..trademark

V……...……....volt

VOC……..……...……..volatile organic compounds

Chapter 1

INTRODUCTION

Since the Clean Air Act was in effect in the United States in 1970s, many harmful pollutants such as hydrocarbon (HC), particular matter (PM), carbon monoxide (CO) and sulfur oxides (SO_2) have been reduced considerably from internal combustion engines. However the amount of nitrogen oxides (NO_x) has drastically increased − 20 percent over last 30 years, and about 25 million tons of NO_x are discharged every year into the atmosphere [1]. NO_x plays an important role in the environment. During summer time, the ground-level ozone (smog) is usually formed when NO_x reacts with other chemicals in the presence of ultra-violet sunlight as shown in Figure 1.1. Ground-level ozone damages the human respiratory system, sometimes leading to serious diseases such as lung cancer or asthma. According to Clean the Air [2], more than 141 million Americans live in areas affected by ground-level ozone, of which 6 million are suffering with asthma attacks, and every year approximately 150,000 Americans are hospitalized in the Eastern half of the United States alone. Moreover, NO_x emissions also contribute to the formation of acid rain, which comes from atmospheric NO_x reacting with water vapor to form nitric acid, and its deposition in water and soil can damage aquatic life and forest.

Unburned hydrocarbon (HC), known as one of the Volatile Organic Compounds (VOC), is another source of smog related to NO_x as shown in Figure 1.1. The hydrocarbon molecule is easily evaporated from incomplete combustion in internal

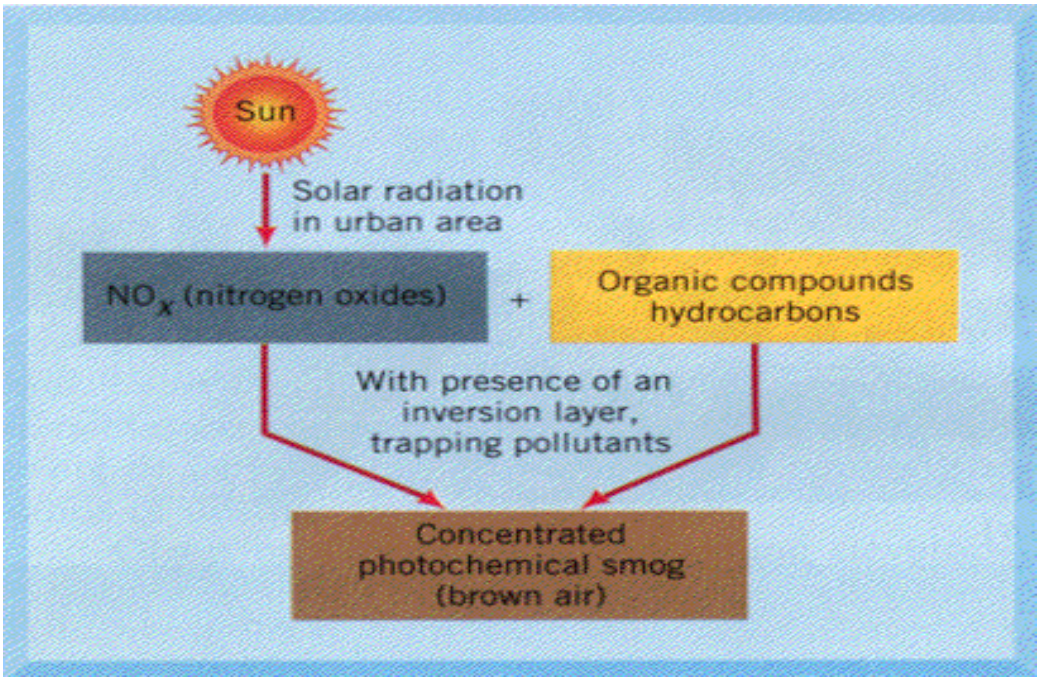

Figure 1.1 Formation of ground-level ozone (smog) from NO_x [4]

combustion engines and participates in the photochemical reactions with NO_x to form brown smog. In high concentration, HC also causes damages to human respiratory.

The Kyoto Protocol was initiated by the United Nations (UN) in May 2000 in order to reduce the emissions of greenhouse gases such as hydrocarbon (HC), carbon dioxide (CO_2), nitrous oxide (N_2O) and etc. CO_2, an inevitable product of combustion from internal combustion engines, becomes a significant pollutant to be considered. Even though CO_2 does not directly impair human life, it traps earth's heat and causes global warming as shown in Figure 1.2. Moreover, one third of total CO_2 emission in the earth's atmosphere is absorbed in the world's oceans, and dissolved CO_2 can acidify the oceans rapidly, which threatens the existence of corals, plankton and other marine life essential to the maritime food chain.

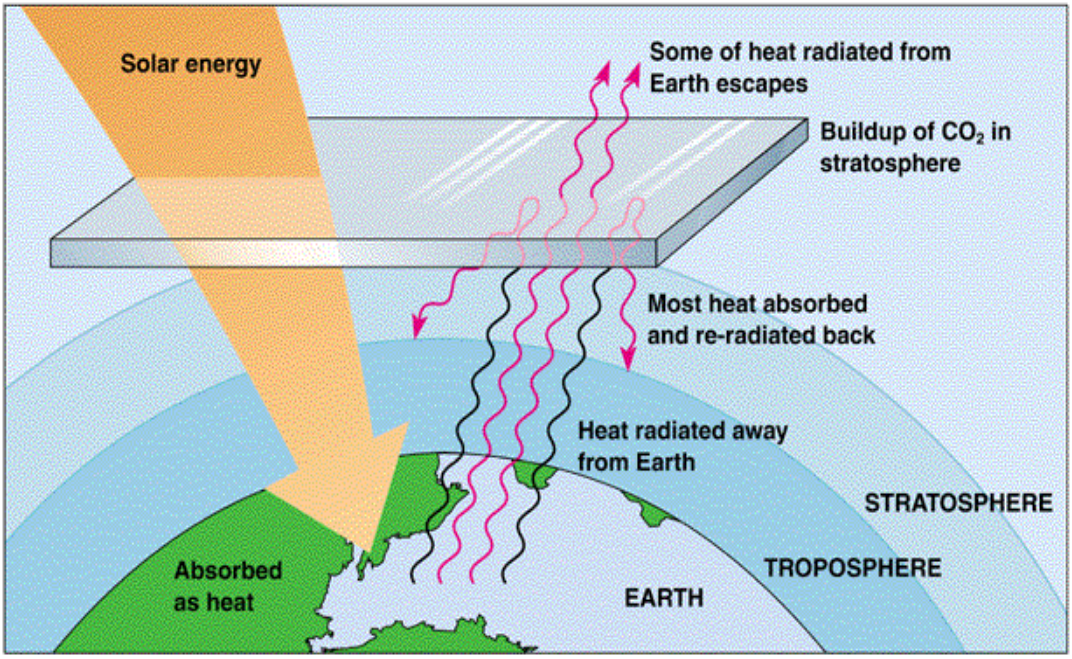

Figure 1.2 Greenhouse effect by CO_2 [5]

Oxides of nitrogen are usually formed by high-temperature combustion in excess of 1100^{o}C, and most internal combustion engines are operated above this temperature to increase fuel efficiency. N_2 and O_2 from air become disassociated with high-temperature combustion, and N and O are combined to form nitric oxide (NO). Figure 1.3 shows the emissions sources for nitrogen oxides in the United States [3]. As can be seen in the figure, more than 50% of NO_x emissions are generated by mobile sources, either on-road or off-road vehicles.

Three-way catalysts (TWCs) have been used by automakers since the 1970s to reduce emissions of HC, CO and and NO_x; however, in order for the TWCs to be effective the engines have to operate at stoichiometric condition—an air-fuel ratio of

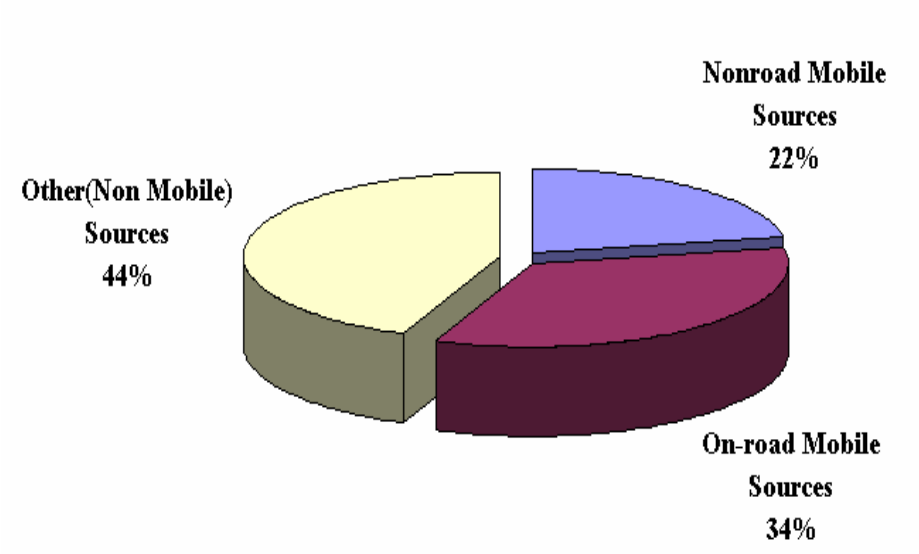

Figure 1.3 Emissions sources for nitrogen oxides in the United States

14.5:1 for gasoline engines. Unfortunately, in oxygen-rich environments such as those of lean-burn engines, TWCs are incapable in removing NO_x from exhaust gases as can be seen in Figure 1.4. Due to the fixed air/fuel ratios of three-way technology, De-NO_x technologies for lean-burn engines have been developed in order to maintain higher fuel efficiencies as well as lower emissions to satisfy the stringent EPA regulations effective since 1984. At a typical air/fuel ratio of 26:1 in lean-burn engines, the fuel consumption is drastically decreased to 50% of that used in stoichiometric engines equipped with TWCs, while lesser amounts of HC, CO and CO_2 emissions will be produced by the complete combustion of fuel. Therefore, the reduction of NO_x emission in lean-burn engines is the most important issue to be solved. Three different De-NO_x technologies have been proposed to reduce NO_x emissions: Selective Catalytic Reduction (SCR), Lean NOx Catalyst (LNC) and Lean NOx Trap (LNT).

SCR has been successfully developed and commercialized for stationary heavy-

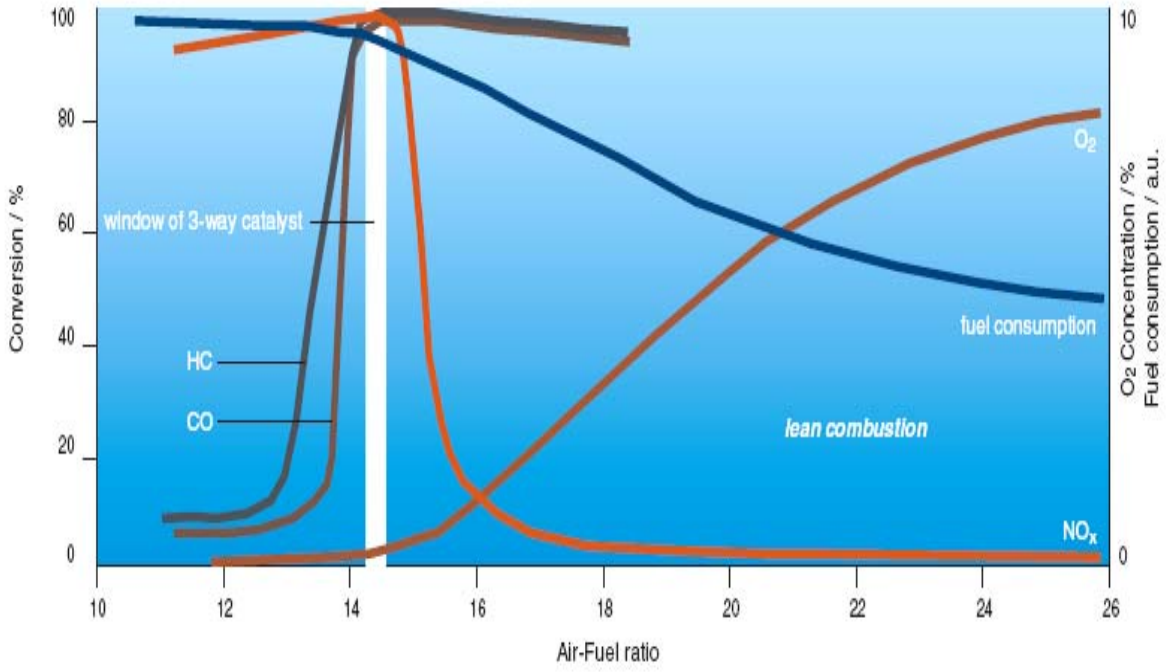

Figure 1.4 Conversion of pollutants in three-way catalyst as a function of air-fuel ratio [6]

duty engines and coal fired power plants. In SCR technology ammonia (NH_3), a reducing agent, is injected into the exhaust stream and reacts with NO_x to form N_2 and H_2O according to the following reactions.

$$4NO + 4NH_3 + O_2 \rightarrow 4N_2 + 6H_2O$$

$$2NO_2 + 4NH_3 + O_2 \rightarrow 3N_2 + 6H_2O$$

According to Helden [7], more than 80% of NO_x conversion is obtained when the operating temperatures are between 350 and 400^{o}C with less than 20 ppm of NH_3 slip. However, the technology requires precise control of reactor temperature to avoid

undesirable byproducts such as ammonium sulfate ($(NH_4)SO_4$) and bisulfate (NH_4HSO_4), which are significant when the operating temperature is below 200^oC. On the other hand, at temperatures above 450^oC NH_3 is converted back to NO_x. Moreover, when the amount of NH_3 injected exceeds the amount of NH_3 required for stoichiometric reaction with NO_x, the excess NH_4 is emitted into the atmosphere as a significant pollutant. Additional tight NH_4 storage and delivery system are also another obstacles for SCR to be applied in light-duty automotive applications.

Lean NO_x catalyst (LNC) based on Cu/ZSM-5 has been developed to reduce NO_x under net oxidizing conditions for automotive applications. Continuous injection of supplemental fuel (HC) in the exhaust stream is required for LNC to maintain the selective NO_x catalytic reduction. Fuel penalty, narrow operating temperature window, insufficient durability and lower NO_x conversion (60%) are still obstacles for LNC technology to be used in automotive applications [8].

Lean NO_x trap (LNT) technology has shown great promise for reducing NO_x in oxygen-rich environments for lean-burn applications because of higher NO_x conversion efficiency and wider operating-temperature window. As shown in Figure 1.5, the operation of LNTs requires engines to operate at two different air/fuel (A/F) ratios corresponding to fuel-lean and fuel-rich phases for storing and reducing NO_x on the catalyst surface, respectively. A typical LNT catalyst consists of a cordierite substrate and γ-Al_2O_3 washcoat impregnated with platinum (Pt) and a NO_x storage medium, an alkali/alkaline earth group such as Ba (barium) or K (potassium). During the fuel-lean phase, NO is oxidized to NO_2 on Pt sites which is stored in the form of nitrites and

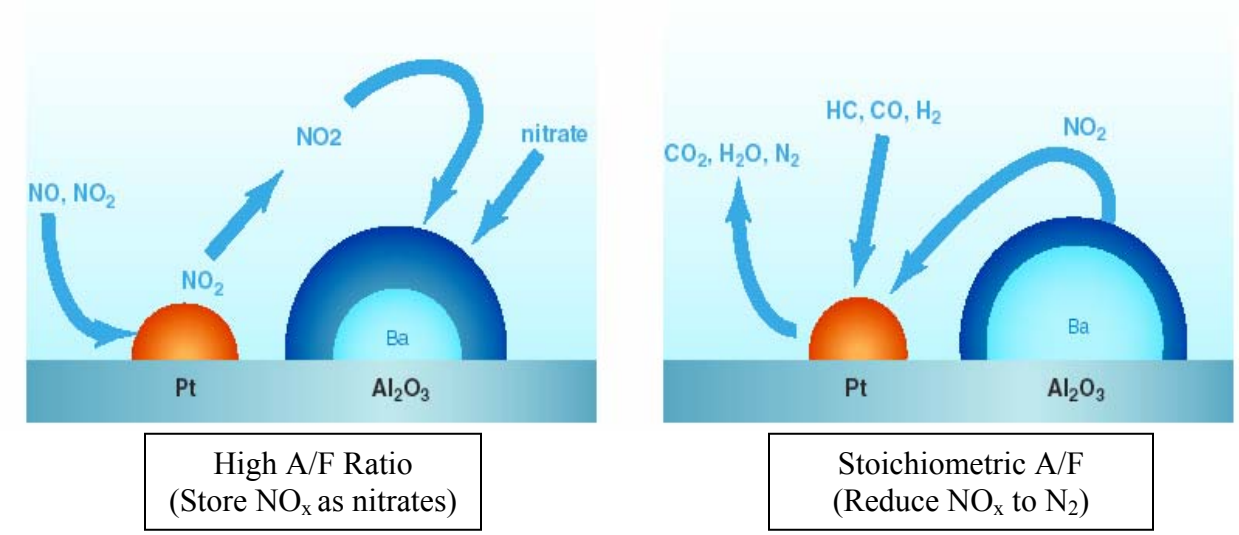

Figure 1.5 Schematic of LNT operation [6]

nitrates on the storage sites. During the rich excursions NO_2 stored in the form of nitrites or nitrates is released from the storage sites and reduced to N_2.

Fuel-lean phase: $NO \xrightarrow[\mathbf{Pt}]{\mathbf{O_2}} NO_2 \xrightarrow[\mathbf{Ba}]{\mathbf{O_2}} Ba(NO_2)_2$ and $Ba(NO_3)_2$

Fuel-rich phase: $Ba(NO_2)_2$ and $Ba(NO_3)_2 \xrightarrow{\mathbf{HC, H_2, CO}} BaO + NO_2 \xrightarrow{\mathbf{HC, H_2, CO}} N_2 + CO_2 + H_2O$

The deactivation of the NO_x storage medium by sulfur poisoning is a major obstacle. Sulfur dioxide (SO_2) in the exhaust gases is oxidized to SO_3 which in turn reacts with the NO_x storage media to form sulfates such as barium sulfate ($BaSO_4$) or potassium sulfate (KSO_4). Since sulfates are more thermally stable than nitrates, the NO_x storage sites are gradually occupied and no longer available for NO_x. Consequently, the NO_x conversion decreases with an increase of sulfates on the NO_x storage sites. To restore the

LNT to its original NO_x storage capacity the LNT is periodically subject to desulphurization at high temperatures in excess of 700^oC under reducing conditions. The frequency of desulphurization is dependent on the amount of sulfur in the fuel − the higher the sulfur level in the fuel the more frequent desulphurization.

In the present study, NO_x absorption isotherm experiments are performed to characterize the NO_x storage capacity and breakthrough time as a function of temperature and gas hourly space velocity (GHSV), from which the optimum operating temperature of the LNT catalysts can be determined. The NO_x desorption isotherm experiments are also performed to ascertain the mechanisms of NO_x desorption process. The NO_x desorption is carried out by shutting off NO_x and O_2 from the simulated exhaust gases, once the LNT catalyst is fully saturated. The understanding of the NO_x desorption mechanisms is further aided by determining the ratio of NO to NO_2 from the absorption isotherms.

Two different regeneration strategies of the LNT catalysts are investigated in the present investigation. In the first strategy the LNT is generated using the lean/rich modulation of the simulated exhaust gases, whereas the regeneration of the LNT is carried by direct fuel injection (DFI) in the second strategy. The purpose of the LNT regeneration lean/rich modulation is to determine the optimum duration of the rich and lean pulses and the optimum concentration of reductants that would produce the highest NO_x conversion efficiency at the predetermined optimum operating temperature of the LNT. Since the fuel efficiency is of primary importance, the optimum rich pulse employed during the regeneration is the one that results in the highest NO_x conversion efficiency in the shortest duration. Regeneration experiments with lean/rich pulses are

performed by varying the time duration of the lean and rich pulses at fixed concentration of the reductants, 4% CO and 1.33% of H_2. The following durations of lean and rich pulses are used in the present investigation:

- 50 s lean and 10 s rich
- 50 s lean and 5 s rich
- 100 s lean and 5 s rich

In the present investigation the optimum time durations of the lean/rich pulses is defined as the one that results in at least 93% NO_x conversion. Once the optimum time durations of the lean/rich pulses are determined, the regeneration experiments are performed at four different concentrations of the reductants.

- 4% of CO and 1.33% of H_2
- 2% of CO and 0.67% of H_2
- 4% of H_2
- 4% of CO

Two separate DFI experiments are carried out: direct fuel injection in the absence and presence of O_2 in the simulated exhaust gases. These two types of experiments are used to simulate two different scenarios in which the rich excursions are generated by manipulating the engine management system (EMS) of the lean-burn engines. In the first scenario, the rich excursions are produced by running the engines under stoichiometric or

rich conditions for a very short time period. In the second scenario the rich excursions are generated by injecting the reductants directly into the lean exhaust gases from on-board supplemental fuel injection system.

To duplicate the first scenario, at the beginning of the rich phase, the flow of O_2 in the simulated exhaust gases is shut off and the reductant, either H_2 or CO, is directly injected into the gas stream. In the second scenario, the rich excursions are generated by injecting the reductant directly into the lean exhaust gas stream. In the present investigation the rich excursions are produced by injecting the reductants, either H_2 or CO using a fast-response piezoelectric valve. Both DFI experiments are performed at the predetermined optimum operating temperature of the LNT and a gas hourly space velocity of 50,000hr^{-1}.

- 2% ~ 4% of CO in the presence O_2 in an increment of 1%
- 2% ~ 4% of CO in the absence O_2 in an increment of 1%
- 2% ~ 4% of H_2 in the presence O_2 in an increment of 1%

The NO_x conversions obtained from DFI with optimum concentration of the reductant in the presence and absence of O_2 are then compared with those found with LNT regeneration using lean/rich cycling. All DFI experiments are performed at the same GHSV and rich duration used in the LNT regeneration experiment lean/ rich modulation.

Chapter 2

LITERATURE REVIEW

This chapter is divided into four main sections in which previous studies of LNT catalysts are reviewed. Section 2.1 discusses the mechanism of NO oxidation on Pt sites while NO_x sorption on Ba sites is reviewed in section 2.2. Sections 2.3 and 2.4 present the mechanisms of NO_x released from the alkaline storage medium and subsequently reduced to N_2 from precious metal sites during the rich phase, respectively. Finally, NO_x reduction on Pt sites is reviewed in Section 2.5.

2.1 NO Oxidation

In engine exhaust gases, NO_x exists primarily as NO. Since NO_2 is the sorption precursor for the LNT trapping materials in the presence of excess O_2, the performance of LNT catalyst is strongly dependent on the efficiency of NO oxidation to NO_2 on precious metal sites. Several precious metals such as platinum (Pt), palladium (Pd), and rhodium (Rh), can be used to oxidize NO to NO_2 . According to Ohusuka et al [35-37], Pt is the first choice for the oxidation of NO in LNT catalyst since Pd and Rh are less active for NO oxidation even though they are more active for NO reduction during the fuel-rich excursion. Experiments with two different LNT formulations, one Pt-based and the other Pd-based, were conducted by Salasc et al. [38] in which the activity of these two metals on the NO oxidation was compared. Pt-containing LNT sample shows 20% of NO

converted to NO_2, while at the same identical conditions no NO conversion was observed with Pd-containing LNT sample.

The prediction of the NO oxidation kinetics over the LNT catalyst sample is not an easy task due to the presence of the NO_x trapping component (BaO). The site of barium oxide can store NO_2 oxidized from Pt as barium nitrate compound ($Ba(NO_3)_2$), and the equilibrium of the NO oxidation over Pt can be shifted by NO_2 adsorption on the storage component as shown in Figure 2.1.

Thermodynamic equilibrium of NO and NO_2 as a function of temperature and O_2 concentration is shown in Figure 2.2. As seen in the figure, NO_2 is the dominant species when the temperature is below 200^oC. As the temperature increases equilibrium dictates lower NO_2 concentrations. Furthermore, increasing O_2 concentration leads to higher NO_2 concentration at equilibrium.

Epling et al. [34] measured the oxidation of NO to NO_2 over a Pt/γ-Al_2O_3 catalyst as a function of temperature and space velocity. The results shown in Figure 2.3 indicate that at temperatures below 200^oC the oxidation of NO is kinetics-limited. At a gas hourly space velocity (GHSV) of 10,000 hr^{-1}, the maximum conversion reaches 57% at 310 ^oC while the maximum reaches 47% at 362 ^oC at a GHSV of 25,000 hr^{-1}. The NO conversion is higher at the lower GHSV due to longer resident time. Since the resident time is inversely proportional to GHSV, and thus longer resident time allows more NO molecules to be oxidized at Pt sites. Above these two maximum temperatures, the NO oxidation is limited by the thermodynamic equilibrium, whereas the conversion is kinetically limited below these two temperatures. Castoldi et al. [11,18,25] conducted several experiments with LNT catalysts having different Ba loadings (from 0-30% wt.) in

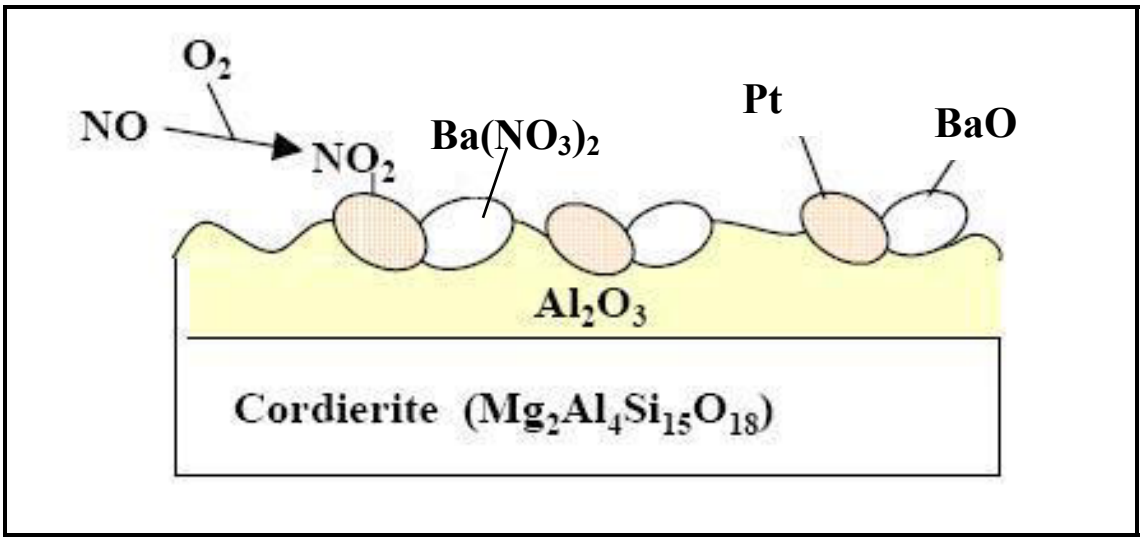

Figure 2.1 Surface oxidation reaction of the LNT catalyst

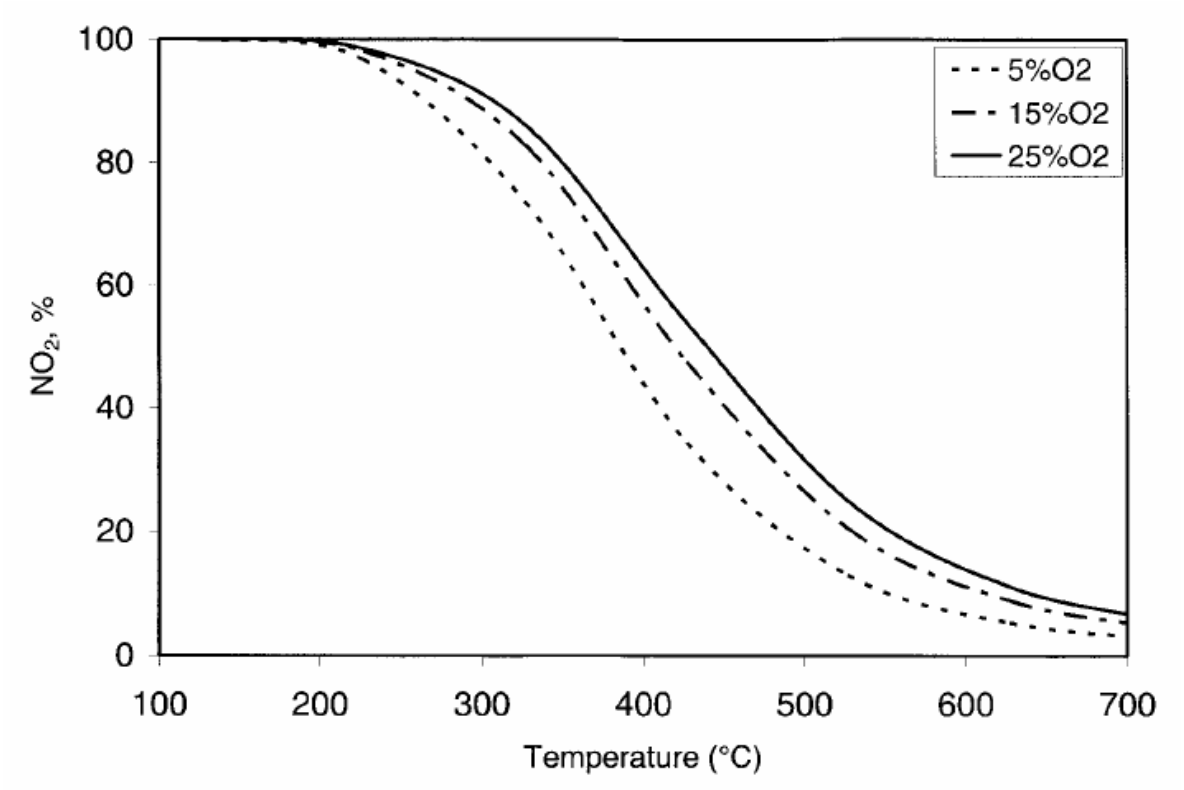

Figure 2.2 Thermodynamic NO_2 / NO equilibrium values as a function of O_2 concentration (250ppm NO_x and a balance of N_2)

the NO_x adsorption-reduction under realistic operating conditions. The role of Pt seems not only to oxidize NO to NO_2, but also to provide sites for both NO or NO_2 adsorption and O_2 dissociation close to BaO sites for nitrate formation. Two kinds of Pt sites seem to operate; sites close to BaO crystallites are active in barium nitrate formation while other sites are responsible for NO_2 formation.

$$NO + 1/2O_2 \rightarrow NO_2 \quad : \text{Oxidation at Pt sites}$$

$$2NO_2 + BaO + 1/2\ O_2 \rightarrow Ba(NO_3)_2 \quad : \text{Storage at Ba sites}$$

2.2 NO_x Sorption

2.2.1 Role of NO_2 in the NO_x Trapping Process

There seems to be a consensus in LNT literature that NO_2 is a precursor for the trapping process by alkaline-earth components. Cant et al. [21, 39, 40] performed NO_x trapping experiment on $BaO/\gamma\text{-}Al_2O_3$ catalyst sample with either NO or NO_2 at the inlet in the presence of O_2. When NO was introduced into the sample, NO_2 was not observed at the surface since the sample did not contain any Pt site to oxidize NO to NO_2. However, when NO_2 was introduced most of NO_2 was successfully absorbed and stored as barium nitrate species as shown in Figure 2.3.

A temperature-programmed absorption with $Pt/BaO/\gamma\text{-}Al_2O_3$ sample was conducted by Salasc et al. [38] to investigate the possibility that NO absorption process could occur under oxygen-free environment; however the result suggested that only a few percent of NO were adsorbed. This minor adsorption was likely occurred due to the residual surface oxygen participating in the oxidation reaction of the pretreatment

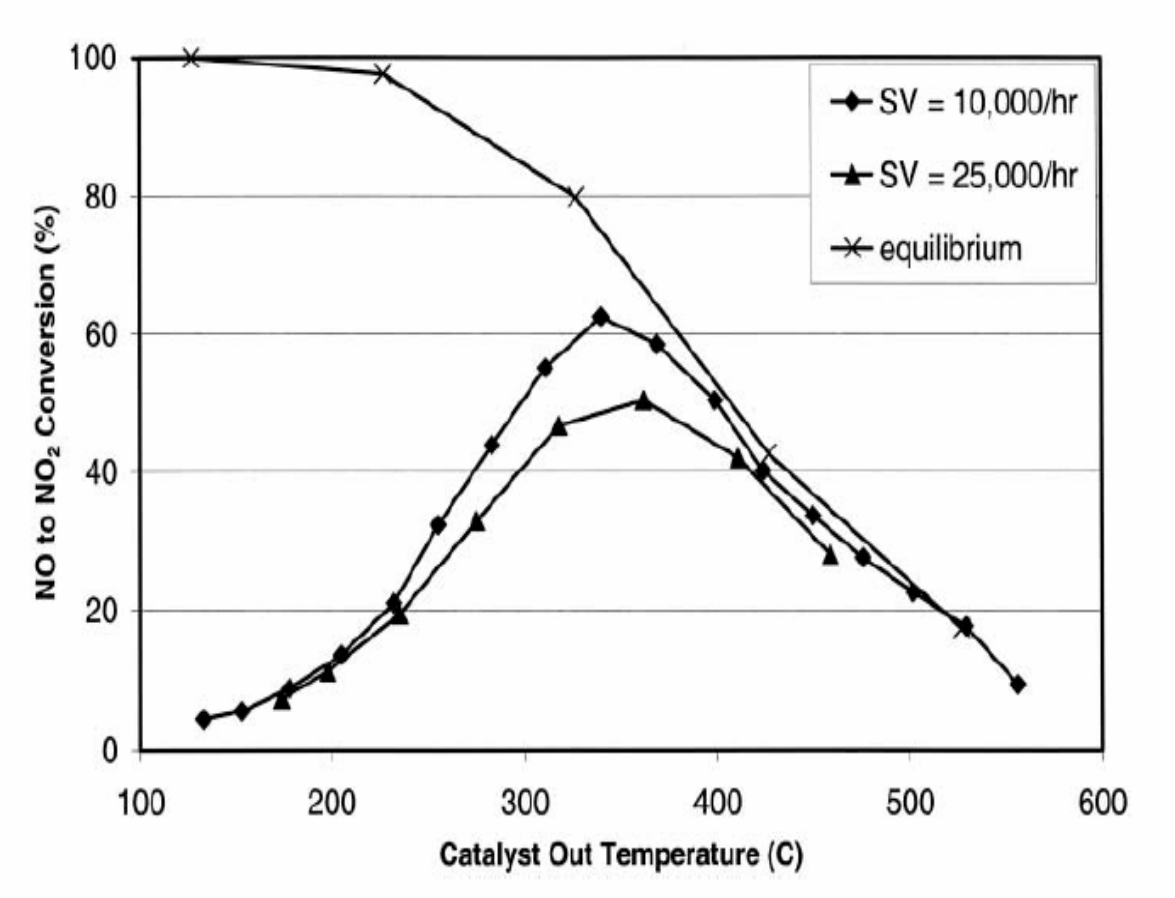

Figure 2.3 NO to NO_2 conversion as a function of gas hourly space velocity and temperature on Pt / Al_2O_3 catalyst (8% O_2, 250ppm NO, and a balance of N_2)

condition, and thus the adsorption of NO by the storage medium is impossible in the absence of O_2.

The results shown in Figure 2.4 were obtained by Epling et al. [34] for LNT catalysts exposed to simulated exhaust gases of 250 ppm of NO or NO_2, 8% of H_2O, 8% of CO_2, O_2 at 0 and 8%, and the balance in N_2. In the presence of O_2 when NO is introduced, the catalyst absorbs NO_x completely in the first 64 seconds. On the other hand, without O_2, the NO_x slip of NO_2 inlet concentration is extended to 220 seconds.

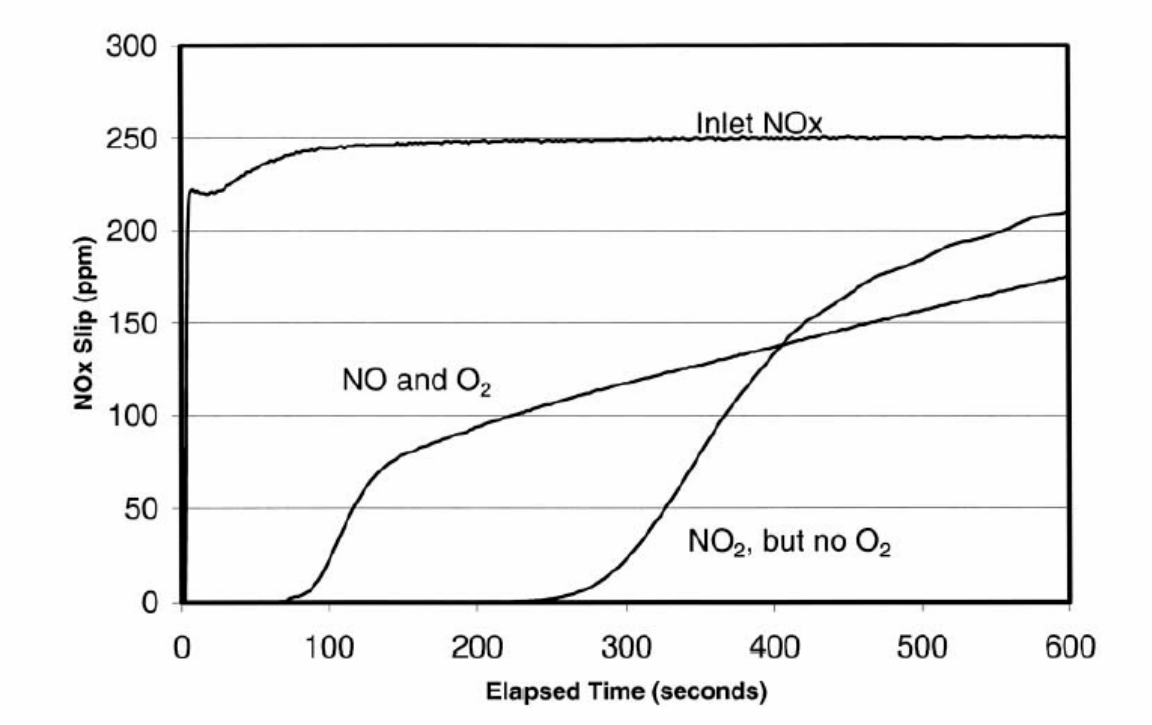

Figure 2.4. Effect of inlet NO_x source, NO (250ppm) or NO_2 (250ppm) on $Pt/BaO/Al_2O_3$ catalyst trapping performance at T=200°C and GHSV=15,000 hr^{-1}

Amount of NO_x stored with NO_2 inlet concentration is greater than with NO and O_2 at the inlet, and consequently NO_2 does play an important role in trapping NO_x regardless of presence of O_2. Furthermore, the integral nature of LNT catalyst suggests that more Pt sites at the front of the catalyst participate in trapping NO_2, whereas less Pt sites participate in trapping NO_2 when NO is introduced to be oxidized at the front of the catalyst.

2.2.2 Effects of Gas Composition and Temperature

The presence of CO_2, H_2O, and O_2 are always present in typical engine exhaust gases. The effect of CO_2, H_2O, and O_2 on the performance of LNT catalyst has been

extensively investigated in previous studies. Epling et al. [34] emphasized that the most important factor in determining the performance of LNT catalysts is the availability of the storage compound, BaO at the beginning of NO_x trapping process. Lietti et al [16, 17] found BaO, $Ba(OH)_2$, and $BaCO_3$ initially coexist at the surface of LNT catalysts, and NO_x storage occurs first on BaO, then barium hydroxyl ($Ba(OH)_2$), and finally barium carbonate ($BaCO_3$). The absorption of NO_x on the storage compounds can not be observed directly, however the order of absorption on the storage compounds can be inferred based on the evolution of H_2O and CO_2 during the regeneration period as shown in Figure 2.5. Prior to the experiment described by panel I, the catalyst was calcined in dry air in order to eliminate any $Ba(OH)_2$, but to retain only $BaCO_3$ in the sample. Under this condition the evolution of CO_2 and NO_x is observed at the same time at 50 s in panel I. The experiment depicted by panel II began after the LNT sample was fully regenerated with 2000ppm of H_2. NO_x slip begins at a much later time of 250 s, which indicates an enhance in NO_x storage. The evolution of CO_2 is still evident, however the amount is much less than that in panel I. This result suggests that CO_2 in $BaCO_3$ is still seconds, Furthermore, the evolution of H_2O is observed prior to the NO_x slip and the evolution of CO_2. These results confirm the order of storage compound decomposed in the following order: first, oxide in BaO is displaced by NO_x to form barium nitrites or nitrates, then hydroxides in $Ba(OH)_2$ with H_2O evolution, and finally carbonates in $BaCO_3$ with CO_2 evolution. The experiment depicted in panel III was obtained using the same reductant with the same concentration in the regeneration as in panel I. NO_x slip occurs at 300 s with less CO_2 evolution, and the catalyst is capturing larger amount of NO_x than in panels I and II. The results confirm that the overall NO_x trapping capacity was recovered after

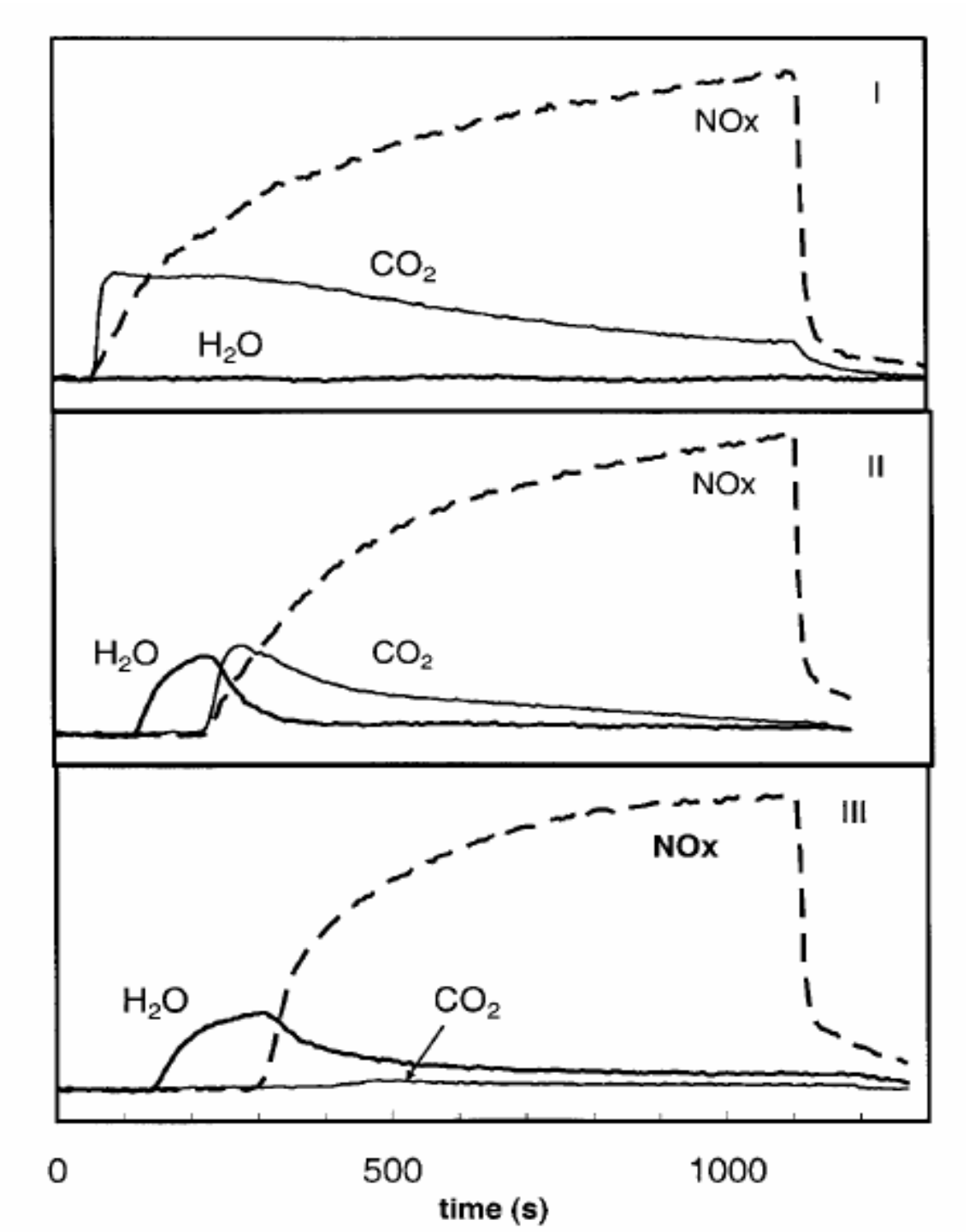

Figure 2.5 A sequence of NO_x storage runs at 350°C with a fresh sample of $Pt/Ba/Al_2O_3$ .The lean phase contained 1000 ppm NO, 3% of O_2, and a balance of He, and the rich phase contained 2000 ppm of H_2 in a balance of He.

all carbonate species were removed by the regeneration. It is obvious that the presence of H_2O and CO_2 in the gas phase have negative effects on NO_x trapping ability of the LNT catalysts and some of the literature confirmed. The presence of CO_2 in lean and rich conditions decreases the trapping capacity of LNT by 45% at 250^oC [13,16,21,40-42].

Toops et al. [40,41] performed a chemisorption experiment with the LNT catalyst; the author injected 5% H_2O at 300^oC into the LNT catalyst and the trapping capacity of LNT was decreased by 16% and reduced the overall performance across a wider operating temperature range. Moreover, Toops et al. [50] found that H_2O reduced the negative impact of CO_2 on NO_x trapping. H_2O in gas phase replaces carbonate species in $BaCO_3$ to form $Ba(OH)_2$ and it can be decomposed to $Ba(NO_3)_2$ by NO_x much easier than $BaCO_3$.

$$BaCO_3 + H_2O \rightarrow Ba(OH)_2 + CO_2$$

As seen in Figure 2.3, NO_x conversion of typical Pt/Ba/γ-Al_2O_3 catalysts (LNT) is a function of temperature, and the maximum conversion usually occurs between 350 and 380^oC [14,16,41,43-47]. The oxidation of NO is an important limiting factor for the overall NO_x trapping process, in which the kinetic limitations always impose on NO oxidation at lower temperatures and equilibrium at high temperatures.

2.2.3 Cycling Fuel Lean and Rich Conditions

Realistic operation condition of LNT catalysts requires periodic rich excursions to regenerate when the catalysts are fully saturated. During the fuel-rich phase, the catalyst

surface may retain some nitrite or nitrate species depending on the efficiency of the LNT catalyst. According to Epling et al. [34], the retained nitrite or nitrate species are continually accumulated after subsequent cycles, and the trapping efficiency of LNT catalysts decreases up to a steady-state level where the rate of desorption is equal the rate of absorption; this subject will be further discussed in section 2.4. After the trapping efficiency reaches the steady-state value, the measured amount of NO_x trapped on surface is less than the total NO_x capacity of the catalyst. The complete regeneration process can be obtained by using longer rich phase (high-temperature transient) or more reductant concentration. An example of cycling lean and rich experiment shown in Figure 2.6, was obtained by Epling et al [43]. NO_x slip during the sorption phase was less than 10ppm before the first NO_x excursion, but it keeps on increasing up to 10 cycles and reaches a steady state value of about 26ppm. The NO_x absorption efficiency is not changing due to the constant furnace temperature, but the amount of NO_x trapped during each cycle is decreasing. Therefore, the decrease in the LNT performance in the cycling experiment is not only due to the performance of LNT catalyst, but the inefficient regeneration due to not enough fuel rich time or reductant concentration.

2.2.4 Reaction Pathways for Nitrate Formation

Epling at al [34] suggested that an oxidation state of N in NO_2 molecule should be changed from +4 to +5 in order to form a nitrate compound. Several simplified and combined pathways have been proposed to explain the nitrate formation during the fuel-lean condition of the LNT catalysts. Due to the significant amount of H_2O and CO_2 presented in the LNT operation condition, Ba, which is highly reactive in combining with

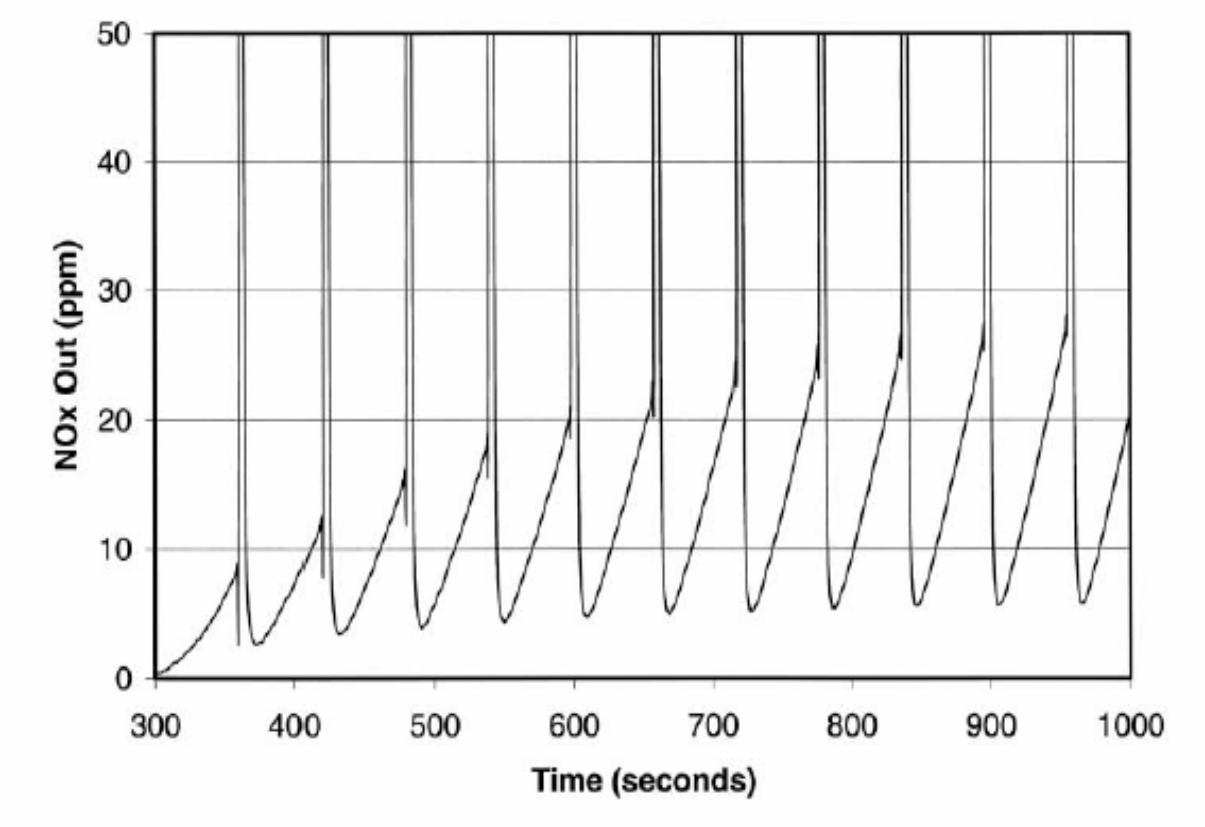

Figure 2.6. Outlet NOx concentration during cycling lean and rich phases over $Pt/Ba/Al_2O_3$ catalyst at 360°C. 250 ppm NO, 8% O_2, 10% CO_2, 8%H_2O, and a balance of N_2 were used for lean phase, and 0 ppm of NO, 4.0% CO, 10% CO_2, 8% H_2O, and a balance of N_2 were used for rich phase.

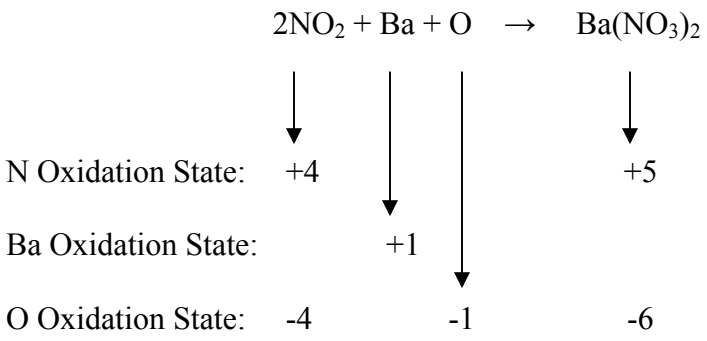

other elements or compounds, would be obtained on the catalyst surface as $Ba(OH)_2$ and $Ba(NO_3)_2$. However, there have been many studies to substitute Ba by other alkali or alkali-earth metals in order to improve the LNT performance, and the following reactions proposed from literatures are not applying to only Ba but any alkali or alkali-earth metal.

1. Nitrates are formed from BaO, NO, and O_2 and subsequent oxidation leads to the nitrate [14,43,47,48]

$$BaO + 2NO + O^* \rightarrow Ba(NO_2)_2$$

$$Ba(NO_2)_2 + 2O^* \rightarrow Ba(NO_3)_2$$

2. NO_2 molecules react with the Ba species precursor and oxygen to form the nitrate [14,16,21,42-44,47-51].

$$BaO + 2NO_2 + O^* \rightarrow Ba(NO_3)_2$$

3. NO molecules react with Ba species precursor and multiple oxygen atoms to form the

nitrate [14,44,48,52]

$$BaO + 2NO_2 + 3O^* \rightarrow Ba(NO_3)_2$$

4. Barium peroxide as an intermediate reacts to form the nitrate [11,15,21,51]

$$BaO_2 + 2NO_2 \rightarrow Ba(NO_3)_2$$

5. An N_2O_4 dimer forms and reacts with the surface to form a mixture of nitrates and nitrates. The nitrite are subsequently oxidized to nitrates [16,53].

$$2NO_2 \rightarrow N_2O_4$$

$$2BaO + N_2O_4 + 2NO_2 \rightarrow Ba(NO_2)_2 + Ba(NO_3)_2$$

$$Ba(NO_2)_2 + 2O^* \rightarrow Ba(NO_3)_2$$

6. A mixture of nitrites and nitrates are formed from NO_2 and oxygen. Again the nitrites are subsequently oxidized to nitrates [48,52,54].

$$2BaO + 4NO_2 \rightarrow Ba(NO_2)_2 + Ba(NO_3)_2,$$

$$Ba(NO_2)_2 + 2O^* \rightarrow Ba(NO_3)_2$$

All six equilibrium reactions are reversible when the fuel-rich phase is introduced into the surface. Equilibrium reactions are easily affected by the concentration of NO_2, since more

NO_2 supplied during lean phase increase the reaction rate to form nitrate compounds. Several FTIR studies [40,55,56] have been undertaken to find evidences for the pathway of nitrate formation. Certainly, it is very difficult to determine the exact pathway of the nitrate formation just by looking at the amount of compounds obtained from FTIR. However, all of FTIR studies confirm the presence of nitrite and nitrate mixtures on the sample surface only during the lean phase. Thus, a reaction to form nitrite species should be proposed in the pathway such as those pathways denoted by 1, 5, and 6. These pathways suggested that nitrite compounds are subsequently oxidized with oxygen atoms captured at Pt sites to form nitrates. The ratio of nitrites to nitrates would increase until the reaction equilibriums are established among nitrites, nitrates, and oxygen atoms. According to Epling et al [34], the pathway number 6 is generally considered to be the mechanism of NO_x trapping because it is consistent with experimental data of LNT catalysts at temperatures lower than the optimum operating temperature (350 to 380^{o}C). However, at higher temperature, the pathway number 6 is in doubt, due to the thermal stability of nitrite compounds. The nitrite compound starts to be decomposed around 270 ^{o}C, above which the compound would not exist.

2.3 Reductant Delivery and Evolution

In a typical operation condition LNT catalysts periodically requires to regenerate the surface occupied by nitrite and nitrate compounds when the catalyst are fully saturated. The regeneration of the catalyst surface is accomplished by subjecting the catalyst periodically to fuel-rich excursions, which consist of unburned hydrocarbons

(HC), carbon monoxide (CO), and hydrogen (H_2). These reductants can be obtained by the combustion of fuel in an oxygen-deficiency environment.

2.3.1 Amount of Reductant

Epling et al [34] proposed that a sufficient amount of reductant must be injected into the main gas stream in order to accomplish the followings:

- creating a net reducing environment by consuming O_2 in the gas phase and, in most cases, O_2 stored on the catalyst:
- releasing stored NO_x
- subsequently reducing NO_x to N_2.

During the regeneration period, the reductant reacts with O_2 trapped on Pt sites, and the exothermic oxidation reaction is one of the NO_x release mechanisms; i.e., thermal release, which will be further discussed in Section 2.4. The remaining reductant then reacts with gas-phase NO_x reducing it to N_2. If only an insufficient amount of reductant remains after the oxidation reaction on the surface, the reduction rate of NO_x in gas phase will decrease. Therefore, after the oxidation reaction, the fuel penalty would be an issue when O_2 still presents on the surface. The overall performance of the catalyst during the regeneration can be affected by the oxygen-storage capacity (OSC), which influences the amount of reductant necessary to complete the oxidation and reduction. The greater the catalyst's OSC, the larger the amount of reductant required for sufficient regeneration.

2.3.2 Significance of Reductant Evolution Over The LNT Catalysts

According to Narula et al. [45,57], H_2 is the most effective reductant to reduce NO_x and regenerate the catalyst surface, while CO and propylene are not effective as reductants. CO reacts with NO_2 selective to N_2, and H_2 known to be the best reductant is produced by the water-gas-shift (WGS) reaction in which CO plays an important role.

$$2CO + 2NO \rightarrow N_2 + 2CO_2 : NO_x \text{ reduction by CO}$$

$$CO + H_2O \rightarrow CO_2 + H_2 \quad : \text{Water-gas-shift reaction}$$

Farrauto et al [59,60] studied the WGS reaction on precious metals, which are the major component of the Three-way Catalytic Converters (TWCs). Since the LNT catalysts also contain precious metals, it is expected that the WGS reaction also occurs. The forward WGS was studied by Li et al [61-63] over $Pt/Ba/\gamma\text{-}Al_2O_3$ samples as well as the reverse WGS reaction [16,64]. Three commercial-available LNT catalysts were used to find the evidence of the forward reaction in experiments performed by Li et al [61]. The authors calculated the theoretical amount of H_2 evolved from the forward WGS reaction in the main stream before they performed actual experiments. The theoretical concentration of H_2 evolved was obtained using the following gas composition - 10% H_2O, 10% CO_2, and 1.2% CO. Under these conditions the amount of H_2 evolved was found to be approximately 1.1%, and a compatible amount of H_2 was observed from experiments. Therefore, author concluded that H_2 was formed via the WGS reaction and their data indicated that H_2 was a better reductant for NO_x conversion. Theis et al [64] studied the reverse reaction of the WGS by injecting H_2 with and without H_2O into the main stream

consisting of N_2 and CO_2. In the presence of H_2O a significant amount of CO was observed, while 64% less CO was observed in the absence of H_2O.

2.4 NO_x Release

Two primary driving forces of NO_x release from the surface were suggested by Epling et al [34]. Heat generated by the oxidation of the reductant is considered to be the first driving force, and the oxidation of the reductant is accomplished either by O_2 in the gas stream or stored on the surface of the catalyst. When the surface temperature increases due to the exothermic reaction, the stability of nitrate stored in the storage component decreases, resulting in NO_x released either into the surface or the gas stream. Evidently, the amount of NO_x released would be significant when the catalyst is fully saturated with NO_x at a given temperature or when the temperature excursions due to the oxidation of reductant are large. Harold et al [65] measured the temperature excursion at the middle LNT powder sample during fuel-rich condition, and they observed a 150^oC temperature rise due to the oxidation reactions.

The second driving force of NO_x release suggested by Epling et al [34] is that the consumption of O_2 stored on the surface from the oxidation reaction reduces the amount of nitrite or nitrate species stored at the equilibrium. As discussed previously in the NO_x Sorption Section, the storage process is partially controlled by the chemical equilibrium at a given temperature. The equilibrium stability of nitrate species is dramatically reduced under conditions with low or zero partial pressures of O_2.

2.4.1 Effect of Temperature

The pathways of NO_x release have been extensively investigated, however the effects of operation parameters on the NO_x release has not been clarified since the inconsistent techniques were adapted to NO_x release experiments. For instance, the NO_x release peak obtained by Fridell et al [44] was measured in the order of increasing furnace temperature after a NO_x storage/reduction cycle, but Nove et al [17,46] measured in the order of decreasing furnace temperature even though propylene was chosen to be the major reductant in both. Moreover the different amounts of NO_x were stored during the fuel lean period in each experiment.

However, Epling et al [34] suggested two different ways to interpret the effects of temperature on the NO_x release. The amount of NO_x release is depending on the material property of the catalyst to trigger the activity of the reductant at lower temperatures where the overall reaction is limited by the chemical kinetic. From this low temperature range, less amount of NO_x release and more reduction of NO_x should be observed as the temperature increases. At higher temperatures, where reductant activation is not an issue, more amount of NO_x release should be obtained due to less stability of the nitrate species. Therefore, most of literatures performed experimental observations on NO_x release and the stability of the nitrate species, agree that the amount of NO_x released increase with temperature, and once the temperatures are higher than 400^oC, the significant amount of NO_x release is observed. Therefore, to minimize the NO_x release at higher operating temperature, the authors concluded three different methods can be utilized; reduce the rate of nitrate decomposition, increase the nitrate stability, or delivering efficient reductants more quickly to match the speed of NO_x release.

2.4.2 Effect of Gas Composition

The amount and type of reductant in exhaust gas composition is an important factor to affect the rate of NO_x release during the rich period. Balcon et al [66] performed NO_x release experiments by using a rapid transition from a NO_x, O_2, and helium (He) mixture to just He, as shown in Figure 2.7. The authors convinced that NO_x release can occur without a reductant present and without temperature increase, since there was no heat evolved from the transition to inert conditions. Since there were only NO_x, O_2, and He introduced to the gas stream, the NO_x release was occurred by a change in equilibrium either from O_2 or NO_x concentration decreases and may be related to decomposition of the less stable nitrite species or release from the γ-Al_2O_3 support [67]. The result of NO_x release experiments performed by Amberntsson et al [68] indicated that O_2 had a suppressive effect on NO_x release. Approximately 75% of the NO_x stored at 450^{o}C was released in a mixture of 5% CO_2 balanced with Ar while 47% of the NO_x stored was released in a mixture of 10% O_2 / 5% CO_2 balanced with Ar. Furthermore, both NO and NO_2 releases were presented, but the release of NO was significantly more influenced than was that of NO_2 by the presence of O_2. This result suggested that the same amount of NO_x was released in both cases, but most of NO_2 species released from the surface could be recaptured regardless of the presence of oxygen. NO released from surface should be oxidized NO_2 with oxygen to be recapture, and the amount of NO recaptured will be significantly less in the absence of O_2. The authors also suggested that the presence of oxygen atoms on Pt sites might cause a decreased amount of NO release because the partial pressure of oxygen presented was affecting the equilibrium amount of nitrite and nitrate species. Liu et al [69] observed that the removal of O_2 broke the

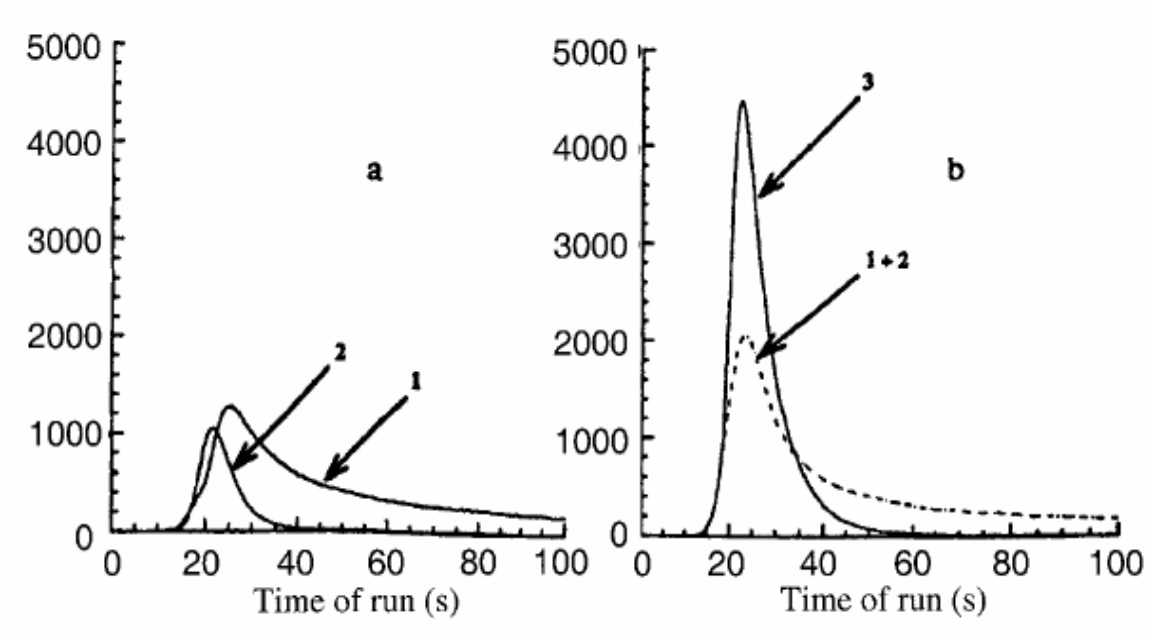

Figure 2.7. NO_x release from a Pt/Rh/Ba/γ-Al_2O_3 catalyst perform at 550°C. The experiment at the panel (a) was performed with two different steps, which was labeled (1) and (2) respectively. NO_x balanced with He was initially exposed on the catalyst, then the gas composition was switched to pure He, and the NO_x release after catalyst was measured (1). After the measurement, 10% CO_2 balanced with He was introduced to catalyst (2). The NO_x release of the panel (b) was obtained from one step experiment. NO_x balanced with He was initially introduced, and the gas composition was continually switched to 10% CO_2 balanced with He (3). The plot labeled (1+2) is the sum of plots (1) and (2) from the left panel.

equilibrium of the nitrate species and destabilized nitrite species to induce NO release.

$$Ba(NO_2)_2 + 2O^* \leftarrow Ba(NO_3)_2$$

$$BaO + 2NO + O^* \leftarrow Ba(NO_2)_2$$

2.5 NO_x Reduction

A number of NO_x reduction mechanisms in the regeneration phase of the LNTs have been proposed. Burch et al [70,71] using propylene (C_3H_6) as the reductant, suggested that NO_x reduction occurs on the unoccupied Pt sites; and this mechanism is also valid for other reductants such as H_2 and CO. To initiate the reduction mechanism atomic oxygen (O) from Pt-O sites absorbed during the lean phase has to be replaced either by the reductant or reductant radicals. Therefore, the reduction of NO to N_2 begins with the reductant radicals generated from the active Pt sites. An example of such a mechanism − the Mars-van Krevelen type − has been proposed for the NO_x reduction in the LNT catalysts [11].

$$C_3H_6(g) + Pt \rightarrow Pt - C_3H_6$$

$$Pt - C_3H_6 + 2Pt \rightarrow 3\ Pt - CH_2$$

$$Pt - CH_2 + 3Pt - O \rightarrow 4Pt + CO_2(g) + H_2O(g)$$

Finally, the reduction of NO_x to N_2 occurs as a result of the reaction between the absorbed reductant radical and NO.

$$Pt - CH_2 + 3Pt - NO \rightarrow 4Pt + CO_2(g) + H_2O(g) + 1.5N_2(g)$$

Chapter 3

EXPERIMENTAL APPARATUS AND PROCEDURE

In this chapter, the experimental apparatus and the testing procedure are described in details. Section 3.1 presents the over-all description of the bench-flow reactor. A detailed description of the LNT system, which consists of the LNT reactor, LNT catalyst samples, and fuel injection system (FIS) for LNT regeneration, is given in Section 3.2, whereas Section 3.3 provides the full description of the BFR components. Sections 3.4 and 3.5 describe the Horiba analyzer bench and emission analyzers. The data acquisition system is presented in Section 3.6, and finally the experimental procedure in Section 3.7.

3.1 Overall Description of the Bench Flow Reactor

An overall schematic and a photograph of the bench flow reactor system (BFRS) are shown in Figures 3.1 and 3.2, respectively. The BFRS consists of a Reverse Flow Oxidation Catalyst Reactor (RFOCR) and a LNT reactor. The two reactors, as seen in Figures 3.1 and 3.2, share the same components such as the instrumentation cabinet, peristaltic pump, and steam generator, which are located in upstream of the reactor branching valves. Since each particular reactor experiment must be run independently, a valve system is devised to direct the gas flow only to the reactor that is being in operation. Due to the high operating temperature range ($140 - 350^{o}C$) of the simulated exhaust gases in upstream of the reactors, three Swagelok high temperature bellow valves (SS-4BW) with maximum operating temperature of $450^{o}C$ are employed for branching the flow.

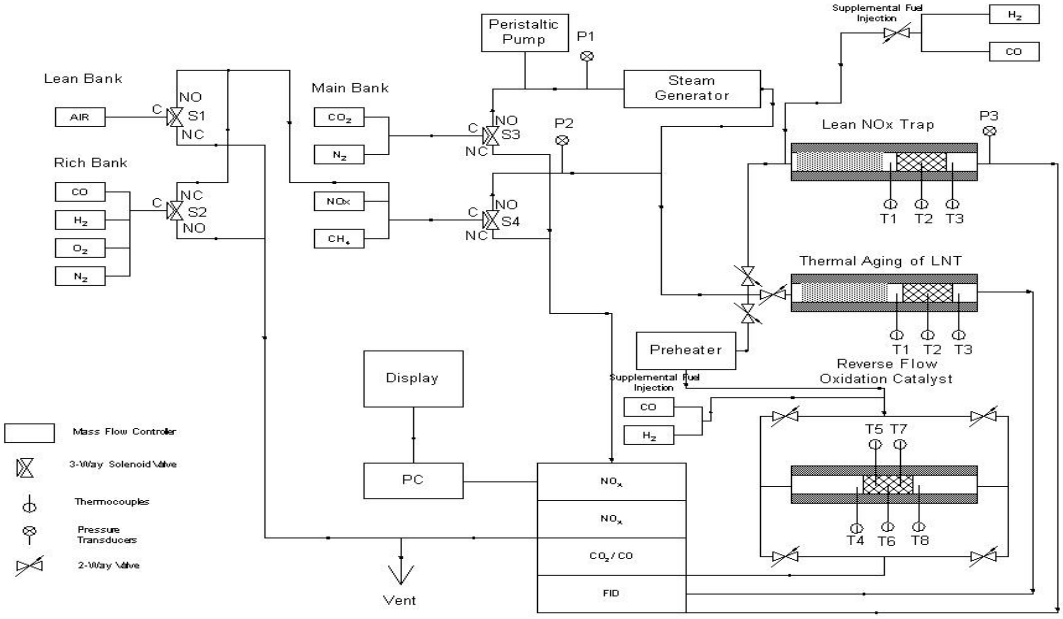

Figure 3.1 Schematic of bench flow reactor system

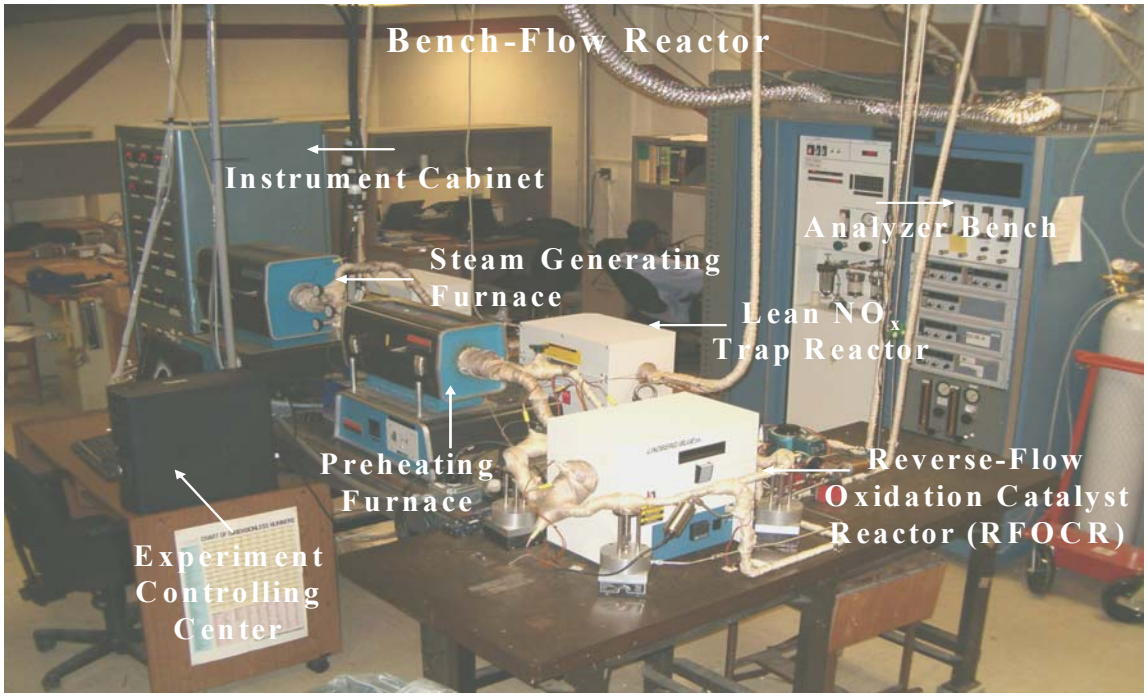

Figure 3.2 Photograph of bench flow reactor system

Simulated exhaust gas consisting of research-grade Air, CO, H_2, O_2, N_2, NO_x, and CO_2 with a composition similar to the exhaust gases from lean-burn natural gas engines, is introduced into the system by means of mass flow controllers (MFCs).

Water vapor is produced via a peristaltic pump into a steam generator, which is then introduced into the simulated exhaust gases. However, the removal of the water vapor from the simulated exhaust gases is necessary prior to the analyzers in order to prevent erroneous reading from the analyzers. For water removal, the Horiba analyzer bench is equipped with a water condenser for removing water vapor from the simulated exhaust gases.

To simulate the fuel lean and rich conditions, three different flow banks are utilized. The main flow bank, which is always present in the flow through the LNT reactor, consists of N_2, CO_2, and NO_x. The rich bank consists of CO and H_2 as reductants, whereas only air is used in the lean bank. During the lean/rich cycling experiments additional N_2 is provided in the rich bank to compensate for the loss of N_2 when the lean bank is shut off. By activating two three-way solenoid valves S1 and S2, the lean and rich cycle of any desired duration can be achieved. Either lean (air) or rich (H_2 and CO) flow stream is sent to the main stream (NO_x) and the remaining flow stream is directed to the vent. The gas flows from S1 and S2 are sent to one flow manifold, which is controlled by a solenoid valve S4. From the solenoid valve S4 the gas flow is sent either to the inlet of the BFRS or directly to the exhaust gas analyzers (BFR system bypass). By using solenoid valve S3, both N_2 and CO_2 are either sent to the steam generator as carrier gases for sweeping out water vapor from the water generator or to the to the gas analyzer via BFR system bypass line.

The exhaust gas mixture is analyzed by the Horiba analyzer bench, which is capable of measuring concentrations of CO, CO_2, THC, NO, and NO_x. National Instruments hardware and LabVIEW 6.1 are used to acquire data during the experimental runs. The hardware components of the data acquisition system consist of a shielded rack mounted terminal block (TC-2095), shielded rack mounted BNC adapter chassis (BNC-2090), and a 4-slot chassis (NI SCXI-1000).

3.2 Lean NO_x Trap System

The Lean NO_x Trap (LNT) system consists of a LNT catalyst sample, quartz-tube reactor with stainless steel end fittings, Lindbergh MiniMite reactor furnace, and Direct Fuel Injection (DFI) system as shown in Figure 3.3. All components are connected by stainless steel tubing and are heated by heating tapes.

3.2.1 Catalyst and Reactor

Monolith LNT catalyst samples with proprietary washcoat formulation are obtained from EmeraChem. The catalyst samples, cored from a "pilot plant" not a "production process" LNT monolith, consist of a ceramic substrate with Pt and BaO and K_2O supported on a γ-Al_2O_3 washcoat. According to the information provided from EmeraChem, Pt is highly loaded with a lager amount of K_20 present in the washcoat than BaO. The detailed description of the EmeraChem LNT washcoat formulation has been registered with U.S. patent 5599758 [71]. A photograph of a LNT catalyst sample is shown in Figure 3.4. A LNT sample of 7.6 cm long and 2.2 cm outside diameter with a

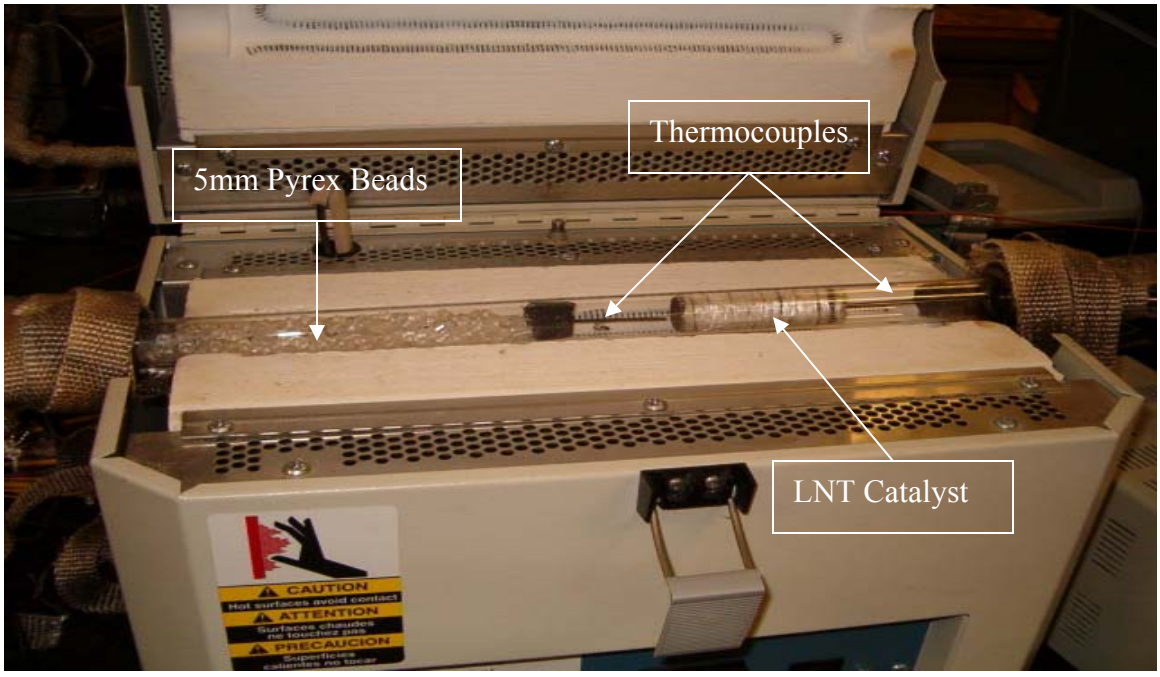

Figure 3.3 Photograph of LNT reactor

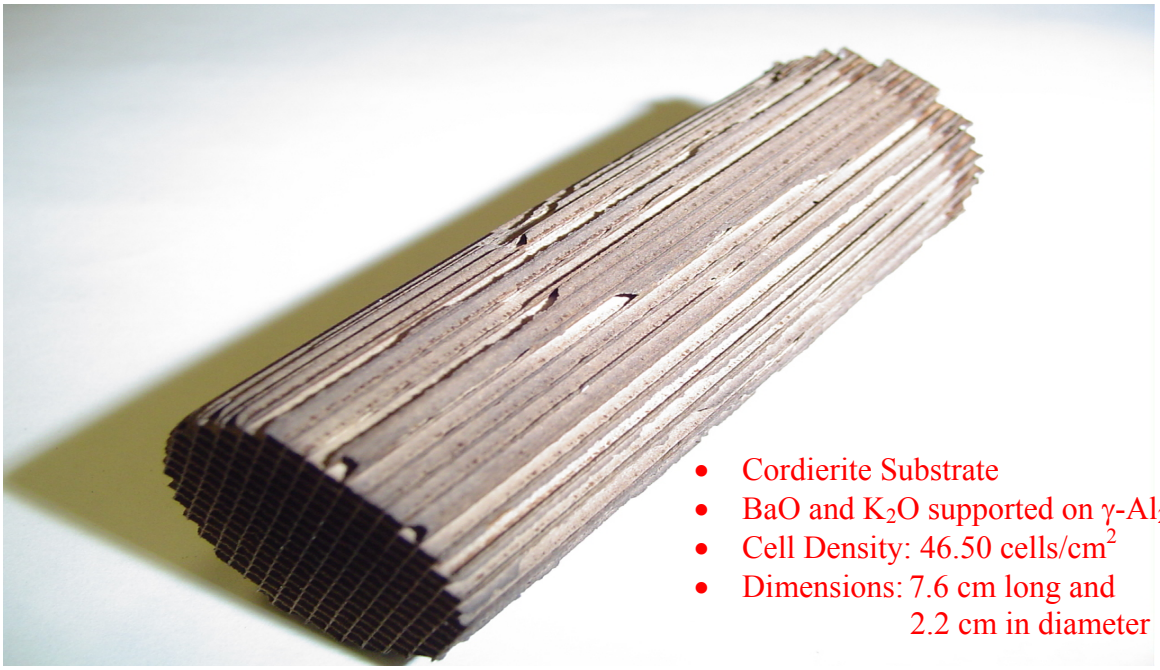

Figure 3.4 Physical dimensions of LNT catalyst sample

cell density of 46.50 cells/cm^2 (300 cells/in^2), is placed in the downstream section of the quartz tube which has an inside diameter of 2.2 cm and an outside diameter of 2.54 cm. The inlet side of the quart tube is filled with 5mm Pyrex beads in order to increase heating surface area for the incoming gases through the reactor as well as to promote mixing of the gases. To eliminate gas bypass around its edges, the catalyst sample is wrapped in FiberFLEX^{TM} glass wool and inserted in the quartz tube. Two type K thermocouples with a diameter of 0.16 cm are used to measure the inlet and the outlet gas temperatures, whereas a third thermocouple of smaller diameter of 0.08 cm is used to measure the temperature at the middle of the catalyst. Shown in Figure 3.3 are two thermocouples placed approximately 5.0 mm from the catalyst entrance and exit. For isothermal operation the LNT reactor is placed inside a Lindberg MiniMite tube furnace, Model TF55035A-1 with a maximum operating temperature of 1100^{o}C. To prevent water vapor condensation in the line prior to the Horiba analyzer bench, the tubing from exit is heated with Omegalux heating tape.

3.2.2 Reactor End Fittings

The present fittings, shown in Figure 3.5, were the modification of the original fittings which experienced serious exhaust mixture leakage at both ends of the quartz tube reactor. The original design of the end fittings was similar to the present set-up, in which Viton O-rings were used to seal the reactor instead of the graphite ferrules. Consequently, the O-rings would degrade and fail over time at high operation temperatures. This failure would cause leaks at the reactor end fittings resulting in errors in the emission data. This component failure was resolved by redesigning the reactor end

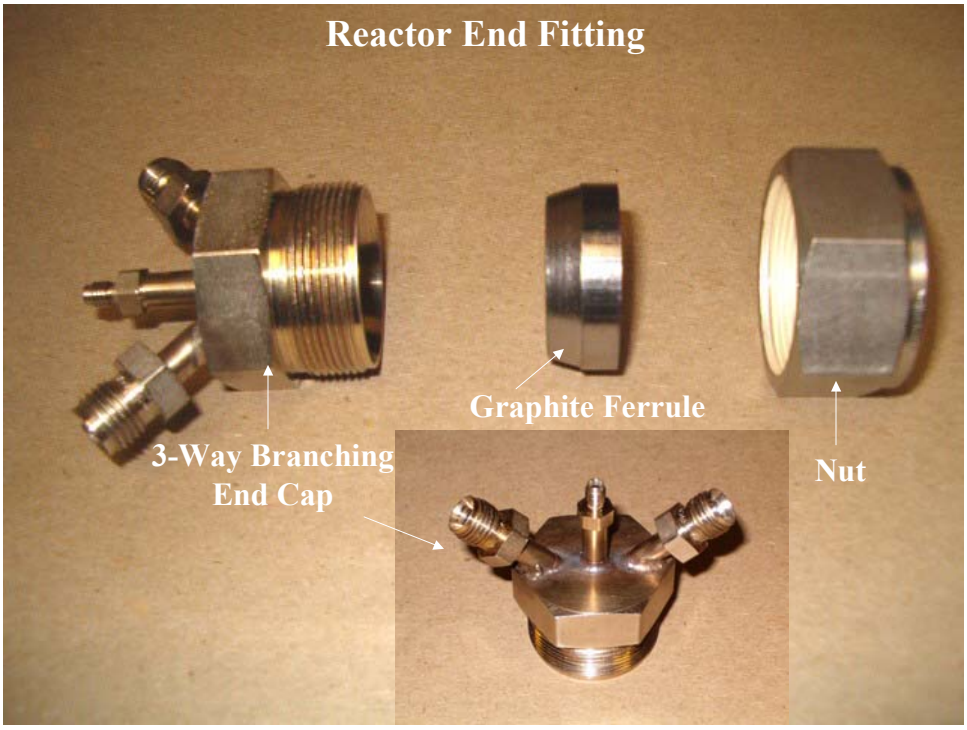

Figure 3.5 Reactor end fittings

fittings. While the basic design is very similar, by using graphite ferrules to seal the reactor allows the LNT system to operate at high temperatures without leakage. Also, by carefully removing the end fittings, the damage of the graphite ferrules can be prevented, and thus they can be reused.

3.2.3 Direct Fuel Injection System

Direct Fuel Injection (DFI) system is added to the LNT system in order to compare two different methods of LNT regeneration. In DFI the LNT is generated by injecting either H_2 or CO directly to the simulated exhaust gases, which is in contrast with LNT regeneration with cycling lean and rich conditions in the main stream. As shown in Figure 3.6, the DFI system has four major components: a pressure regulator

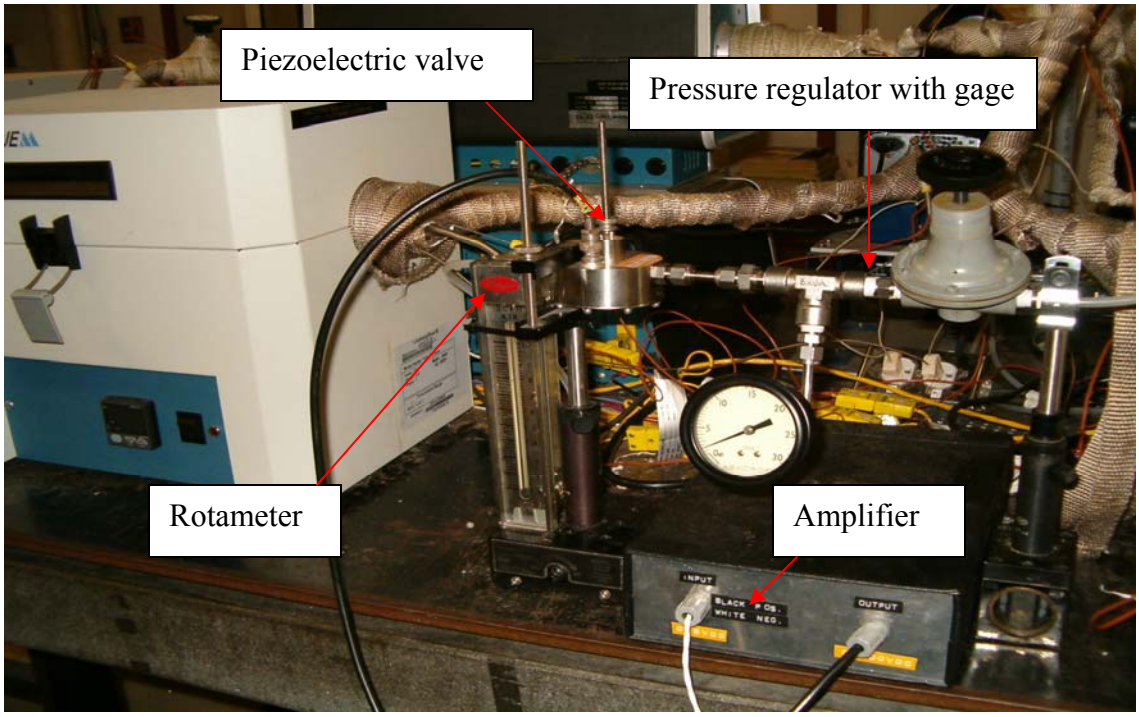

Figure 3.6 Components of direct fuel injection system

with pressure gage, a piezoelectric valve, an amplifier, and a rotameter. The fuel delivery pressure is precisely regulated since the flow rate of fuel through the piezoelectric valve is strongly dependent on the pressure. A small change in fuel delivery pressure can induce a large change in the amount of fuel injected. The amplifier is used to step up the voltage of the output signal from LabVIEW program from 0 to 5V to 0 to 100V for controlling the piezoelectric valve. The Maxtek MV-112 piezoelectric valve with a response time of 2 ms is the main component of the DFI system; it regulates the precise amount of fuel to be injected into the LNT reactor. Flow range of the valve is 0 to 0.5 L/min (LPM) at standard pressure, but it can be increased by operating at higher pressures (max 4.46 bar or 64.7 psia). A Dwyer rotameter with a range between 0 and

4.717 LPM is used to measure the fuel flow rate from the piezoelectric valve in the DFI system.

3.3 Components of Bench Flow Reactor

3.3.1 Instrument Panel

The instrument panel, shown in Figure 3.7, houses four major components of the Bench Flow Reactor System: mass flow controllers, temperature and pressure displays, heating tape controllers and data acquisition system. Mass flow controllers (MFCs) are used to regulate precisely the mass flow rate of the simulated exhaust gas mixture through the LNT catalyst reactor. The data acquisition system (DAS) interfaces output signals from the analyzers with LabVIEW for easy data storage. The instrument panel houses a number of temperature and pressure displays, showing the temperatures and pressure at specific locations in the BFR system. Two heating tape controllers mounted on the cabinet are used to maintain constant wall temperature of the stainless steel tubing between the cabinet and the inlet of the LNT reactor.

3.3.1.1 Mass Flow Controllers

The Mass Flow Controllers (MFCs) are used to regulate the mass flow rate of all the components of the simulated exhaust gases through the bench flow reactor. As shown in Figure 3.8, a MFC is used for each of the gas species used such as CO, CO_2, NO_x, H_2, Air, and N_2. MFCs require a 24 VDC power supply and are controlled by LabVIEW. Since the MFCs are linear within the intended flow range, by varying the command signals between 0 and 5 V the flow of all constituents of the simulated exhaust

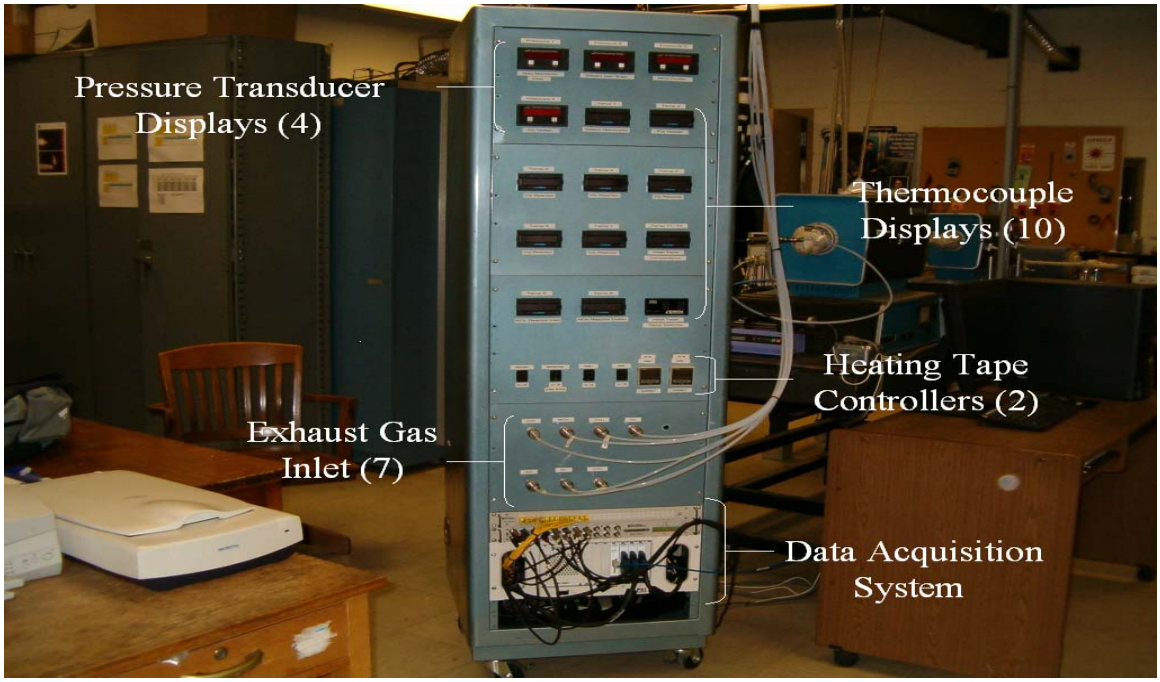

Figure 3.7 Photograph of front panel of instrumentation cabinet

Figure 3.8 Wiring of displays and mass flow controllers inside the cabinet (back view)

gases can be adjusted to any desired flow rate. Since the manufacturer used N_2 to calibrate the MFCs, a correction factor, called the K-factor, is employed when other gaseous species are being used. The operational ranges and the K factor of mass flow controllers are listed in Table 3.1.

3.3.1.2 Pressure and Temperature Displays

The BFR system includes three Cole Parmer pressure transducers, Model 68072 – 06, and five Omega type-K thermocouples of 0.16 cm in diameter. The outputs of the pressure transducers and the thermocouples are connected to three Cole Parmer, Model 94785 – 00 pressure displays and five Omega, Model DP 18-KC1 temperature displays, respectively. All the displays are housed in the instrumentation cabinet. The temperatures of the heating tapes are displayed by an Omega, Model MDP – 18 single temperature scanner. The analog output from the pressure transducer is 4 to 20mA which corresponds to a pressure range of 0 to 4.46 bar (64.7 psia). The temperature displays have a range of 0 – 1250^{o}C. The three pressure transducers are positioned at the inlet and outlet of the LNT reactor, and the inlet of the steam generator. Two thermocouples are located at the outlet of the steam generator, steam generator bypass. The remaining three thermocouples are located at the inlet, middle and exit of the LNT catalyst.

3.3.1.3 Heating Tape Controllers

There are two heating tape controllers (Model – XT16) mounted on the front side of the cabinet. They are used to control two Omega heavily insulated Samox heating tapes with a maximum operating temperature of 760^{o}C; one is used to heat up the LNT

Table 3.1 Operational ranges and K factors of mass flow controllers

Main Flow	Volumetric Flow Rate (LPM)	K Factor	Manufacturer
N_2	0 – 10	1.000	Omega
CO_2	0 – 10	0.737	Omega
NO_x	0 – 5	0.976	Omega
Lean Flow			
Air	0 – 20	1.006	Omega
Rich Flow			
CO	0 – 20	1.000	Tylan
H_2	0 – 5	1.010	Omega
N_2	0 – 5	1.000	Omega
O_2	0 – 2	0.992	Tylan

furnace inlet manifold and the other to maintain the steam generator bypass at high temperature.

3.3.1.4 Manually-Operated Switches

Three manual switches mounted on the front of the cabinet are used to control:

- Analyzer bypass
- Heating tape between steam generator and three-way branching valves
- Heating tape between three-way branching valves and LNT inlet manifold

3.3.2 Peristaltic Pump

To properly simulate an actual engine exhaust mixture, it is necessary to introduce water vapor into the feed stream. A Harvard syringe pump was initially utilized for water injection into the steam generator. Due to the relatively small volume of the syringe

pump, it was impractical to use the device for experimental runs with longer durations, i.e., 4 hours or more. Consequently, a Masterflex^{TM} peristaltic pump, shown in Figure 3.9, is used to replace the syringe pump. The peristaltic pump with water flow rate varied between 0.1 and 580 mL/min, allows for continuous water injection due to the pump's inlet being placed into a refillable large water reservoir.

3.3.3 Steam Generator

A photograph of the steam generator is shown in Figure 3.10. The steam generator is used to generate water vapor for the simulated exhaust gases. It is constructed from stainless steel tubing of 51mm in outside diameter and a wall thickness of 3.2mm. Both the inlet and outlet flanges of the steam generator are sealed with copper gaskets (44.5mm ID and 9.5mm OD). The flanges are tightened using a torque wrench to ensure no leakage from the steam generator. To prevent liquid water from accumulating a strip of FiberFLEX^{TM} is placed horizontally inside the steam generator. Depending on the gas hourly space velocity (GHSV) the peristaltic pump continuously injects a predetermined amount of water into the stainless steel steam generator maintained at 200^{o}C. The generated water vapor is then swept out by a flow of carrier gases consisting of N_2 and CO_2.

3.3.4 Reactor Branching Valves

The BFR consists of three reactors: the LNT reactor, the LNT thermal aging reactor, and the Reverse Flow Oxidation Catalyst Reactor (RFOCR). All reactors share

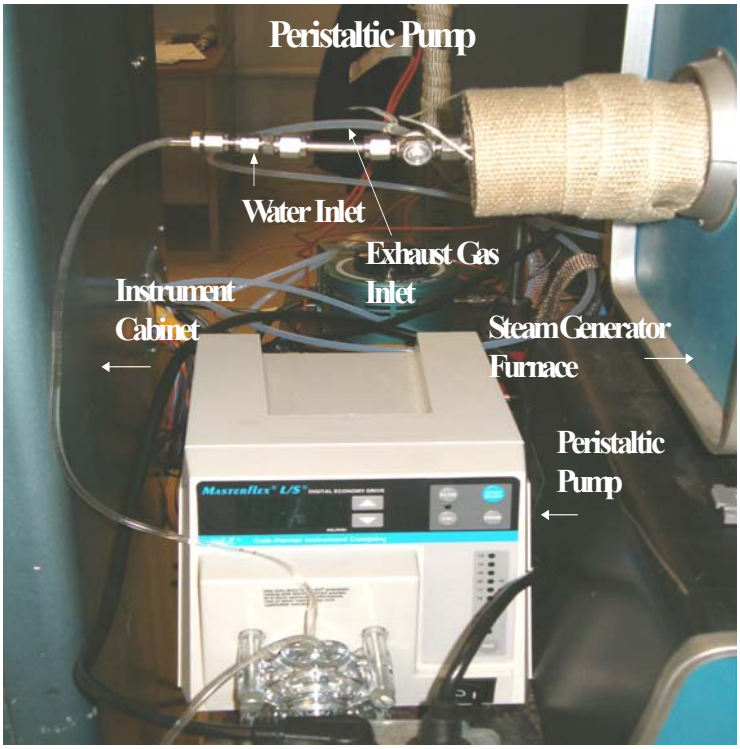

Figure 3.9 Photograph of peristaltic pump

Figure 3.10 Photograph of steam generator

the same components such as the instrument cabinet, the peristaltic pump, and the steam generator, which are located in upstream of the reactor branching valves, as shown in Figure 3.11. Since each reactor must be run independently, a valve system is used to direct the gas flow only to the reactor that is being in operation. Due to the high operating temperatures (140 − 350^{o}C) of the simulated exhaust gases in upstream of the three reactors, three Swagelok high-temperature bellow valves (SS-4BW) with a maximum operational temperature of 450^{o}C are employed for branching the flow.

3.3.5 Pressure Transducers

Three pressure transducers are positioned in the BFR system to ensure there is no pressure loss or high backpressure in the system. Cole Parmer pressure transducers are used in the BFR system, and these are mounted at the steam generator bypass line and downstream of the LNT reactor. The purpose of positioning a pressure transducer between the inlet of the steam generator bypass line and the outlet of the LNT reactor is twofold: to ensure that there is no pressure drop due to leakage of exhaust gases, and to monitor pressure buildup during the exothermic regeneration of the LNT.

3.4 Horiba Analyzer Bench

The exhaust gases flow into the Horiba analyzer bench are pressurized to 1.06 bar (15.4 psia) by the sample pump since the Horiba and California NO_x analyzers require a minimum operating pressure of exhaust gases. The pressure of exhaust gases inside the Horiba bench can be controlled by the manifold pressure knobs located on the front of the analyzer bench. A water condenser in the cabinet, as shown in Figure 3.11, is used to

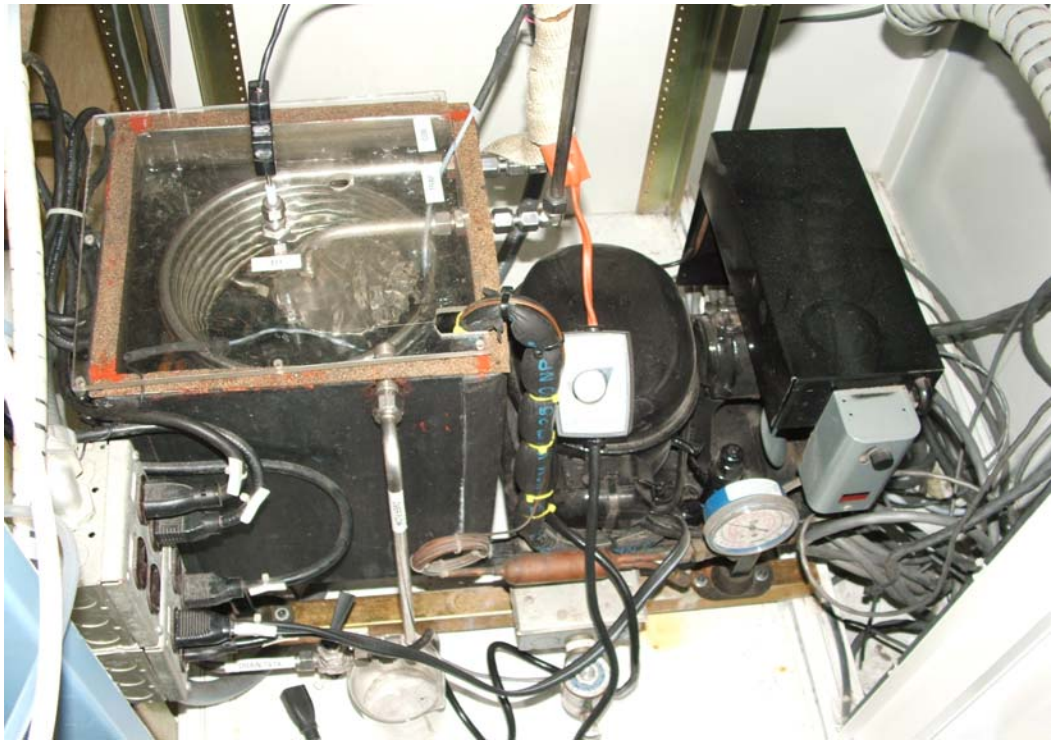

Figure 3.11 Water condenser inside of the Horiba analyzer bench

remove the water vapor from the simulated exhaust gases since all gas analyses are carried out on a dry gas basis.

3.5 Emission Analyzers

Exhaust emission conversion efficiency is of primary concern for the BFR system, namely methane (CH_4) and nitric oxides (NO_x) conversion. This is accomplished via the Horiba analyzer bench, shown in Figure 3.12, which consists of four analyzers: CO(Low)/CO_2 and CO (High) (AIA-220), Hydrocarbon (FIA-210), and NO_x (CLA-220). Calibration and spanning procedures for each analyzer are strictly followed per protocol of Horiba Instruments. Prior to each experimental run of the BFR, each analyzer is

Figure 3.12 Front panel of Horiba exhaust gas analyzers

spanned for accuracy. Both the span gas and the inert gas (N_2) are introduced through the gas divider and to the analyzers at various percentages of the span gas concentration. Full calibration of the analyzers is performed monthly, as per Horiba instructions.

3.5.1 Horiba NO_x Analyzer

The Horiba CLA-220 analyzer uses chemiluminescence to measure the concentration of nitrogen oxides (NO or NO_x). The chemiluminescent emission is based upon the reaction between ozone and nitric oxide, yielding electronically excited NO_2 and O_2. The transition from the electronically excited state of NO_2 to the normal state produces light, which has the intensity proportional to the mass flow rate of NO_2 into the reaction chamber.

3.5.2 California Analytical Instrument NO_x Analyzer

The California Analytical Instrument 400HCLD NO_x analyzer is used to measure the NO concentration from the simulated exhaust gases using the chemiluminescent method. A built-in internal pump and heated sample line are installed in 400HCLD so that the analyzer can be operated without the sample pump and water condenser such as those required by Horiba analyzers.

3.5.3 Horiba CO Analyzer

A non-dispersive infrared absorptiometry method is employed by two Horiba CO analyzers (AIA-220) to measure both high range CO (0 to 50,000 ppm) and the low range CO (0 to 500 ppm) concentrations simultaneously.

3.5.4. Horiba CO_2 Analyzer

Horiba CO_2 analyzer (AIA-220) employs non-dispersive infrared absorptiometry, to detect CO_2 concentration from the simulated exhaust gases.

3.6 Data Acquisition System

The purpose of data acquisition system (DAS) is to provide the integrated interface between LabVIEW and the components of the BFR system in order to monitor and store the experimental data. With the aid of LabVIEW software, the DAS allows the control of the flow rates of all constituent of the exhaust gases via the MFCs, and to save data obtained from temperature, pressure transducer, and analyzers in real time. The DAS consists of a Dell personal computer, National Instruments LabVIEW 6.1 software, and

data acquisition boards. LabVIEW software provides a user friendly feed-back and control loop for the components of the BFR and facilitates the user to operate the BFR system and collect data simultaneously. Data acquisition boards mounted in the PC are a link between LabVIEW and the BFR system. A photograph of the hardware components of the data acquisition board is shown in Figure 3.13.

3.6.1 Computer

Dell PWS 350 personal computer with 2.8GHz Intel Pentium 4 processor is chosen to house both LabVIEW software and data acquisition boards.

3.6.2 LabVIEW 6.1

LabVIEW allows the user to modify and operate the input data; the flow rate of MFCs, time duration of opening solenoid valves to regulate lean and rich condition, and time duration of DFI. At the same time, all temperature, pressure, concentration profiles are stored in LabVIEW database, which can be converted to an Excel file format for the further data analysis.

3.6.3 Data Acquisition Boards

Data acquisition boards are used to convert analog signals from thermocouples, pressure transducers, and analyzers, to digital signals in order to save the data in LabVIEW. The boards also convert the output digital signals from LabVIEW to analog signals for operating the MFCs, solenoid valves, and DFI. The boards house hardware components consisting of the following: a shielded rack mounted BNC adapter chassis

Figure 3.13 Data acquisition system – interface boards

(BNC-2090), PXI-1002, a shielded rack mounted terminal block (TC-2095), and a 4-slot chassis (NI SCXI-1000).

3.7 Experimental Procedure

3.7.1 Startup Procedure

Every experiment begins with the safety checkup of the exhaust fan and CO detector in the laboratory. After the initial checkup, the power switches of the BFR cabinet, desk top computer installed with LabVIEW, gas analyzers, water condenser in the Horiba analyzer bench, and exhaust fan of the Horiba analyzer bench are turned on. Oxygen at pressures of 1.91 bar (27.7 psia) and 2.94 bar (42.7 psia) is then introduced to Horiba and California Analytical Instrument NO_x analyzers, respectively; oxygen is used to generate ozone for NO_x detection. Approximately, one hour of warm-up time is required for the analyzers and the water condenser to be fully operational. Once all the instruments are warmed up, appropriate gas cylinders are opened and regulated to a

supply pressure of 2.74 bar (39.7 psia), and the reactor branching valves are used to divert the gas flow to the LNT reactor. The gas outlet of the LNT reactor is then connected to the inlet of the Horiba analyzer bench, and the sampling pump is turned on.

Prior to the experiment, the LNT reactor and the gas analyzers are purged with a flow of N_2 for at least one hour. During the purge, the heat tapes and the LNT furnace are turned on in order for the LNT reactor to reach steady state operating temperature. The purpose of the N_2 flow is two-fold: to preheat the LNT reactor to the desired operating temperature; and to stabilize the analyzers before the actual run. The gas flow from the LNT reactor exit is directed to the gas analyzers by selecting the appropriate analyzer matrix switches, located on the front panel of the Horiba analyzer bench. It is imperative not to have a large pressure or vacuum across the LNT reactor since a low or high pressure can cause damage to the quartz tube of the LNT reactor. For the present setup an optimum operating pressure of 1.08 bar (15.7 psia) is required, and by adjusting the pressure of the sampling pump inside the analyzer bench the desired pressure can be achieved.

3.7.2 Composition of Simulated Exhausted Gases

Table 3.2 lists the composition of the lean and rich phases used in the present investigation. Both the lean and rich phases are used for the absorption isotherm experiments, however only the lean phase is used in the desorption isotherm experiments in which the mechanism of NO_x desorption process is investigated following the shutting off of NO and O_2. Two different regeneration experiments − lean and rich cycling, and direct fuel injection − are performed by varying the concentration of two reductants, H_2

Table 3.2. Gas composition of rich and lean phases

Gas	Fuel Lean	Fuel Rich
NO, ppm	500	500
CO_2, %	5	5
CO, ppm	0	40,000
H_2, ppm	0	13,333
O_2, %	10	0
H_2O, %	10	10

and CO in the rich phase. In contrast to lean and rich cycling, the regeneration experiment by DFI is accomplished by injecting either H_2 or CO into the fuel-lean exhaust gases.

3.7.3 Absorption and Desorption Isotherm Experiments

The purpose of the NO_x absorption isotherm experiments is to characterize the NO_x storage capacity and breakthrough time as a function of temperature and gas hourly space velocity (GHSV) from which the optimum operating conditions of the LNT catalyst can be determined. The absorption isotherm experiments are carried out at temperatures of 250, 300, 350, 400, and 500^oC, and GHSVs of 25,000, 50,000, and 75,000 hr^1. At each GHSV, a new LNT catalyst sample is used to minimize the effect of aging on the catalyst performance. Once the optimum operating temperature of the LNT catalyst is obtained, two different regeneration experiments are performed at this temperature. The purpose of the NO_x desorption isotherm experiment is to investigate the NO_x desorption process from the LNT catalyst without reductants. The NO_x desorption

occurs by shutting off the flow of NO_x and O_2, once the LNT catalyst is fully saturated. From results of two experiments performed at 350 and 500^oC, the temperature dependency of the NO_x desorption process at a gas hourly space velocity of 25,000 hr^{-1} is investigated. In addition the NO_x desorption process is further investigate by characterizing the ratio of NO and NO_2 as a function of temperature at a GHSV of 75,000 hr^{-1}.

3.7.4 Regeneration Experiments

3.7.4.1 Regeneration by Cycling Lean and Rich in Main Stream

The purpose of the LNT regeneration by cycling between fuel lean and rich conditions is to determine the optimum duration of the rich and lean pulses and the optimum concentration of reductants that would produce the highest NO_x conversion efficiency at the optimum operating temperature of the LNT. Since the fuel efficiency is of primary important the optimum rich pulse employed during the regeneration is the one that results in the highest NO_x conversion efficiency in the shortest duration. Regeneration experiments with lean/rich pulses are performed by varying the time duration of the lean and rich pulses at fixed amount reductants, 4% CO and 1.333% of H_2. The following durations of lean and rich pulses are used in the present investigation:

- 50s lean and 10s rich
- 50s lean and 5s rich
- 100s lean and 5s rich

The optimum time duration of the lean/rich pulses is defined as the one that results in at least 93% NOx conversion. Once the optimum time duration is determined, the regeneration experiments are performed at four different concentrations of the reductants.

- 4% of CO and 1.33% of H_2
- 2% of CO and 0.67% of H_2
- 4% of H_2
- 4% of CO

3.7.4.2 Regeneration by Direct Fuel Injection

Two separate DFI experiments are carried out: direct fuel injection in the absence and presence of O_2 in the simulated exhaust gases. These two types of experiments are used to simulate two different scenarios in which the rich excursions are generated in the operation of lean-burn engines. In the first scenario, the rich excursions are produced by running the engines under stoichiometric or rich conditions for a very short period. In the second scenario the rich excursions are generated by injecting the reductants directly into the lean exhaust gases.

To duplicate the first scenario, at the beginning of the rich phase, the flow of O_2 in the simulated exhaust gases is shut off and the reductant, either H_2 or CO, is directly injected by DFI system into the gas stream. In the second scenario, the rich excursions are generated by injecting the reductant directly into the lean exhaust gas stream. Both

experiments are performed at the predetermined optimum operating temperature of the LNT and a space velocity of 50,000 hr^{-1}.

The second objective is to compare the performance of DFI in the absence of O_2 with lean/rich cycling method. The NO_x conversions obtained from DFI with optimum concentration of the reductant in the presence and absence of O_2 are then compared with those found with LNT regeneration using lean/rich cycling. All DFI experiments are performed at the same GHSV and rich duration used in the LNT regeneration experiment by using lean/rich modulation.

- 2% of CO ~ 4% of CO with O_2 in an increment of 1%
- 2% of CO ~ 4% of CO without O_2 in an increment of 1%
- 2% of H_2 ~ 4% of H_2 with O_2 in an increment of 1%
- 2% of H_2 ~ 4% of H_2 without O_2 in an increment of 1%

Chapter 4

RESULTS AND DISCUSSIONS

The results obtained from NO_x isothermal absorption experiments are presented in this chapter in which the effect of temperature and gas hourly space velocity (GHSV) on the performance of EmeraChem LNT catalysts is investigated. Section 4.1 encompasses the results obtained from the absorption isotherms such as NO_x storage capacity, breakthrough time and ratio of NO_2 to NO as a function of temperature and gas hourly space velocity, while section 4.2 discusses the mechanisms of NO_x desorption from the surface of LNTs as related to the stability of nitrate compounds.

4.1 Absorption and Desorption Experiments

4.1.1 Absorption Isotherm

A series of isothermal absorption experiment are carried out at different temperatures and gas hourly space velocities (GHSV) in order to investigate the effect of temperature and GHSV on the NO_x trapping capacity of EmeraChem LNT catalysts. From the isothermal absorption experiments the optimum operating temperature of the EmeraChem LNT catalysts can be determined. Consequently, experiments are conducted at three different gas hourly space-velocities of 25,000, 50,000, and 75,000 hr^{-1} and five different temperatures of 250, 300, 350, 400 and 500^oC. All experiments are performed at a concentration of 500ppm NO with the composition of lean and rich excursions shown

in Table 4.1. The rich excursion is used only to restore the original trapping capacity of the LNT at the end of the isothermal absorption experiments.

A typical absorption isotherm at 350°C and a GHSV of 25,000 hr^{-1} is shown in Figure 4.1, in which the outlet concentration of NO_x is plotted versus time. For discussion purposes this concentration profile can be conveniently divided into three separate stages. The first stage, which lasts approximately 7 minutes for this particular experiment, no NO_x is observed at the exit of the LNT catalyst, which indicates that the inlet NO_x has been completely trapped on the surface of the LNT. This is one of the primary attractions of the LNT technology for NO_x emission control applications in lean-burn engines. At the end of the first stage breakthrough or NO_x slip begins, and in the second stage rapid uptake of NO_x occurs. In the absorption isotherm experiment illustrated by Figure 4.1, this second stage lasts approximately from 5 to 47 minutes. As the NO_x storage sites are gradually filled up, the rate of NO_x trapping decreases, which leads to a slower NO_x uptake in the third stage. This later stage can last for a period of time; for this particular experiment the duration of the third stage is approximately 110 minutes. At the end of the third stage, the LNT is regenerated by subjecting it to a rich excursion until the end of this experiment. The rich excursion with the composition given in Table 4.1, consisting of 1.33% H_2 and 4.0% of CO, induces NO_x release as indicated by a sharp NO_x spike in Figure 4.1, and subsequent reduction to N_2. As a result of the rich excursion the LNT has been restored to its original trapping capacity. Results obtained for other absorption isotherms at a GHSV of 25,000 hr^{-1} are shown in Figure 4.2. Absorption isotherms at GHSVs of 50,000 and 75,000 hr^{-1} are shown in Figures 4.3 and 4.4, respectively. As seen in these figures the absorption isotherms are qualitative similar at all GHSVs investigated

Table 4.1 Gas composition used in isothermal absorption

Gas	Fuel Lean	Fuel Rich
NO, ppm	500	500
CO_2 , %	5	5
CO, ppm	0	40,000
H_2, ppm	0	13,333
O_2, %	10	0
H_2O, %	10	10
Lambda	2.07	0.89

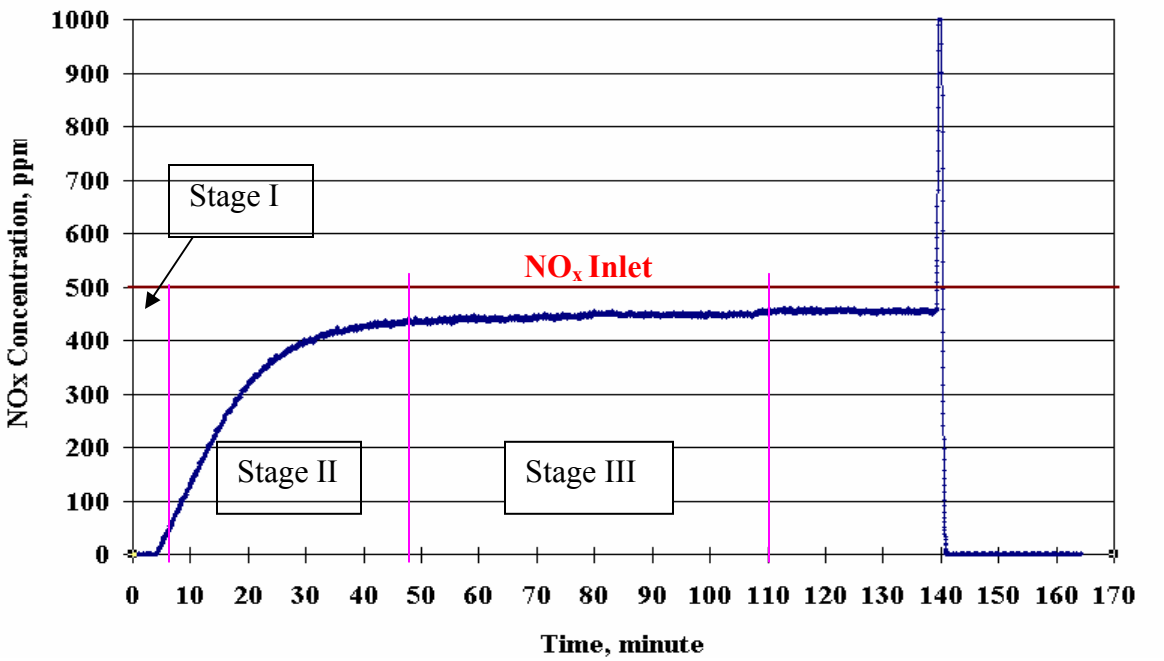

Figure 4.1 Outlet NO_x concentration versus time at a temperature of 350°C and a GHSV=25,000 hr^{-1} with 500ppm of inlet NO_x concentration

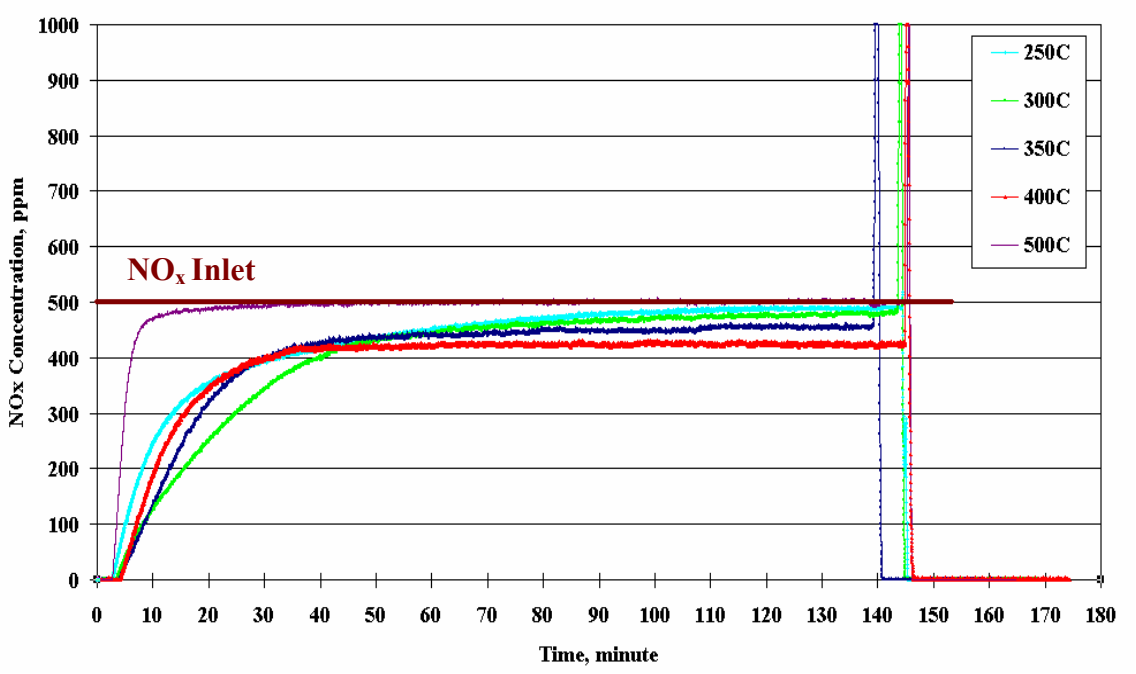

Figure 4.2 Effect of temperature on NO_x absorption isotherms with 500ppm of inlet NO_x concentration at GHSV=25,000 hr^{-1}

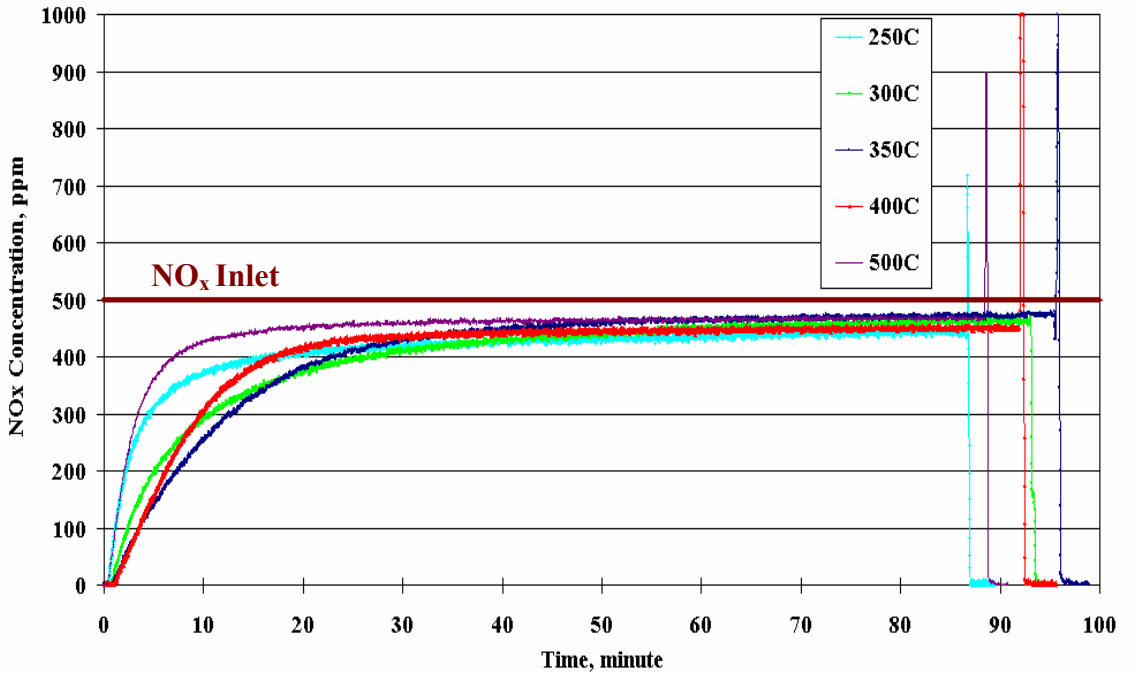

Figure 4.3 Effect of temperature on NO_x absorption isotherms with 500ppm of inlet NO_x concentration at GHSV=50,000 hr^{-1}

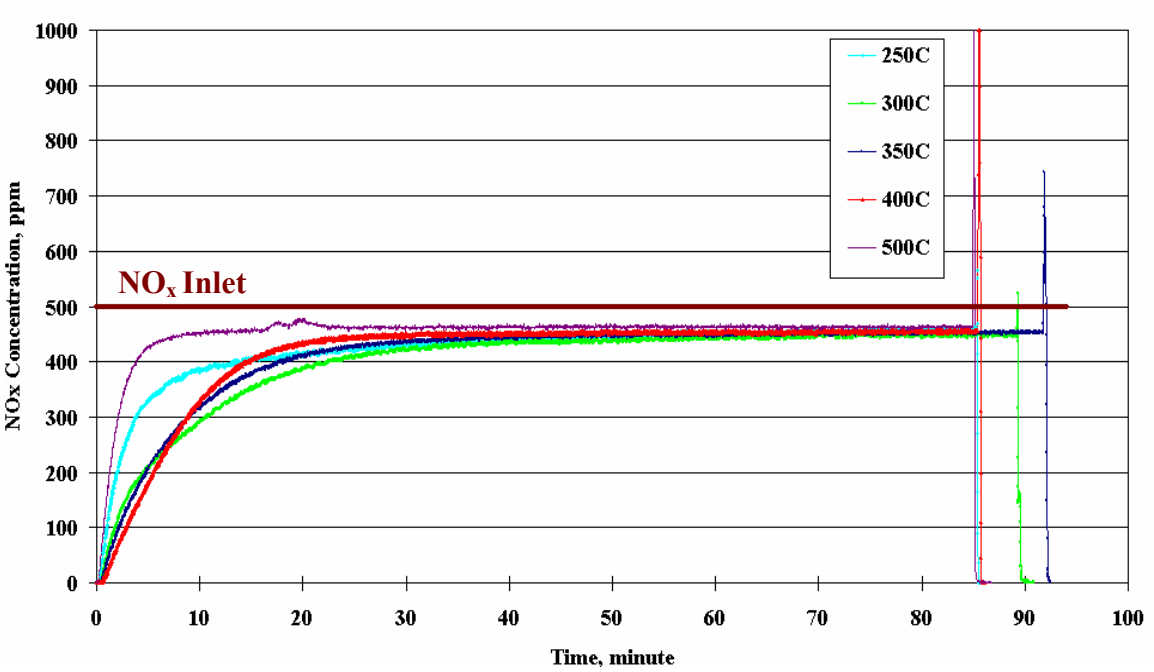

Figure 4.4 Effect of temperature on NO_x absorption isotherms with 500ppm of inlet NO_x concentration at GHSV=75,000 hr^{-1}

in the present study. In addition, at any given GHSV the breakthrough or NO_x slip and the time to reach saturation occur much earlier for the absorption isotherms at 250 and 500°C. The reasons for the discrepancies between isotherms at 250 and 500°C and at other temperatures will be given in detail in section 4.1.3. Typical temperature and NO_x concentration histories during the regeneration phase of an absorption isotherm experiment performed at 400℃ and a GHSV of 25,000 hr^{-1} are shown in Figure 4.5. The fuel rich excursion consisting of 1.33% of H_2 and 4% of CO is used to reduce NO_x to N_2. Since the reduction reactions are highly exothermic, the maximum temperature always occurs inside the LNT during the regeneration phase as can be seen in Figure 4.5. In this particular isothermal absorption experiment an increase of 130°C in catalyst temperature is observed. No significant temperature change is seen for the gas phase at the inlet,

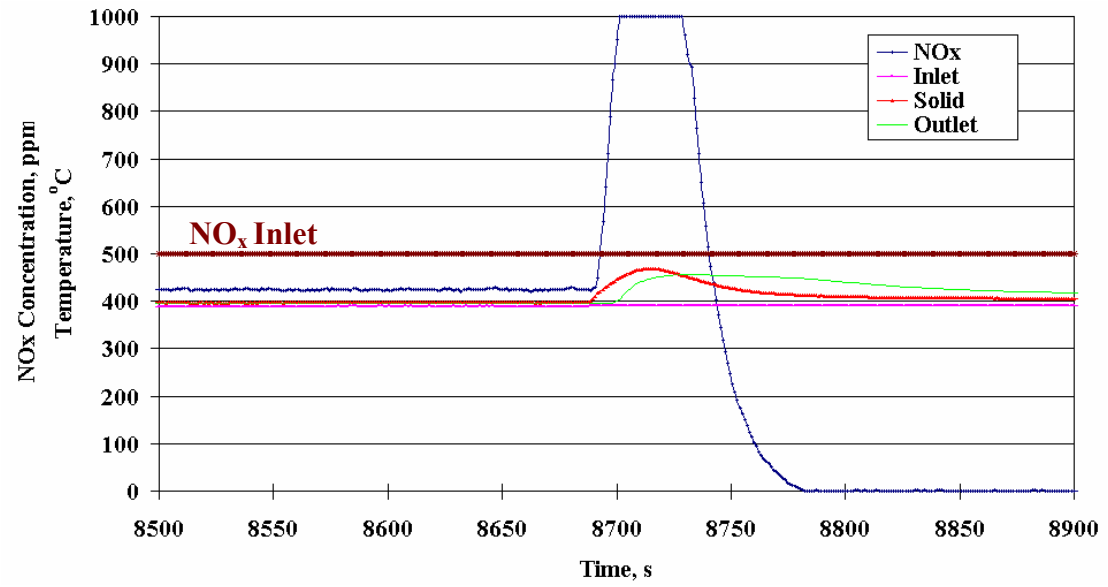

Figure 4.5 Temperature and outlet NO_x concentration histories during regeneration phase of absorption isotherm performed at 400°C and GHSV of 25,000 hr^{-1}

which indicates that gas-phase reactions are insignificant. On the other hand due to the heat transfer from the catalyst, the exit temperature of the gas phase has increased approximately 100°C. The increase in the exit temperature of the gas phase always lags behind the increase in catalyst temperature. Since the NO_x analyzer is set in the range of 0 to 1000ppm, any NO_x excursion above 1000ppm is recorded as a straight line. As can also be seen in Figure 4.5 the rich excursion has successfully recovered all of the original NO_x trapping capacity of the LNT.

4.1.1.1 NO_x Storage Capacity of LNT

From the isothermal absorption experiments the NO_x storage capacity as a function of temperature is obtained. The area enclosed by the inlet and the outlet NO_x concentration profiles is proportional to the amount of NO_x absorbed by the catalyst

during the fuel-lean condition, as shown in Figure 4.6. The area under the outlet NO_x concentration profile is numerically integrated using Matlab, and from which the amount of NO_x absorbed during the fuel-lean condition is estimated by the following equation.

Amount of NO_x Stored in ppm.s

= Amount of NO_x Introduced – Amount of NO_x Released

The volumetric flow rate is used to convert the total amount of NO_x stored in ppm·s to liter. By using the ideal gas equation of state the amount of NO_x stored can then be expressed in term of gmol. The NO_x storage capacity per unit mass of the catalyst is obtained by dividing the stored NO_x in gmol by the weight of the LNT catalyst in g. The effect of temperature and GHSV on the NO_x storage capacity of EmeraChem LNTs is shown in Figure 4.7 and Table 4.2 to 4.4. As seen in the figure at a given GHSV the NO_x storage capacity exhibits a volcano-type dependence on the temperature, with a maximum in storage capacity of 3.2×10^{-3} mol NO_x/g of catalyst occurring at 350°C. Since NO_2 is a precursor for the trapping process at alkaline-earth components, i.e., Ba, the lower NO_x storage capacity at temperature below 350°C is due to kinetic limitation on the oxidation of NO to NO_2. On the other hand the decrease in the NO_x storage capacity at temperatures above 350°C is due to equilibrium-limited. Consequently, the effect of kinetics at low temperatures and equilibrium at high temperatures give rise to the characteristic volcano- type dependence of the temperature of the LNT's storage capacity. As the GHSV increases the NO_x storage capacity of the LNT decreases. At a GHSV of 25,000 hr^{-1}, the maximum NO_x storage capacity at 350°C is 3.2×10^{-3}

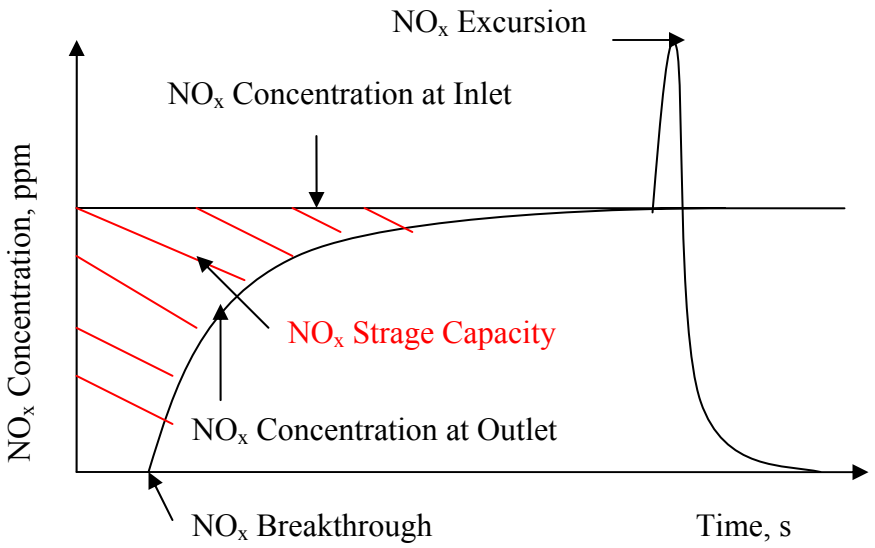

Figure 4.6 Shaded area represented the amount of NO_x stored at given temperature and gas hourly space velocity

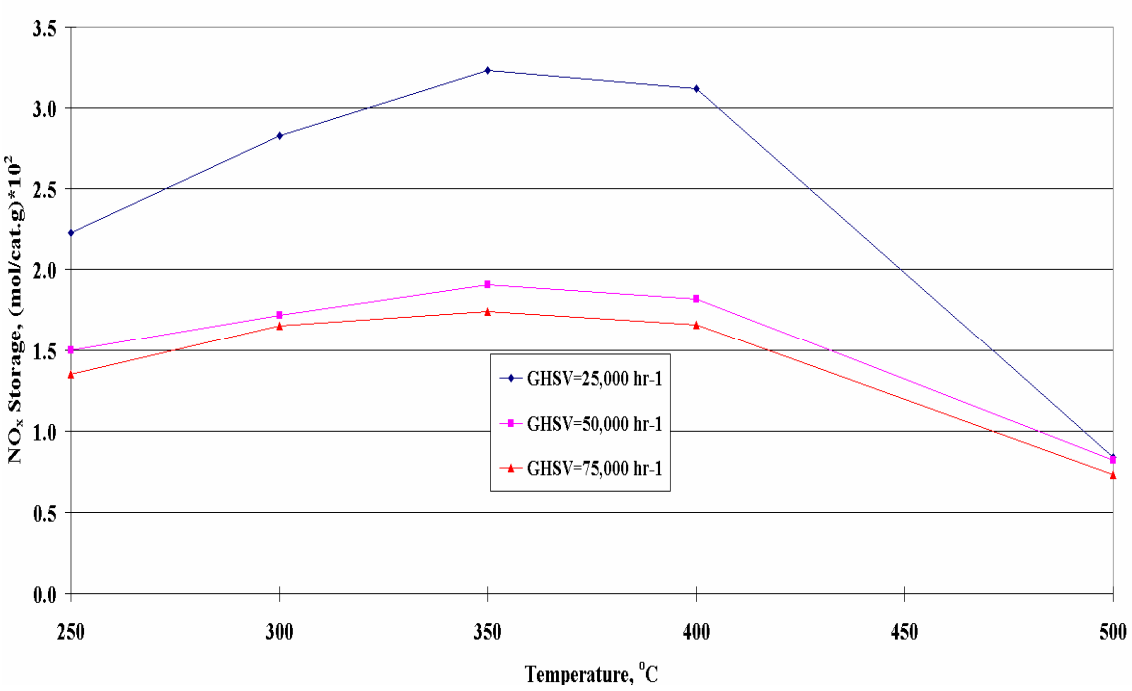

Figure 4.7 NO_x storage capacity as a function of temperature and GHSV

Table 4.2 Effect of temperature on NO_x storage capacities at 25,000 hr^{-1}

Temperature, ^oC	NO_x Storage, mol/g of Catalyst
250	0.0223
300	0.0283
350	0.0323
400	0.0312
500	0.0084

Table 4.3 Effect of temperature on NO_x storage capacities at 50,000 hr^{-1}

Temperature, ^oC	NO_x Storage, mol/g of Catalyst
250	0.0150
300	0.0172
350	0.0191
400	0.0182
500	0.0082

Table 4.4 Effect of temperature on NO_x storage capacities at 75,000 hr^{-1}

Temperature, ^oC	NO_x Storage, mol/g of Catalyst
250	0.0135
300	0.0165
350	0.0174
400	0.0166
500	0.0073

mol NO_x/g of catalyst, while at a GHSV of 75,000 hr^{-1} and at the same temperature, it is 1.75×10^{-3} mol NO_x/g of catalyst. As seen in Figure 4.7 the effects of kinetics and equilibrium on the NO_x storage capacity are preserved even at high GHSVs. The decrease in NO_x storage capacity with increasing GHSV is due to shorter resident time of NO_x in the simulated lean-burn exhaust gas stream. Based on the results of the present study the optimum operating temperature for the EmeraChem LNT is 350°C at all GHSVs investigated.

4.1.1.2 NO_x Breakthrough Time

In the present investigation breakthrough time is defined as the time at which the concentration of NO_x in the simulated exhaust gas starts to increase, i.e., the onset of NO_x slip as seen on Figure 4.8. The effect of temperature and GHSV on the breakthrough time is shown in Figure 4.9 and Table 4.5 to 4.7. Similar to the NO_x storage capacity the breakthrough time exhibits a similar volcano-type dependence on the temperature, and a maximum in breakthrough time occurs at a temperature of 400°C for all three different GHSVs investigated in the present study. However, the temperature at which the maximum breakthrough times occur is approximately 50°C higher than the temperature at which the maximum NO_x storage occurs. In order to confirm the repeatability of the data at a given temperature three different absorption isotherms experiments were carried out, with exception of the isotherm at 325°C, at a GHSV of 25,000 hr^{-1} from which the breakthrough times were obtained. As can be seen in Table 4.5, the difference in the breakthrough time is within the experimental error.

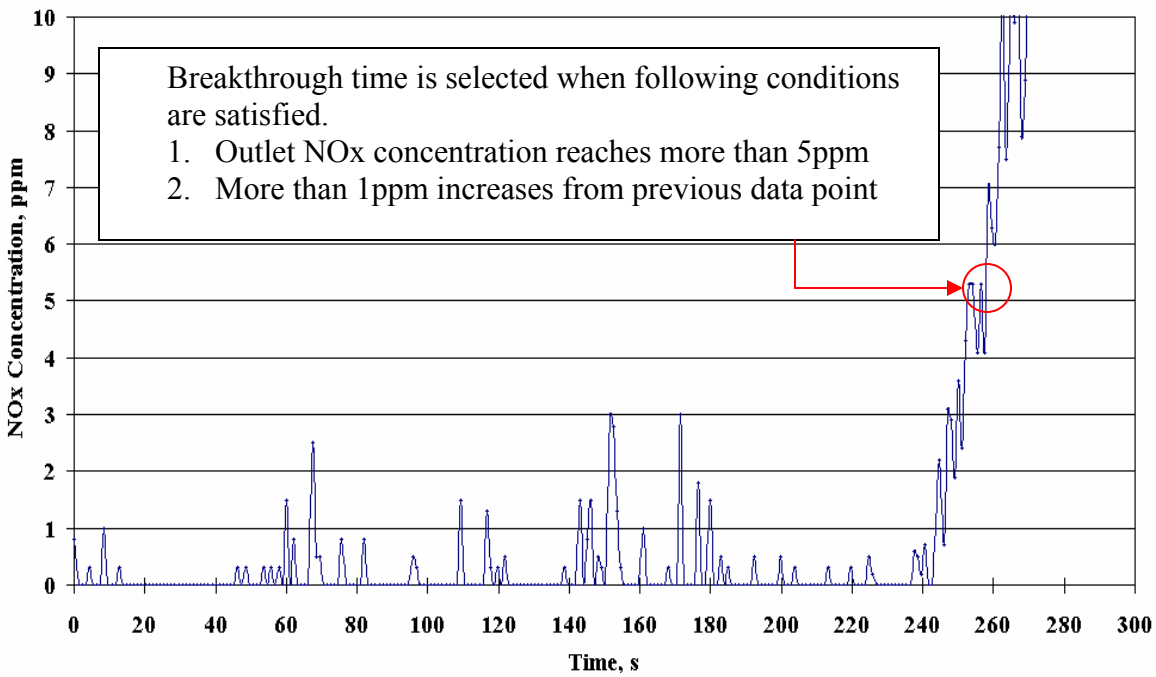

Figure 4.8 Breakthrough experiment performed at a temperature of 350°C and GHSV of 25,000 hr^{-1}

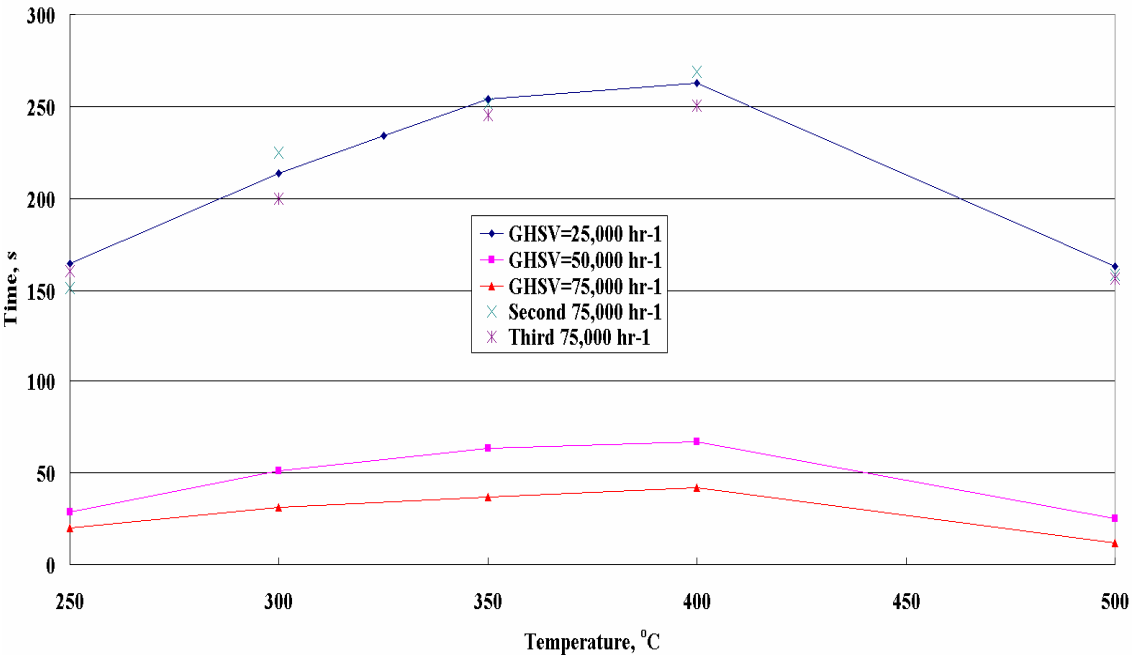

Figure 4.9 Effects of temperature and gas hourly space velocity on breakthrough time

Table 4.5 Effect of temperature on breakthrough at 25,000 hr^{-1}

Temperature, ^{o}C	Breakthrough, s
250	165, 151*, 161**
300	214, 225*, 200**
325	234
350	254, 252*, 246**
400	263, 269*, 250**
500	163, 159*, 157**

* Second measurement ** Third measurement

Table 4.6 Effect of temperature on breakthrough at 50,000 hr^{-1}

Temperature, ^{o}C	Breakthrough, s
250	28
300	51
350	63
400	67
500	25

Table 4.7 Effect of temperature on breakthrough at 75,000 hr^{-1}

Temperature, ^{o}C	Breakthrough, s
250	20
300	31
350	37
400	42
500	12

4.1.1.3 Ratio of NO_2 to NO

The most important role of precious metal during the storage process is to oxidize NO to NO_2, which in turn is stored in the storage compound in the form of nitrates. Consequently the NO_x storage capacity of LNT is strongly dependant on NO_2 conversion on Pt sites. The effect of temperature on the ratio of NO_2 to NO obtained from the isothermal absorption experiment performed at a GHSV of 75,000 hr^{-1} is shown in Figure 4.10. The curve exhibits a volcano-shape dependency on the temperature with a maximum NO_2/NO ratio occurring at 400^oC. Chemical equilibrium between NO and NO_2 shows that NO_2 is the dominant species below 220^oC, and the amount of NO_2 decreases with increasing temperature. The result suggests that below 400^oC NO oxidation is kinetically-limited, and equilibrium-limited at temperature above 400^oC.

4.1.2 Desorption Isotherm

There are two primary mechanisms of NO_x desorption from the LNT surface. The first mechanism is thermal in nature in which NO_x is desorbed due to the exothermic oxidation of the reductants by O_2, either in the gas stream or absorbed on the LNT surface. As the temperature of the catalyst increases, NO_x is released since the stability of nitrates decreases with an increase in temperature. In the second mechanism NO_x is desorbed in the absence of O_2 in the gas stream. Since the trapping of NO_x is driven by equilibrium, the stability of nitrites species is significantly reduced. Thus, the shutting of O_2 in the gas stream will provide a driving force for the decomposition of nitrate species with subsequent release of NO_x from the LNT surface. The second mechanism is predominant in the regeneration phase in which rich excursion is introduced, resulting in

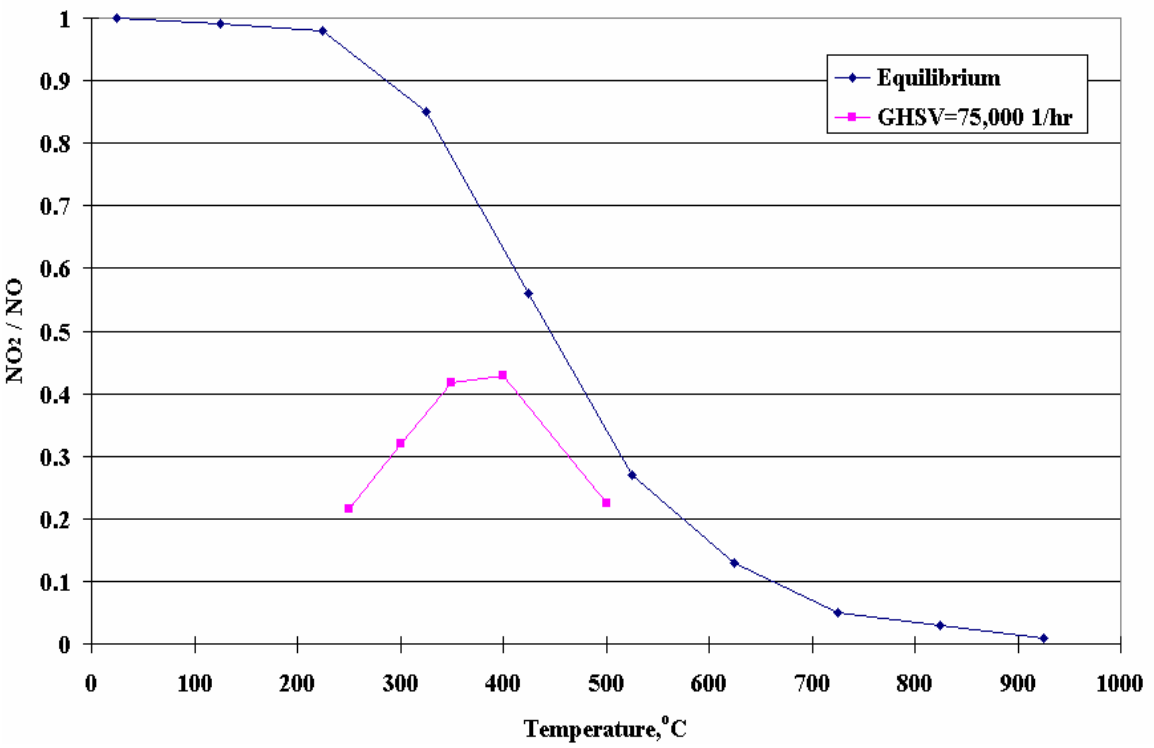

Figure 4.10 Ratio of outlet NO_2 to NO outlet concentration during absorption isotherm performed at a GHSV of 75,000 hr^{-1}. Also shown is the equilibrium ratio of NO_2 to NO

a net reducing environment. The NO_x desorption experiments were conducted at two different temperatures of 350 and 500°C and at a GHSV of 25,000 hr^{-1} in which the flow of O_2 and NO_x shut off at the end of the NO_x absorption period. The primary objective of the desorption experiment is to ascertain the thermal nature of the NO_x desorption mechanism. As shown in Figures 4.11 and 4.12, LNT catalysts in both experiments are fully saturated after 8000 s, and immediately after which the flows O_2 and NO_x are shut off around 9000 s. As can be seen in Figures 4.11 and 4.12, NO_x desorption is greater at 500°C than 350°C, and the result suggests that more NO_x is desorbed at higher temperature due to the higher decomposition rate of nitrite or nitrate compounds.

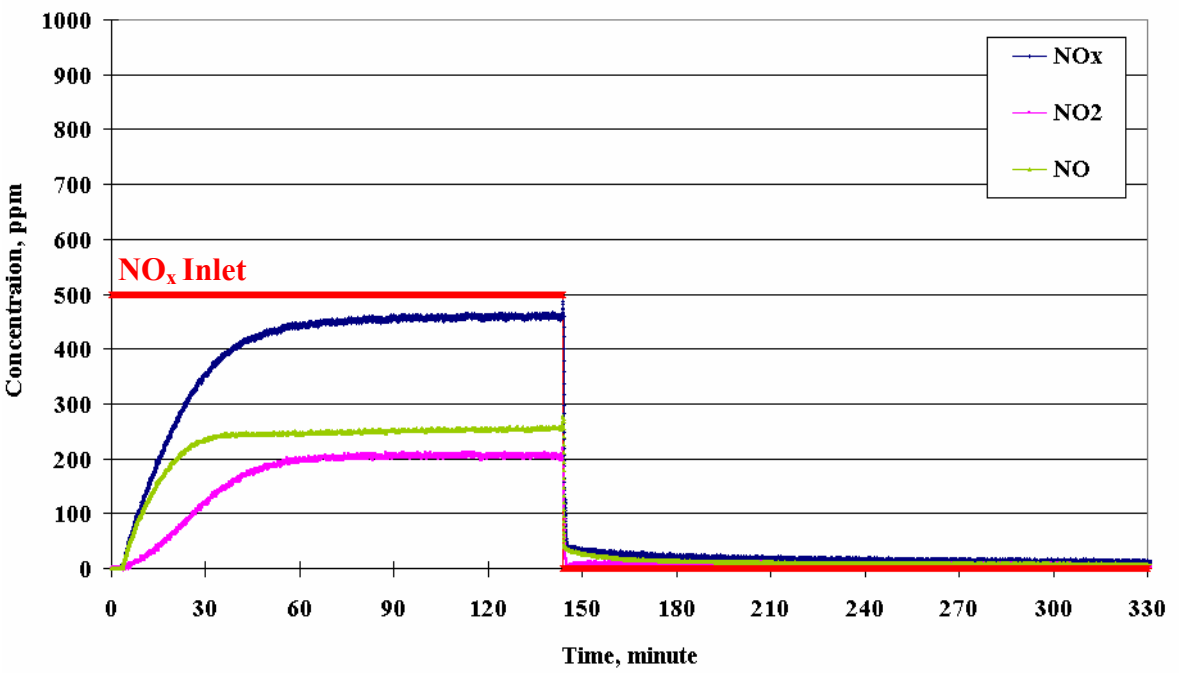

Figure 4.11 Desorption experiment performed at T = 350°C and GHSV = 25,000 hr^{-1}

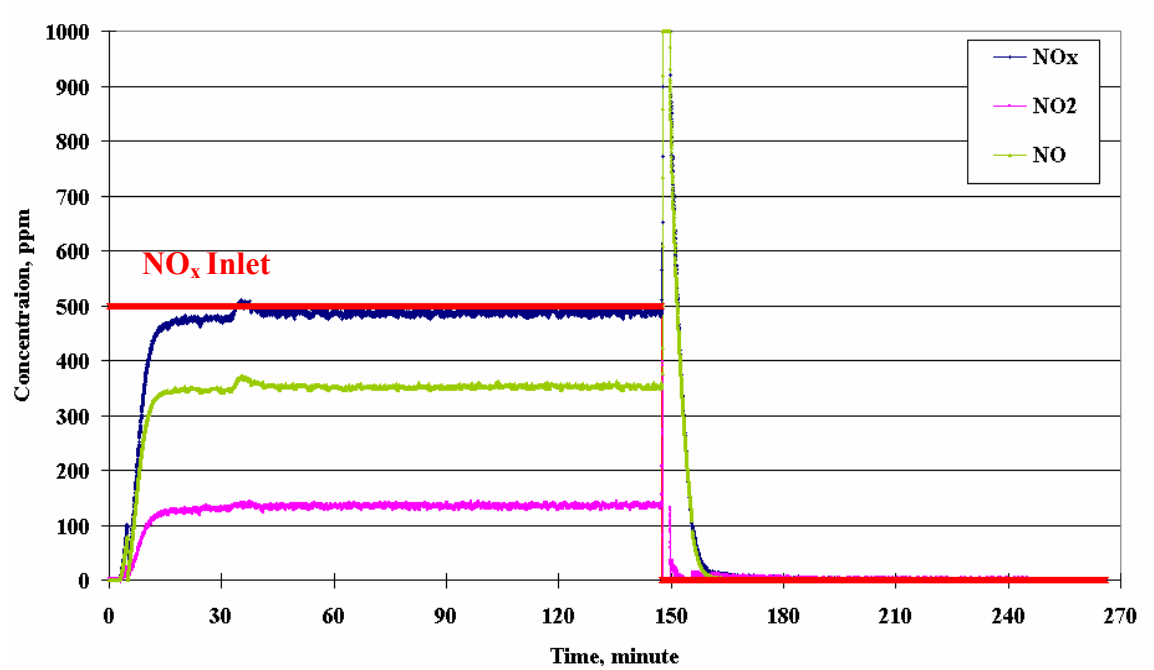

Figure 4.12 Desorption experiment performed at T = 500°C and GHSV = 25,000 hr^{-1}

4.2 LNT Regeneration

The objective of this section is to investigate the optimum combination of fuel lean and fuel-rich pulses, the minimum amount of reductants required, and the best reductant species used in the regeneration of the EmeraChem LNTs. This section is divided into two subsections and compares the performance of LNT regeneration techniques, cycling lean and rich and direct fuel injection. Section 4.2.1 presents the LNT regeneration by cycling between the rich and lean pulses, whereas LNT regeneration by direct fuel injection is discussed in section 4.2.2.

4.2.1 Cycling Lean and Rich in Main Stream

The effects of lean and rich duration and type of reductants on the regeneration of the LNT catalyst are investigated at an operating temperature of 350^{o}C and a space velocity of 50,000 hr^{-1}. The operating temperature is selected to be 350^{o}C since the catalyst was determined previously to have a maximum NO_x storage capacity at that temperature. All experiments are carried out with 500ppm NO, 5% CO_2, 10% O_2, 10% H_2O with balance N_2 in the lean phase; and 500ppm NO, 5% CO_2, 4% CO, 1.33% H_2, 0% H_2O with balance N_2 in the rich phase. The experiments are performed for two different cases. In the first case, the time durations of the lean and rich phase are varied at a fixed concentration of CO and H_2. In the second case, the reductant concentrations − CO and H_2 − are varied at constant time durations of the lean and the rich phase. The objectives of the first case are to investigate the effect of time duration of fuel lean and rich on the performance of the LNT catalyst and to determine the optimum time durations to regenerate the LNT catalyst with the minimum amount of reductants. On the other

hand, the objective of second case is to investigate the effect of the reductant concentrations on the NO_x conversion efficiency using the optimum time durations obtained from the first case.

4.2.1.1 Varying Time Duration

Three different lean/rich cycles − 50 s lean and 10 s rich, 50 s lean and 5 s rich, and 100 s lean and 5 s rich − are used to investigate the effect of lean and rich durations on the NO_x conversion of the EmeraChem LNT catalysts. The reductants in the rich phase of the three investigated cycles consist of 4% CO and 1.33% H_2.

Figures 4.13 and 4.14 show NO_x concentration, NO_x conversion and corresponding catalyst and gas temperatures in six cycles of a cycling experiment at a temperature of 350^oC and a GHSV of 50,000 hr^{-1} with 50 s lean and 10 s rich for a total cycle time of 60 s. For this particular experiment NO_x excursion occurs only in the first lean/rich cycle but not in successive cycles. This anomaly is attributed to the pre-existing conditions of the LNT; the inadequacy of previous regeneration in "cleansing off " NO_x from the surface of the catalyst. During the first 10 s of the lean cycle, NO_x is absorbed by the LNT, resulting in almost no NO_x slip and 100% NO_x conversion. As the storage sites are gradually occupied, NO_x breakthrough commences as reflected in a gradual increase in NO_x concentration and a decrease in NO_x conversion. As seen in Figure 4.14, during the lean phase there is negligible change in temperature of the inlet and exit gas phase as well as the LNT. The difference in these temperatures is due the inability of maintaining isothermal condition for the LNT reactor. As the rich phase commences at 50 s, the reductants, H_2 and CO, induce NO_x release due to thermal decomposition of surface

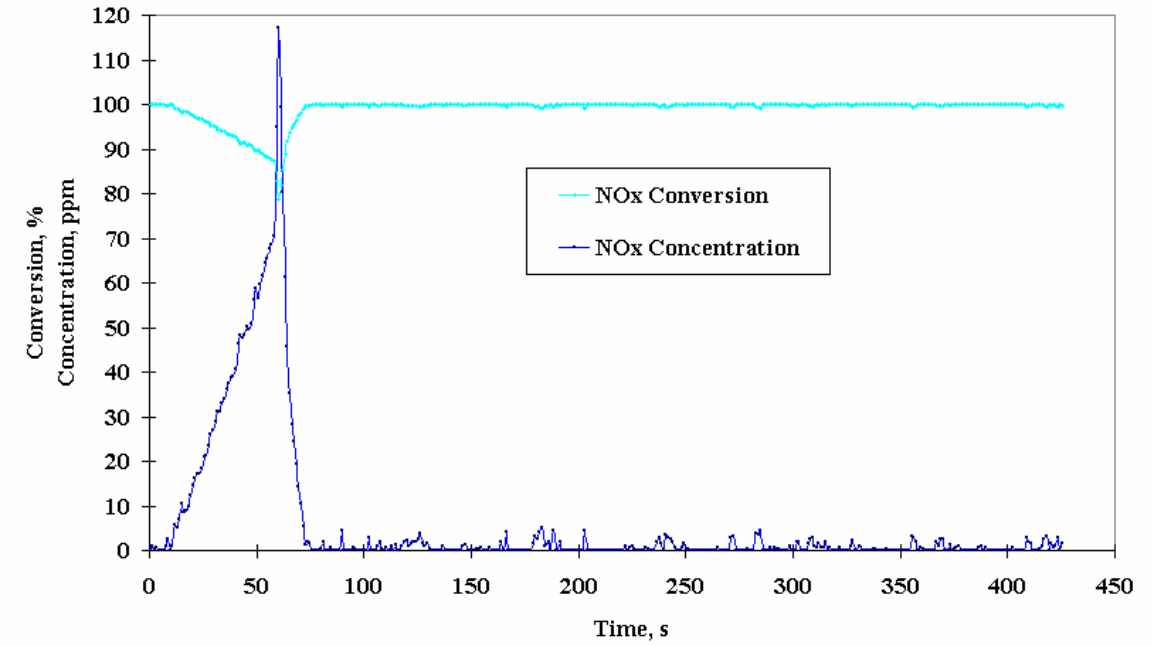

Figure 4.13 NO_x conversion and concentration histories of cycling regeneration with 500ppm of NO_x inlet concentration (50 s lean and 10 s rich, CO=4%, H_2=1.33%, T=350°C, GHSV=50,000 hr^{-1})

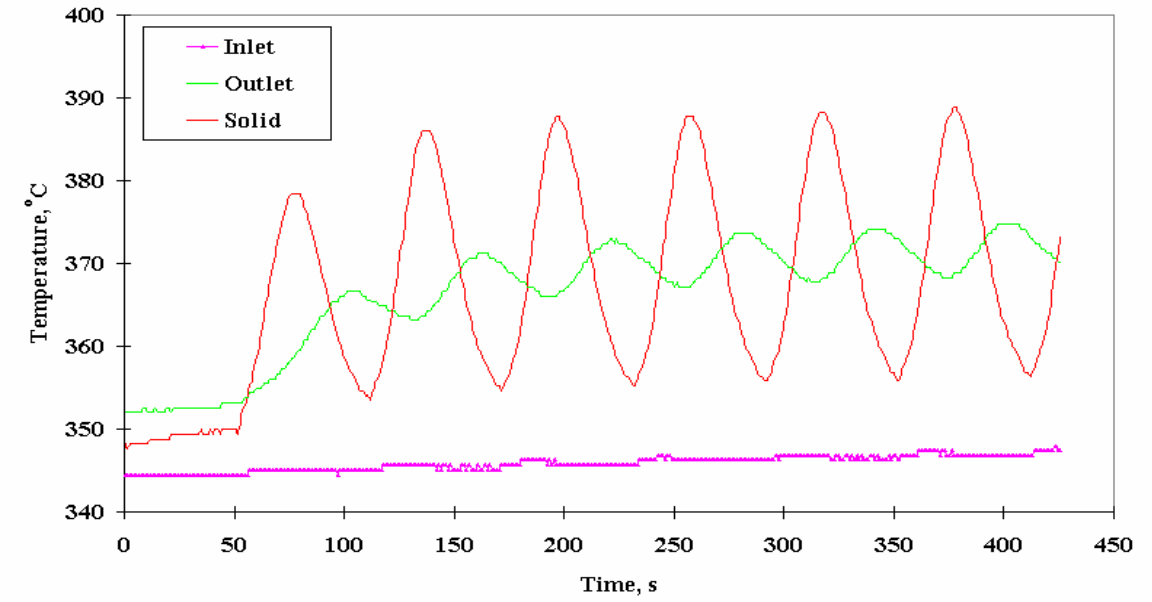

Figure 4.14 Temperature histories of cycling regeneration with 500ppm of NO_x inlet concentration (50 s lean and 10 s rich, CO=4%, H_2=1.33%, T=350°C, GHSV=50,000 hr^{-1})

nitrites and nitrates, as indicated by a sudden increase in NO_x concentration and a corresponding decrease in NO_x conversion. During the rich phase, the NO_x excursion is followed instantaneously by a sharp decrease of NO_x to nearly zero, which is indicative of subsequent reduction of stored nitrites and nitrates to N_2. The sudden NO_x excursion is accompanied by an increase in the LNT and the exit gas phase temperatures. The increase in the temperature of the LNT in the rich phase is a result of two different exothermic catalytic reactions; one between the reductants and absorbed O_2 on the surface of the LNT catalyst during the lean phase, and the other between the reductants and NO_x. For this particular experiment, a 10 s duration of the rich phase results in a maximum increase of 35^oC of the catalyst temperature. At the end of the first cycle with the termination of the rich phase, the LNT temperature decreases and this decrease in temperature continues well into the lean phase of the second cycle until the next rich phase. As a result of convection the temperature of the exit gas phase increases with the maximum temperatures occurring approximately 35 s behind those of the catalyst. This time lag is a result of the distance between two thermocouples used to measure the catalyst and the exit gas temperatures. On the other hand the increase in the inlet gas phase temperature is negligible, which indicates insignificant gas-phase reactions. Once the LNT's surface is "cleansed off", leaving more accessible trapping sites for the next cycle, no NO_x excursions are observed in the successive lean/rich cycles. The amount of NO_x slip is negligible and within the resolution of the NO_x analyzers, culminating in an average NO_x conversion in 6 cycles close to 100 %.

Figures 4.15 and 4.16 show NO_x concentration, NO_x conversion and corresponding catalyst and gas temperatures in six cycles of a lean/rich modulation

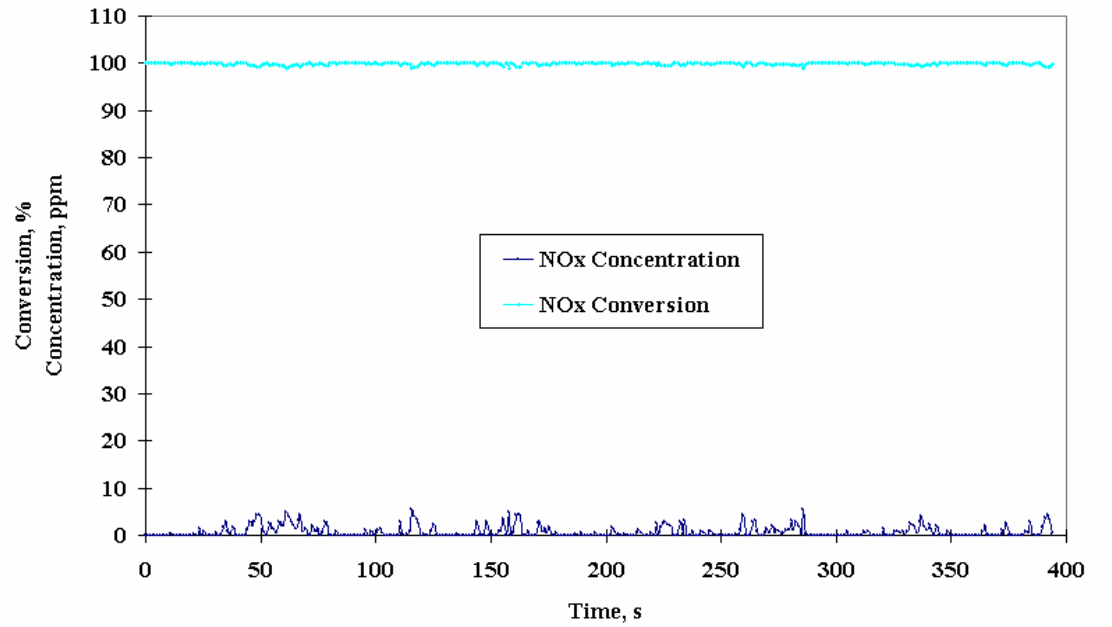

Figure 4.15 NO_x conversion and concentration histories of cycling regeneration with 500ppm of NO_x inlet concentration (50 s lean and 5 s rich, CO=4%, H_2=1.33%,T=350°C, GHSV=50,000 hr^{-1})

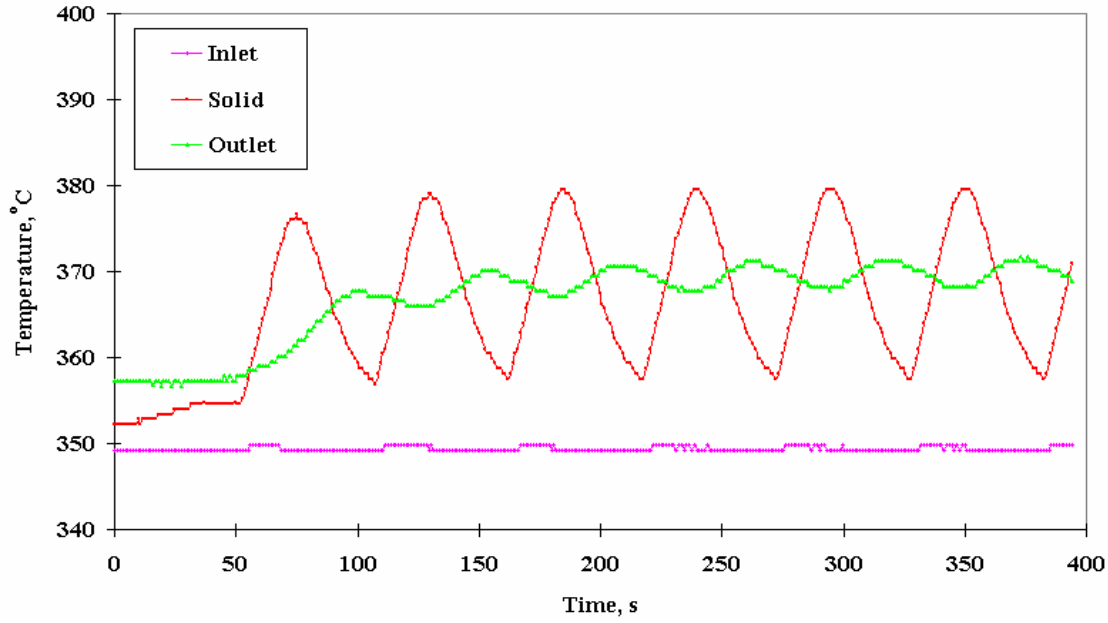

Figure 4.16 Temperature histories of cycling regeneration with 500ppm of NO_x inlet concentration (50 s lean and 5 s rich, CO=4%, H_2=1.33%, T=350°C, GHSV=50,000 hr^{-1})

experiment at a temperature of 350°C and a GHSV of 50,000 hr^{-1} with 50 s lean and 5 s rich for a total cycle time of 60 s. In contrast to the previous run no NO_x excursion is observed in this experiment. It is apparent that the surface of this particular LNT is free of NO_x accumulation prior to the experiment. Even though the duration of the rich pulse is half of the previous run, NO_x slip is of similar magnitude, resulting in a NO_x conversion of 99.9%. As seen in Figures 4.13 and 4.15, more than 99.9% NO_x conversion is obtained for the first two lean/rich cycles, whereas the NO_x conversion decreases to 98.0% for the 100 s lean and 5 s rich cycles, as shown in Figure 4.17. The catalyst and gas temperatures of 100 s lean and 5 s rich cycles are shown in Figure 4.18, which are very similar to Figure 4.16. Since there is not much difference in NO_x conversion between the three different lean/rich cycles, a lean/rich cycle of 100 s lean and 5 s rich hereafter is selected, since this cycle would offer the best fuel efficiency in regenerating the LNT catalysts.

4.2.1.2 Varying Concentration of Reductant

Experiments are performed at 350°C − the optimum operating temperature of the EmeraChem LNT catalyst − and a GHSV of 50,000 hr^{-1}, using four different concentrations of the reductants in the rich or regeneration phase. For this particular series of experiments, the objectives are twofold. The first objective is to determine the minimum concentration of CO and H_2 when the two reductants are used in the rich phase which produces high NO_x conversion. Only two different concentrations of the reductants are used: 4% CO and 1.33% H_2 and 2% CO and 0.67% H_2. The second objective is to find between CO and H_2 the most effective reductant for the regeneration of the LNTs.

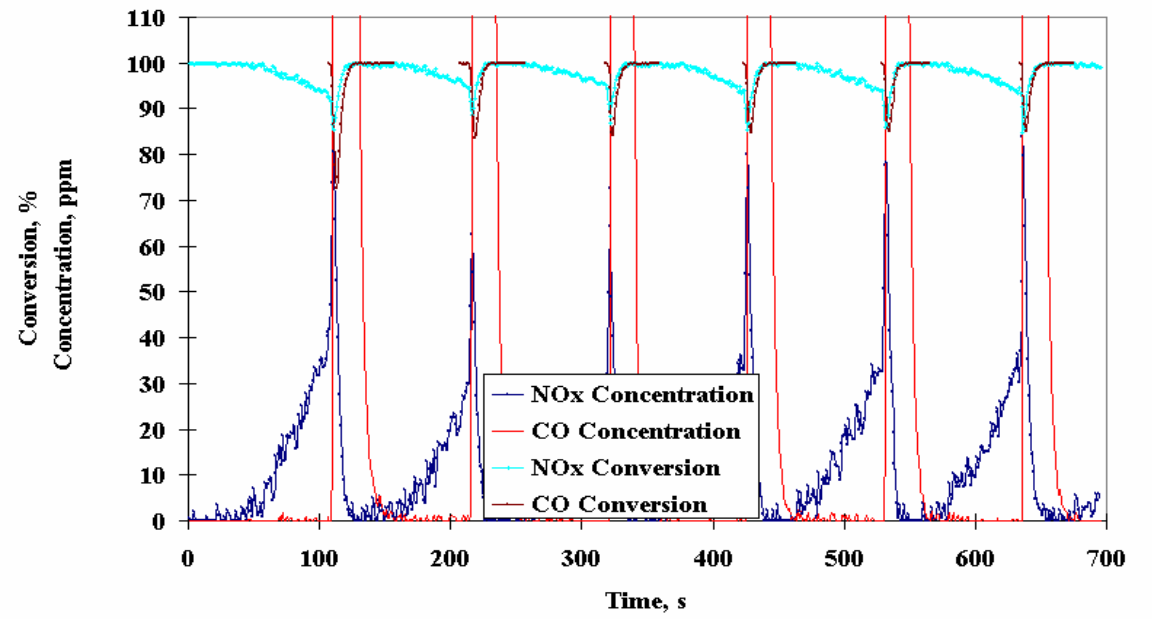

Figure 4.17 NO_x and CO conversion and concentration histories of cycling regeneration with 500ppm of NO_x inlet concentration (100 s lean and 5 s rich, CO=4%, H_2=1.33%, T=350°C, GHSV=50,000 hr^{-1})

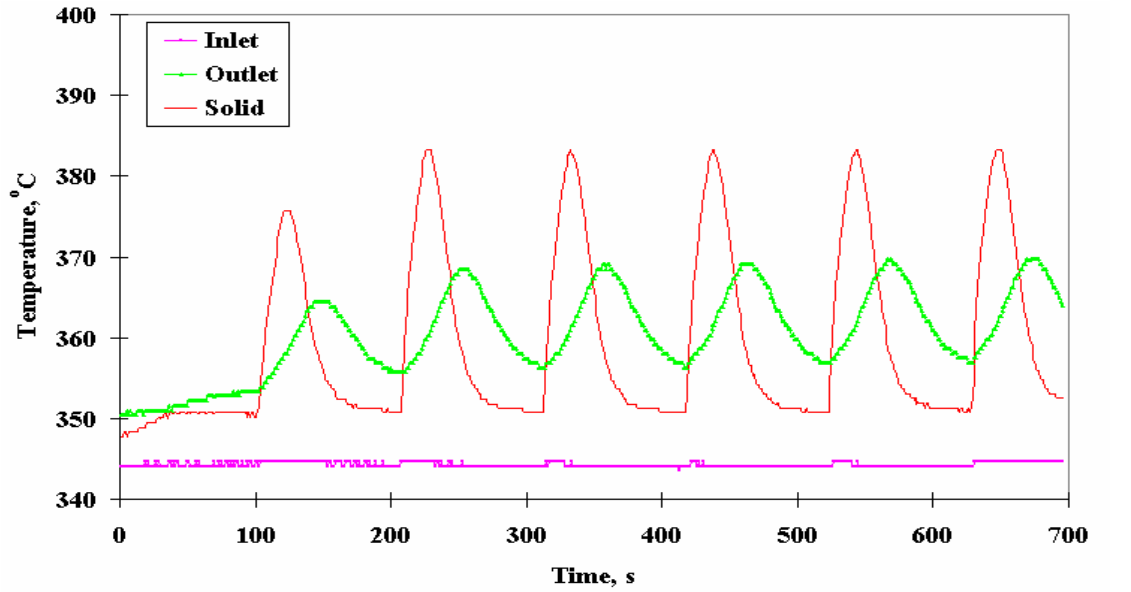

Figure 4.18 Temperature histories of cycling regeneration with 500ppm of NO_x inlet concentration (100 s lean and 5 s rich, CO=4%, H_2=1.33%, T=350°C, GHSV=50,000 hr^{-1})

For the second objective experiments are performed at a concentration of 4% of either CO or H_2 in the rich phase. All experiments are conducted using an optimum lean/rich modulation of 100 s lean and 5 s rich. The results obtained from cycling experiment with 4% CO and 1.33% H_2 in the rich phase and lean/rich modulation of 100 s lean and 5 s rich − has been discussed in Section 4.2.1.1(see Figures 4.17 and 4.18). Figures 4.19 and 4.20 show NO_x concentration, NO_x conversion and corresponding catalyst and gas temperatures in 10 cycles of a cycling experiment with 2% CO and 0.67% H_2 in the rich phase at a temperature of 350^oC and a GHSV of 50,000 hr^{-1}. For this particular experiment NO_x slip and excursion gradually increase with increasing number of cycles. The increase in NO_x slip and excursion is attributed to insufficient amount of reductants; i.e., 2% CO and 0.67% H_2, used in regenerating the LNT. As seen in Figure 4.19, the CO conversion is almost 100% in the rich phases, which indicates that most of CO is consumed by the NO_x reduction reaction. As some of the storage sites are occupied with NO_x from previous incomplete regenerations, the LNT has less accessible trapping sites for the next lean phase. Therefore the rate of NO_x reduction with insufficient amount of reductants is less than that of NO_x accumulation in the lean phase, resulting in an increase in NO_x slip and excursion with each successive cycle and a corresponding decrease in NO_x conversion. It is interesting to observe that at low concentration of reductants the temperatures of LNT and inlet and outlet gas decrease with successive cycles as in contrast to the previous experiment, in which the temperatures of LNT and inlet and outlet gas reach a steady-state condition only after two cycles (see Figure 4.18). For this particular concentration of the reductants in the rich phase; i.e., 2% CO and 0.67% H_2, the outlet gas temperature is less but the LNT temperature is higher than those in the

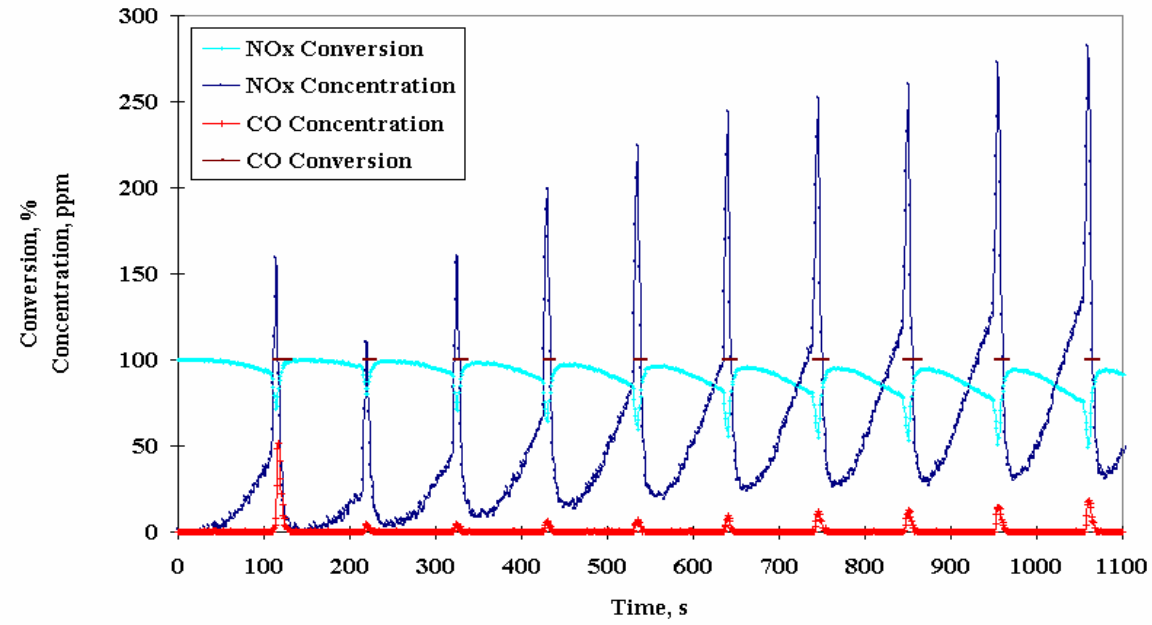

Figure 4.19 NO_x and CO conversion and concentration histories of cycling regeneration with 500 ppm of NO_x inlet concentration (100 s lean and 5 s rich, CO=2%, H_2=0.67%, T=350°C, GHSV=50,000 hr^{-1})

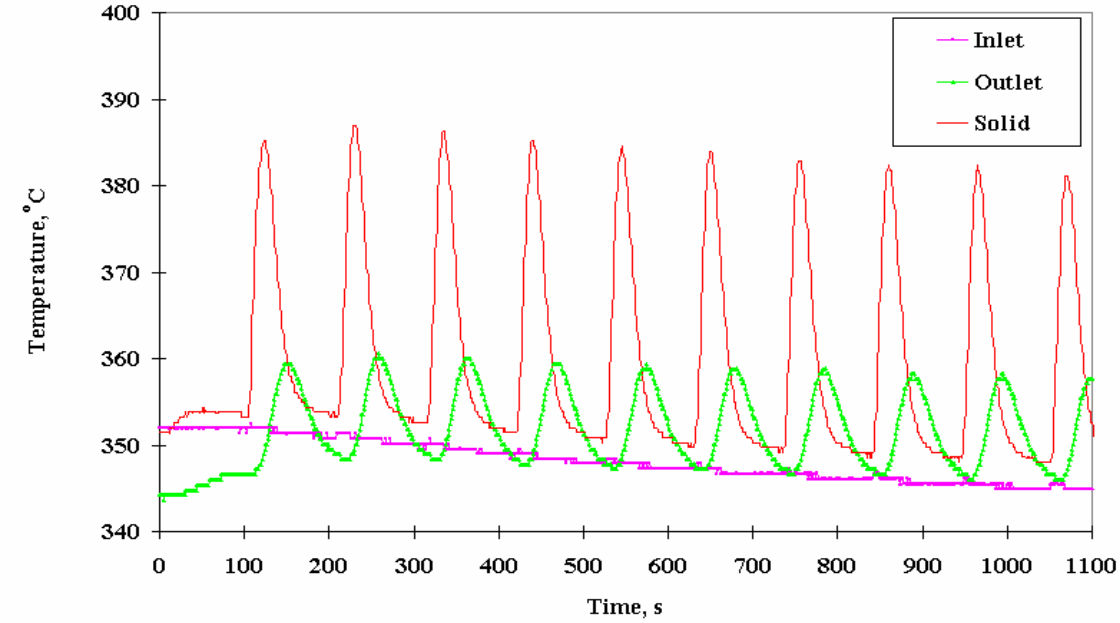

Figure 4.20 Temperature histories of cycling regeneration with 500ppm of NO_x inlet concentration (100 s lean and 5 s rich, CO=2%, H_2=0.67%, T=350°C, GHSV=50,000 hr^{-1})

previous case in which the concentration of the reductants is doubled. These results seem to indicate that for reductants of insufficient strength most of the reductants are consumed in the front half of the LNT, and not much reductants are left to react with NO_x stored in rear half. Since NO_x slip and excursion increase as the number of cycles increases, it appears that the amount of NO_x accumulation increases with each successive cycle resulting in higher NO_x slip, which in turn produces higher NO_x excursion in the next cycle. It is also interesting to note that the concentration of CO increases with increasing number of cycle even though the amount is negligible. The increase in CO concentration is indicative of the reduction reactions becoming less efficient due to more absorbed NO_x on the LNT surface blocking the diffusion of O_2 to ceria sites during the lean phase. NO_x concentration, NO_x conversion and temperature histories in 10 cycles of a cycling experiment with either 4% CO or 4% H_2 in the rich phase with a lean/rich modulation of 100 s lean and 5 s rich are shown in Figures 4.21 to 4.24. As seen in Figures 4.21 and 4.23, regardless of the reductant used, highest NO_x slip and excursion occur only in the first cycle due to the inadequacy of previous regeneration in "cleansing off" stored NO_x from the surface of the LNT. After the first cycle, NO_x slip and excursion decrease and reach steady-state values. Since NO_x slip and excursion with H_2 as the reductant are less than those with CO, the average NO_x conversion for H_2 is higher than that of CO. Figure 4.21 also shows CO excursions during the rich pulses, which indicates that not all CO is consumed by NO_x reduction reaction and in the absence of O_2, large amount of CO slip occurs. Average CO conversion for this experiment decreases to 99%, whereas about 100% of CO conversion is obtained from the cycling experiment with 2% CO and 1.33% H_2 in the rich pulse (see Figure 4.19). The temperature histories of LNT, inlet and outlet

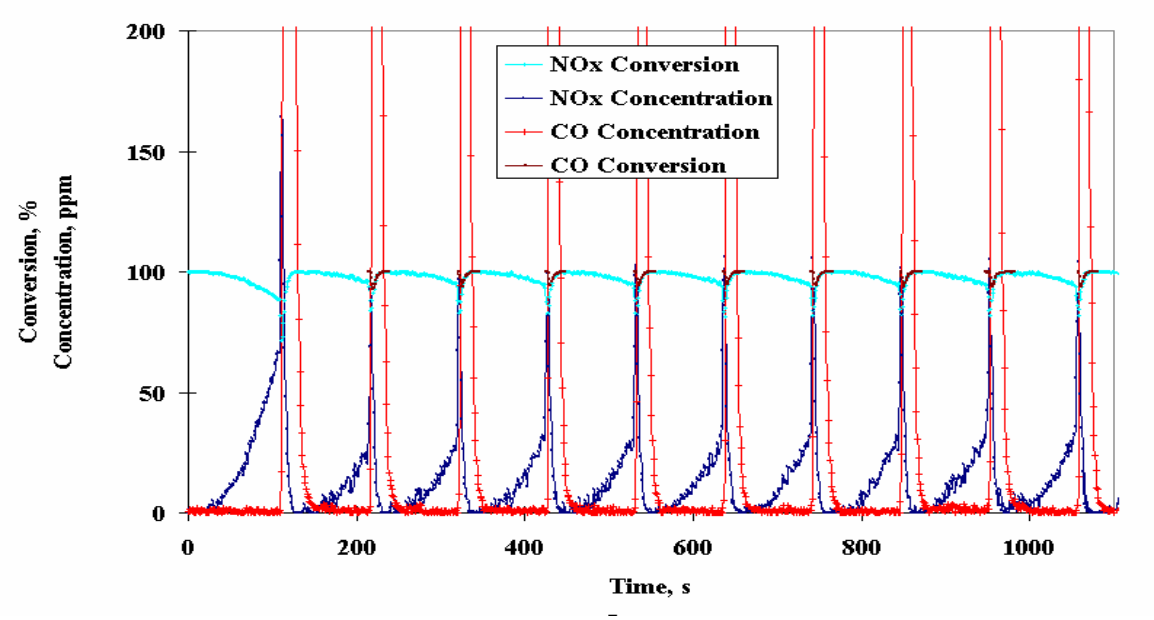

Figure 4.21 NO_x and CO conversion and concentration histories of cycling regeneration with 500ppm of NO_x inlet concentration (100 s lean and 5 s rich, CO = 4%, T=350°C, GHSV=50,000 hr^{-1})

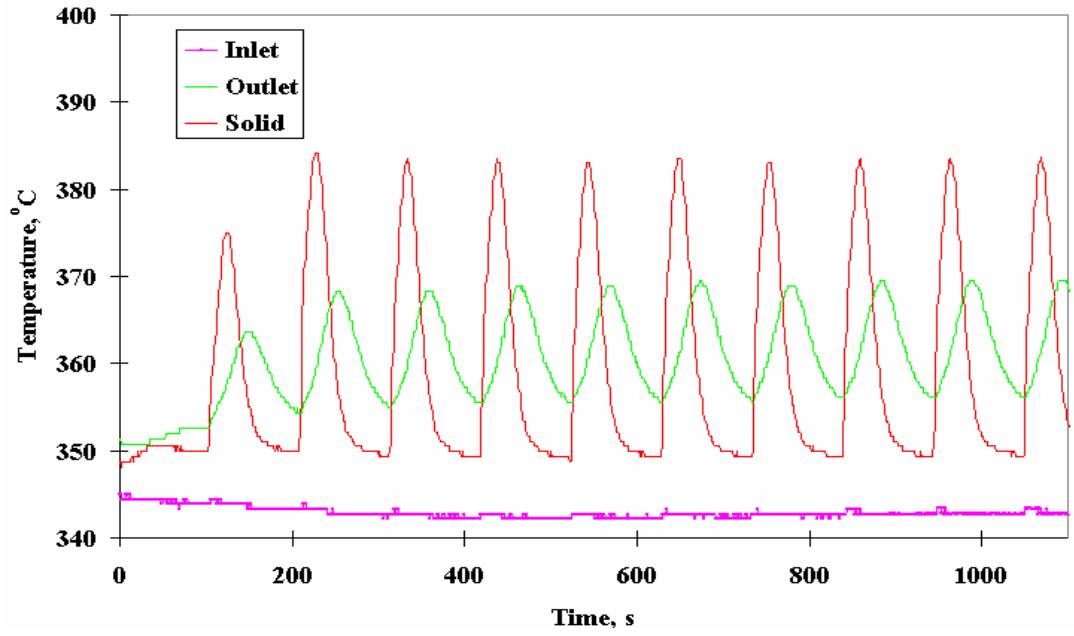

Figure 4.22 Temperature histories of cycling regeneration with 500ppm of NO_x inlet concentration (100 s lean and 5 s rich, CO = 4%, T=350°C, GHSV=50,000 hr^{-1})

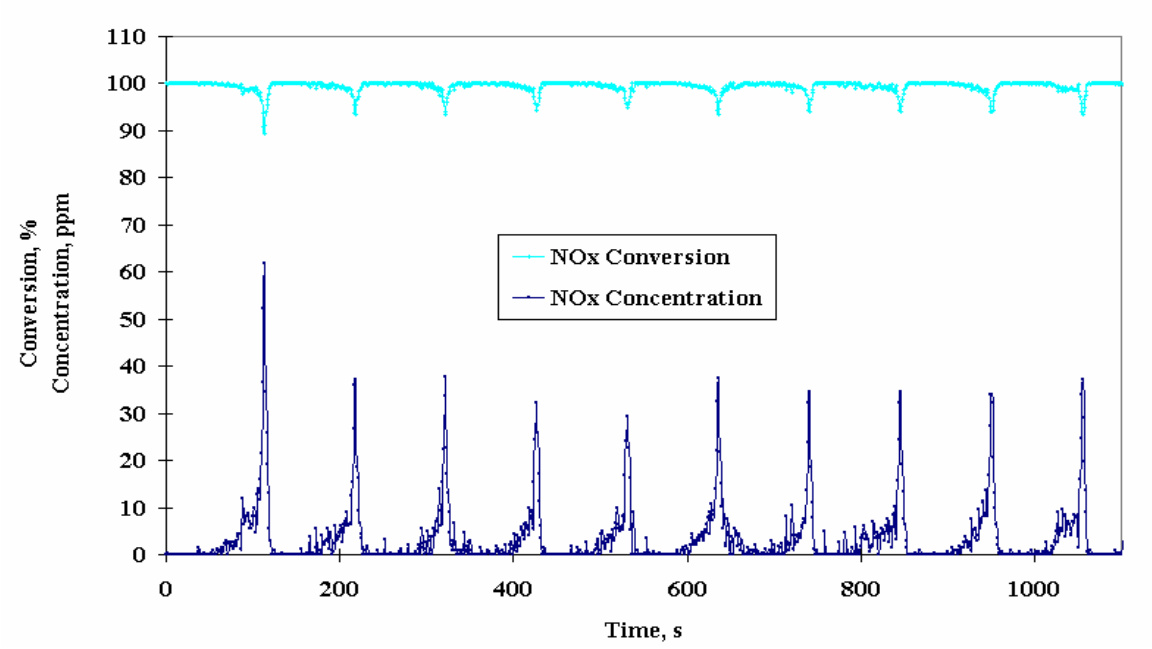

Figure 4.23 NO_x conversion and concentration histories of cycling regeneration with 500ppm of NO_x inlet concentration (100 s lean and 5 s rich, H_2 = 4%, T=350^oC, GHSV=50,000 hr^{-1})

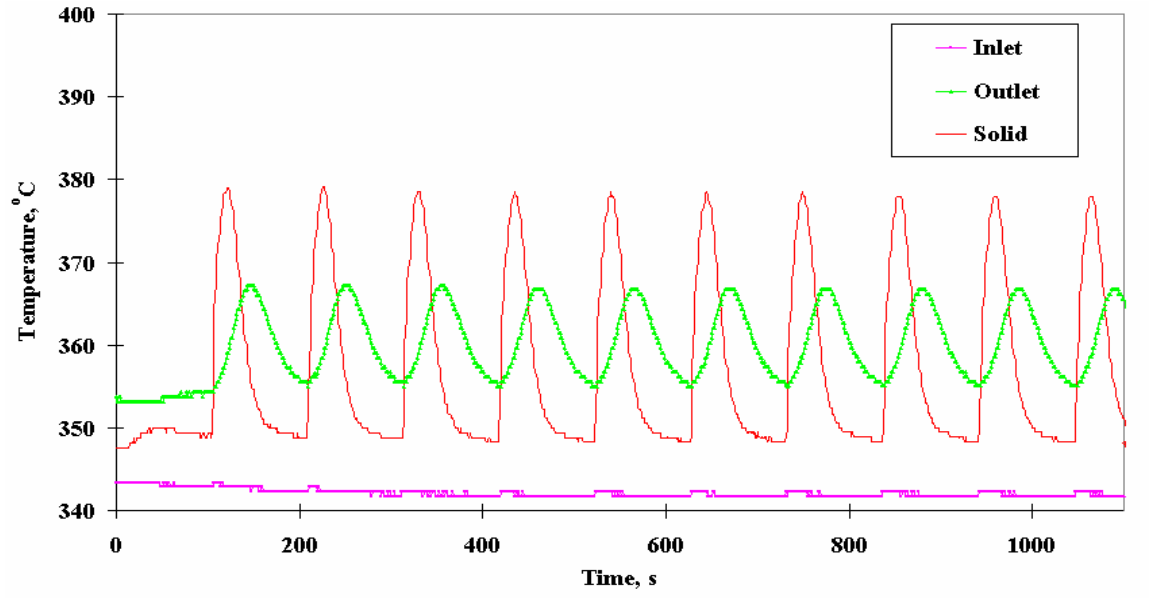

Figure 4.24 Temperature histories of cycling regeneration with 500ppm of NO_x inlet concentration (100 s lean and 5 s rich, H_2 = 4%, T=350^oC, GHSV=50,000 hr^{-1})

gas for CO and H_2 are shown in Figures 4.22 and 4.24, respectively. These temperature histories are similar to those obtained from the cycling experiment with 50 s lean and 10 s rich (see Figure 4.14). NO_x and CO conversion efficiencies are listed in Table 4.8. As seen in Table 4.8, it is apparent that H_2 is a slightly better reductant in reducing NO_x than CO.

4.2.2 Direct Fuel Injection (DFI)

Two separate DFI experiments are carried out: direct fuel injection in the absence and presence of oxygen in the simulated exhaust gases. These two types of experiments were used to simulate two different scenarios in which the rich excursions are generated in the operation of lean-burn natural gas engines. In the first scenario, the rich excursions are produced by running the engines under stoichiometric or rich conditions for a very short period. In the second scenario the rich excursions are generated by injecting the reductants directly into the lean exhaust gases. To duplicate the first scenario, at the beginning of the rich phase, oxygen is shut off and the reductant, either H_2 or CO, is directly injected into the reactor gas stream. In the second scenario, the rich excursions are generated by injecting the reductant into the lean exhaust gas stream. Both experiments are performed at the optimum operating temperature of 350^oC and a space velocity of 50,000 hr^{-1} with an optimum lean/rich cycle of 100 s lean and 5 s rich.

Figures 4.25 and 4.38 show the effect of reductant chemical species and concentration on the NO_x concentration profiles at the exit of the LNT catalysts in the absence of O_2 in the rich phase. CO and H_2 are selected as the reductants, and the results are listed in Table 4.9. As seen in Figure 4.25, at a concentration of 2% CO the amount of

Table 4.8 Results of cycling 100 s lean and 5 s rich experiment with T=350°C and GHSV=50,000 hr^{-1}

Reductants	NO_x Conversion, %	CO Conversion, %	Temperature Increase During Regeneration, °C
4% CO & 1.33% H_2	98.0	97.5	33
2% CO & 0.67% H_2	90.9	100.0	34
4% CO	97.7	98.7	34
4% H_2	99.4	–	30

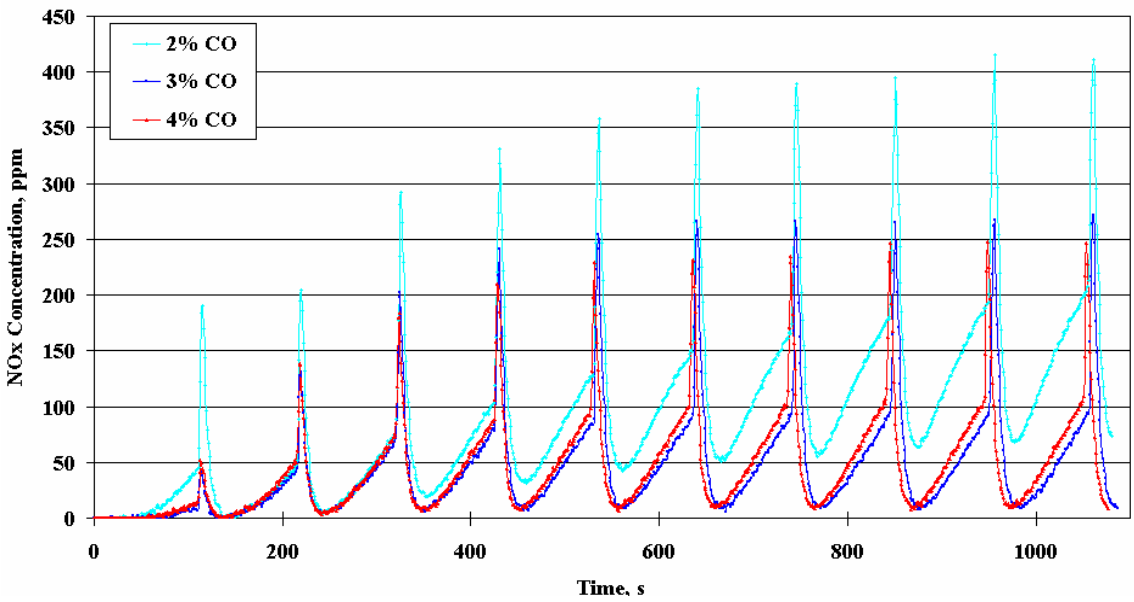

Figure 4.25 NO_x conversion versus time for various CO injections using DFI in absence of O_2 with 500ppm of NO_x inlet concentration (100 s lean and 5 s rich, T=350°C, GHSV=50,000 hr^{-1})

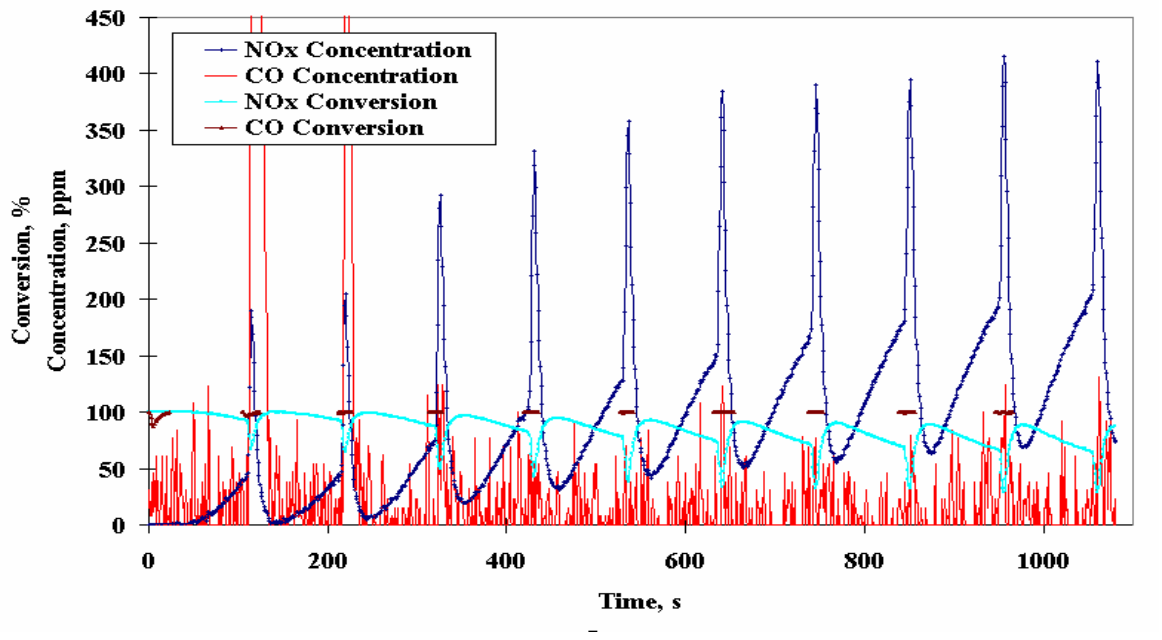

Figure 4.26 NO_x and CO conversion and concentration histories for 2% CO injections using DFI in absence of O_2 with 500ppm of NO_x inlet concentration (100 s lean and 5 s rich, T=350°C, GHSV=50,000 hr^{-1})

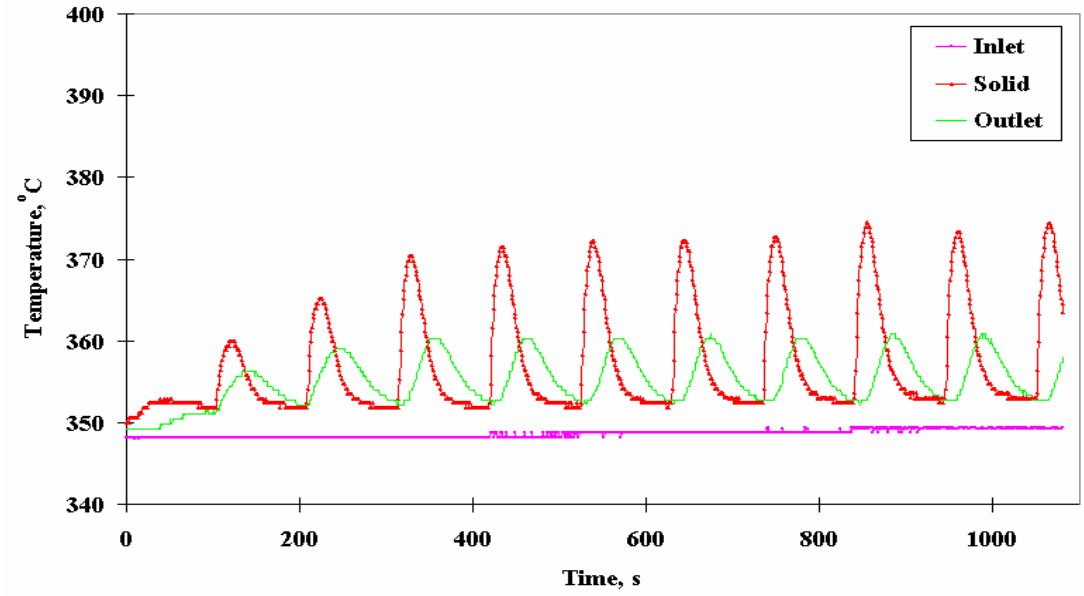

Figure 4.27 Temperature histories for 2% CO injections using DFI in absence of O_2 with 500ppm of NO_x inlet concentration (100 s lean and 5 s rich, T=350°C, GHSV=50,000 hr^{-1})

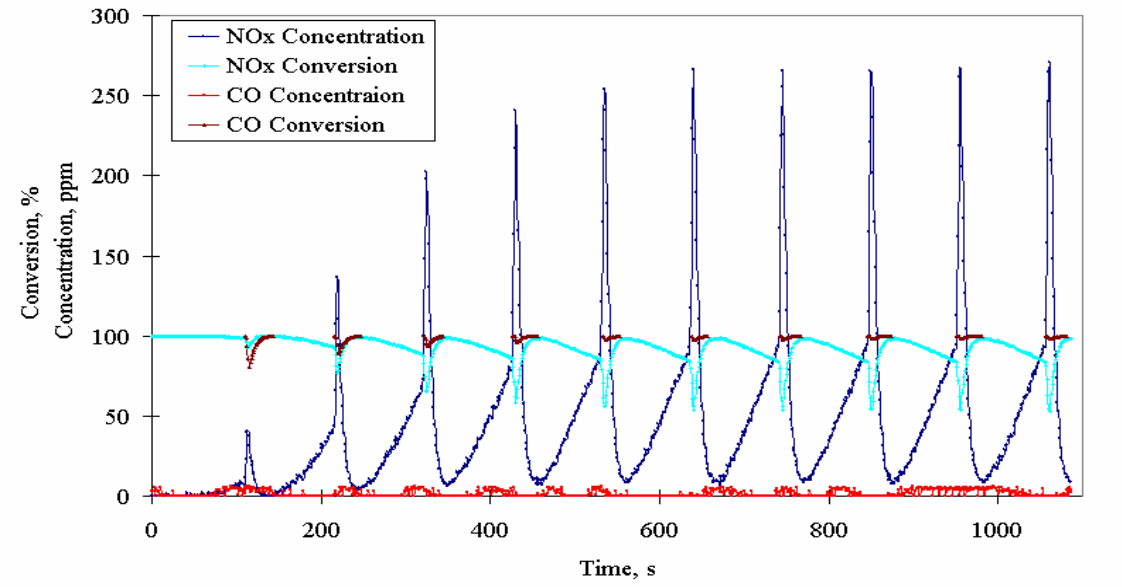

Figure 4.28 NO_x and CO conversion and concentration histories for 3% CO injections using DFI in absence of O_2 with 500ppm of NO_x inlet concentration (100 s lean and 5 s rich, T=350°C, GHSV=50,000 hr^{-1})

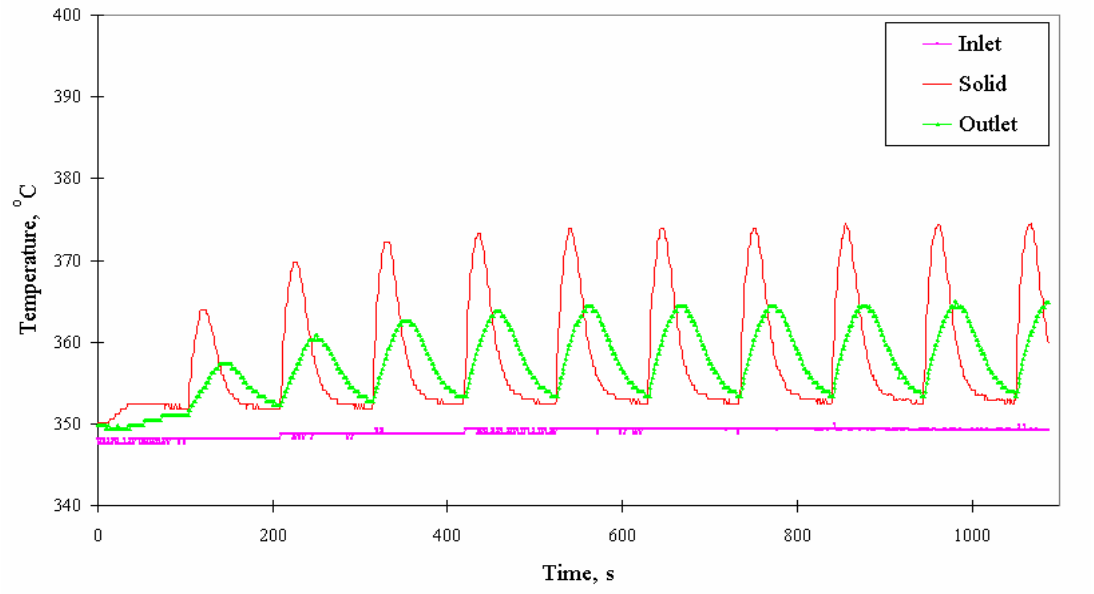

Figure 4.29 Temperature histories for 3% CO injections using DFI in absence of O_2 with 500ppm of NO_x inlet concentration (100 s lean and 5 s rich, T=350°C, GHSV=50,000 hr^{-1})

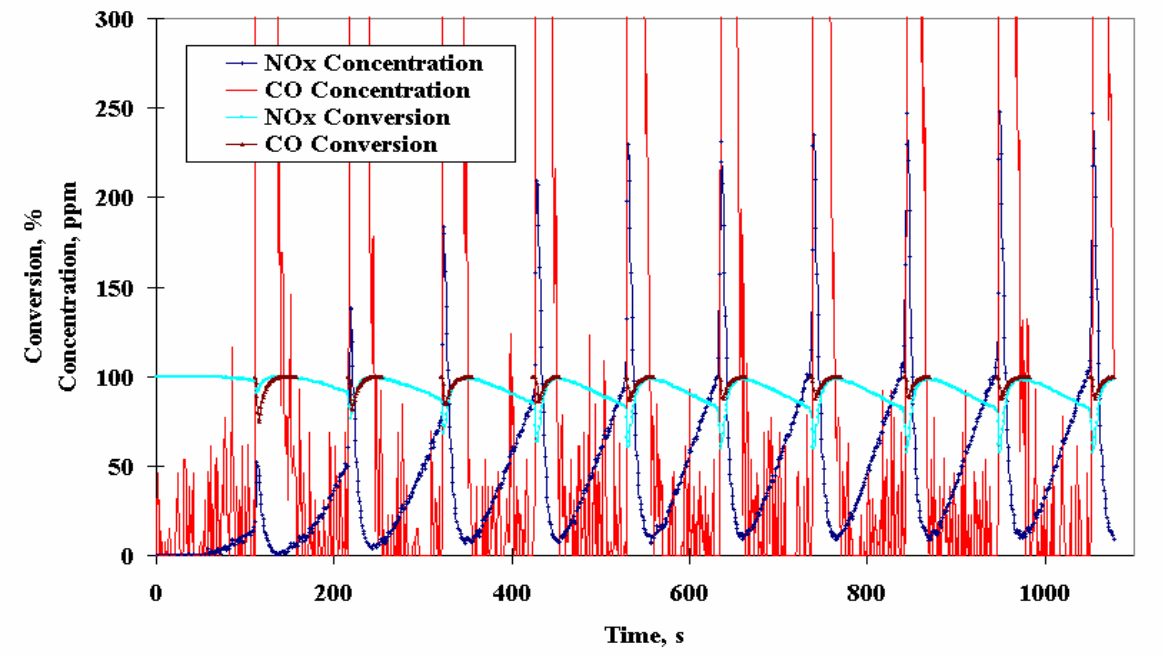

Figure 4.30 NO_x and CO conversion and concentration histories for 4% CO injections using DFI in absence of O_2 with 500ppm of NO_x inlet concentration (100 s lean and 5 s rich, T=350°C, GHSV=50,000 hr^{-1})

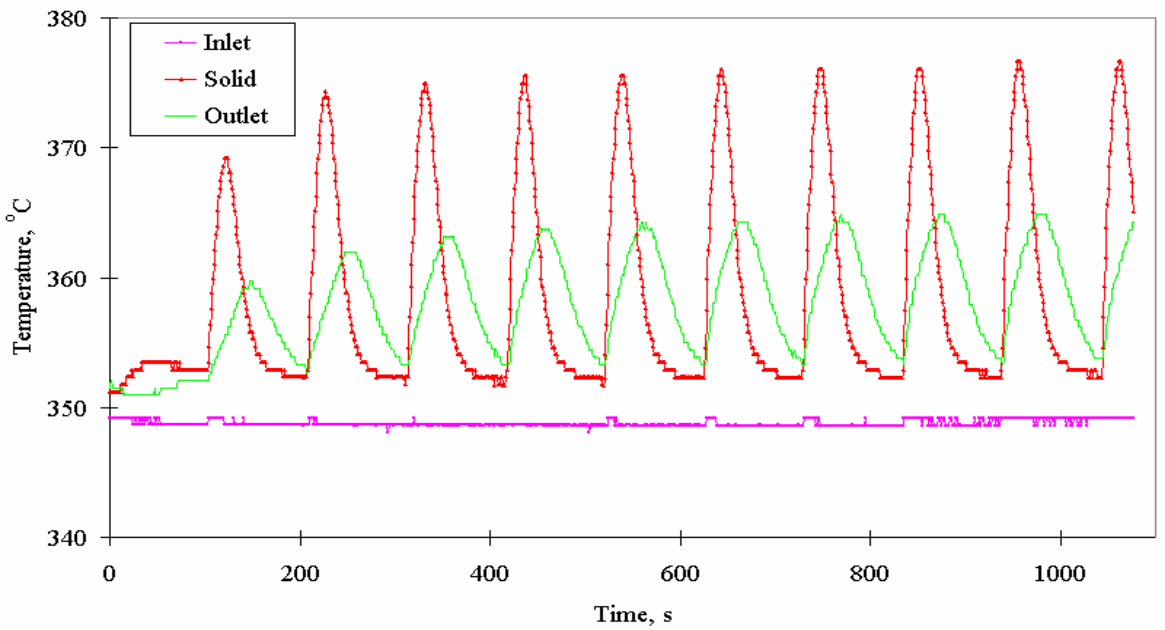

Figure 4.31 Temperature histories for 4% CO injections using DFI in absence of O_2 with 500ppm of NO_x inlet concentration (100 s lean and 5 s rich, T=350°C, GHSV=50,000 hr^{-1})

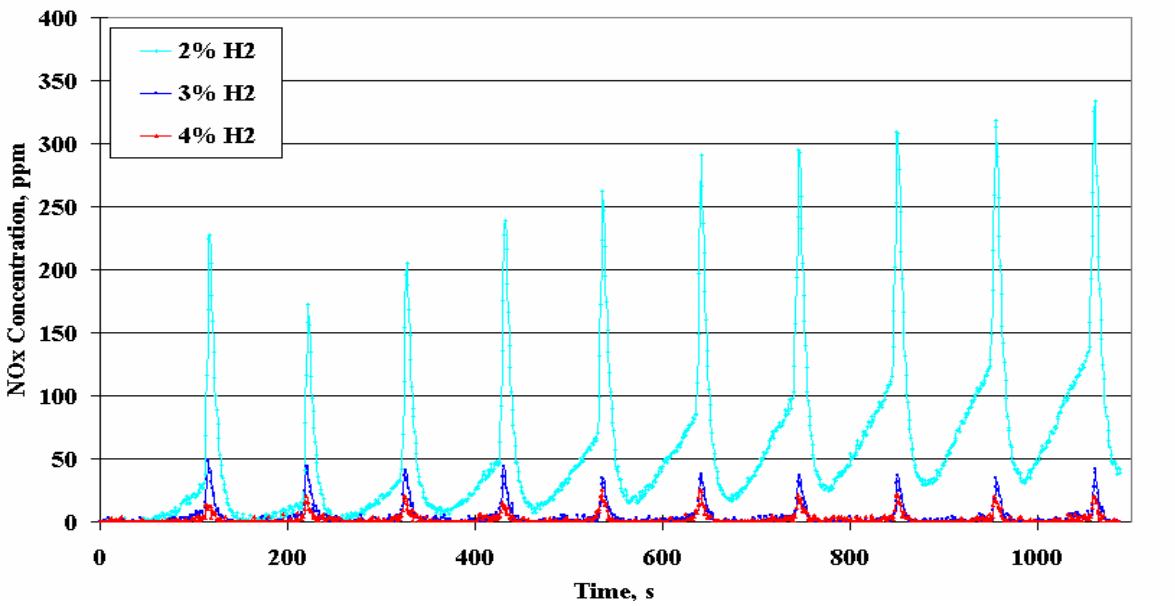

Figure 4.32 NO_x Conversion versus time for various H_2 injections using DFI in absence of O_2 with 500ppm of NO_x inlet concentration (100 s lean and 5 s rich, T=350°C, GHSV=50,000hr^{-1})

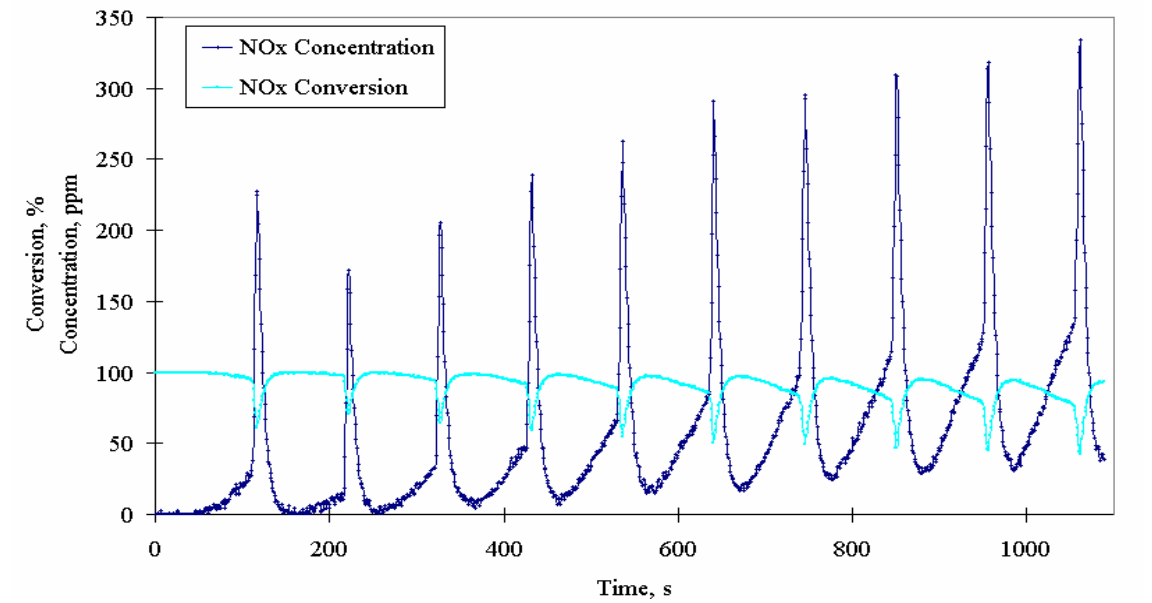

Figure 4.33 NO_x conversion and concentration histories for 2% H_2 injections using DFI in absence of O_2 with 500ppm of NO_x inlet concentration (100 s lean and 5 s rich, T=350°C, GHSV=50,000 hr^{-1})

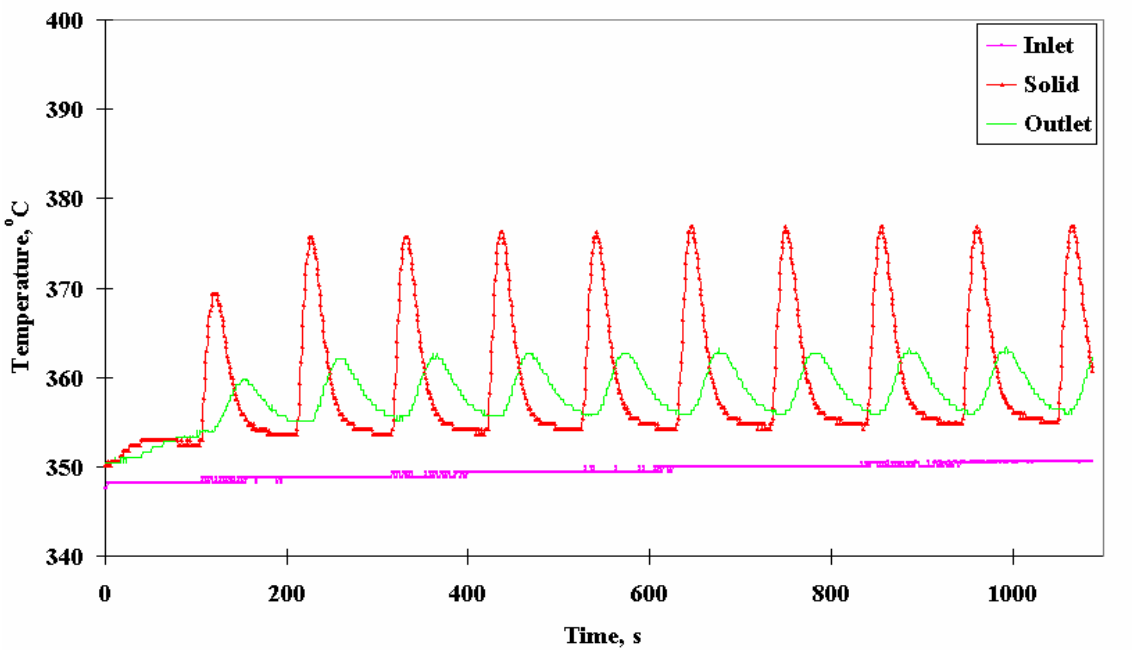

Figure 4.34 Temperature histories for 2% H_2 injections using DFI in absence of O_2 with 500ppm of NO_x inlet concentration (100 s lean and 5 s rich, T=350°C, GHSV=50,000 hr^{-1})

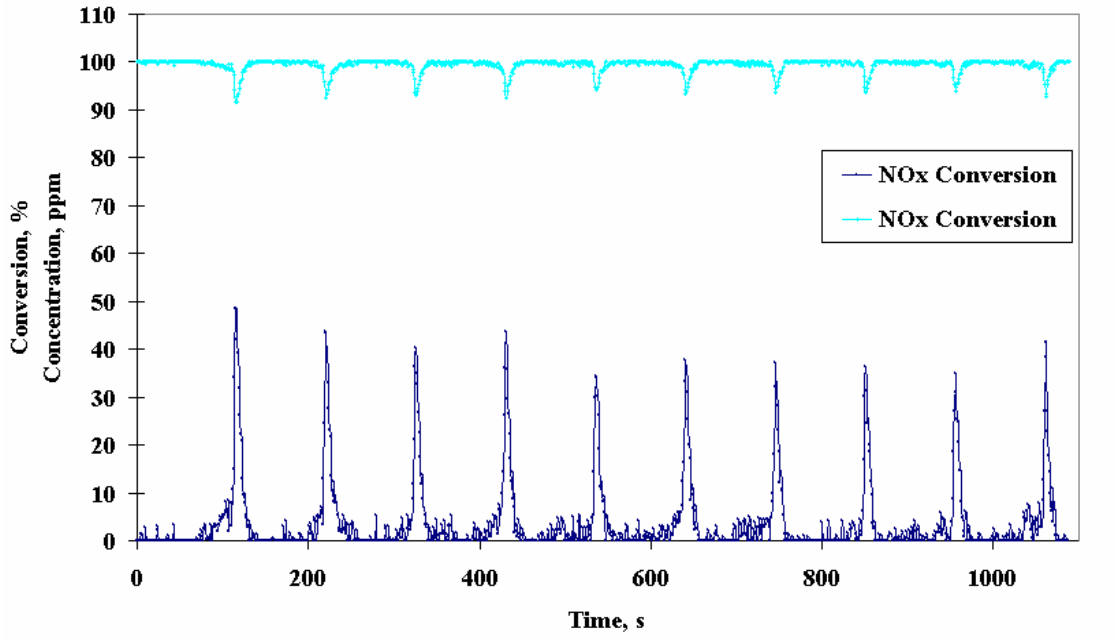

Figure 4.35 NO_x conversion and concentration histories for 3% H_2 injections using DFI in absence of O_2 with 500ppm of NO_x inlet concentration (100 s lean and 5 s rich, T=350°C, GHSV=50,000 hr^{-1})

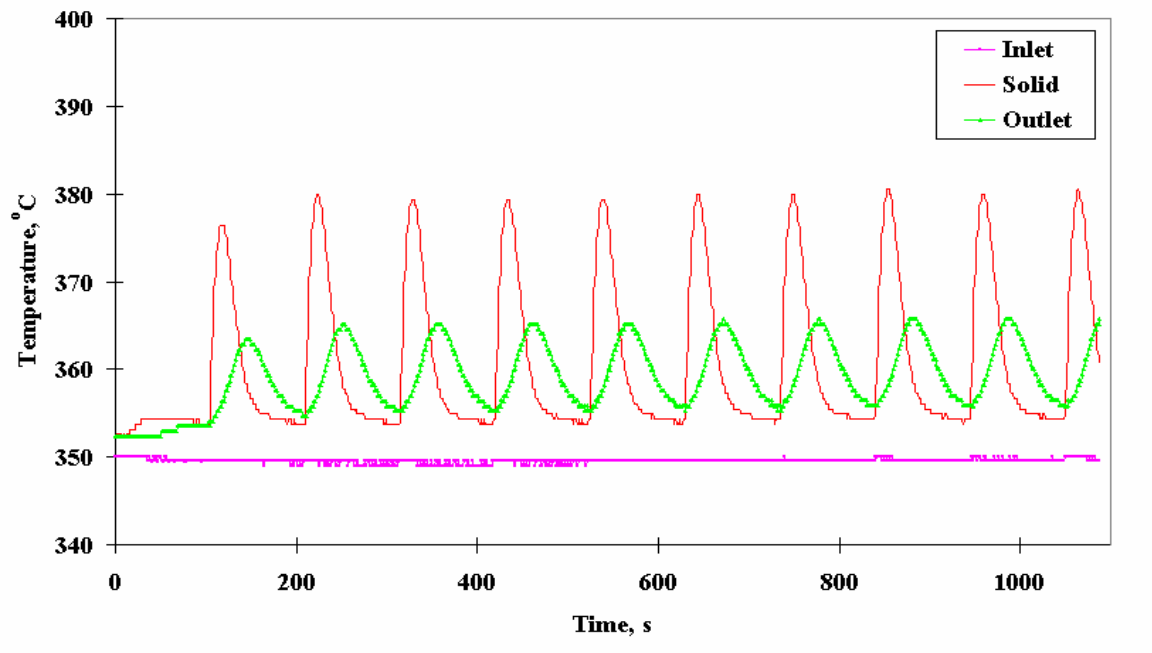

Figure 4.36 Temperature histories for 3% H_2 injections using DFI in absence of O_2 with 500ppm of NO_x inlet concentration (100 s lean and 5 s rich,T=350°C, GHSV=50,000 hr^{-1})

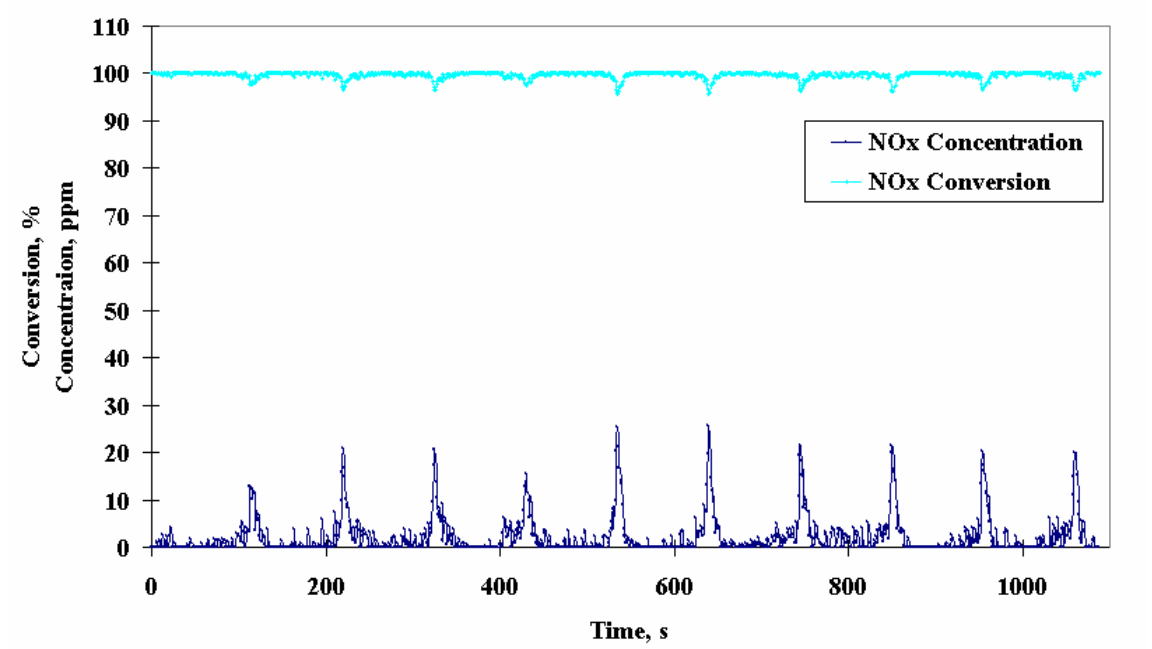

Figure 4.37 NO_x conversion and concentration histories for 4% H_2 injections using DFI in absence of O_2 with 500ppm of NO_x inlet concentration (100 s lean and 5 s rich, T=350°C, GHSV=50,000 hr^{-1})

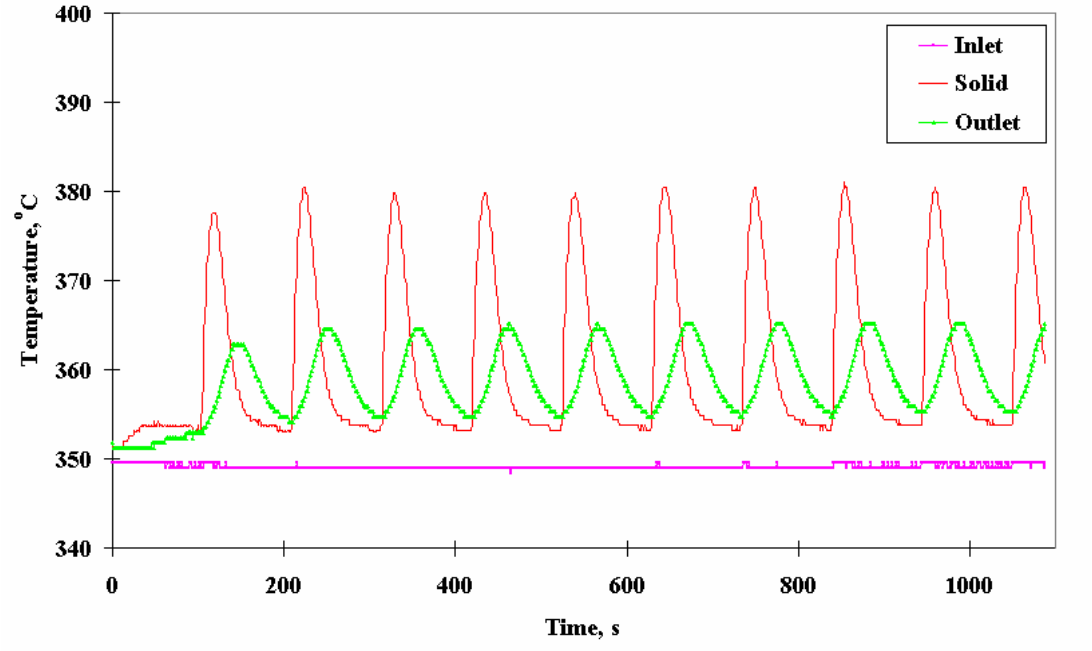

Figure 4.38 Temperature histories for 4% H_2 injections using DFI in absence of O_2 with 500ppm of NO_x inlet concentration (100 s lean and 5 s rich, T=350°C, GHSV=50,000 hr^{-1})

Table 4.9 Results from direct fuel injection without O_2 (5 s rich and 100 s lean, T=350°C, GHSV=50,000 hr^{-1})

Reductant	NO_x Conversion,%	CO Conversion,%	LNT Temperature Increase, °C
2% CO injection	84.0	99.2	22
3% CO injection	92.3	98.0	22
4% CO injection	92.0	96.6	24
2% H_2 injection	90.5	-	23
3% H_2 injection	99.3	-	26
4% H_2 injection	99.6	-	28

NO_x slip at the end of the lean phase and the NO_x excursion at the end of the rich phase increase with each successive cycle. Similar behavior is observed for H_2 as a reductant at the same concentration even though the amount of NO_x slip and the NO_x excursion is relatively lower. The increase in the amount of NO_x slip and the NO_x excursion is due to not only in the decrease in the trapping efficiency of LNT, but also the inadequacy of the a steady value immediately after the first cycle. This indicates that H_2 is a better reductant in "cleansing off" the surface of the LNT, leaving more accessible trapping sites for the next lean phase. strength of the reductant in "cleansing off" the surface of the catalyst in the generation phase. As the concentration of the reductant increases, the amount of NO_x slip and NO_x excursion decreases, and reaches a steady value. For CO at concentrations of 3 and 4% the steady state performance is achieved after 10 cycles.

On the other hand with H_2 as the reductant at the same concentrations, the amount of NO_x slip and NO_x excursion reaches the catalyst out NO_x concentrations during DFI in the presence of O_2 with either CO or H_2 as the reductant, are shown in Figure 4.39 and 4.52, respectively. Table 4.9 and 4.10 list the NO_x conversion averaged over 10 cycles obtained at different concentrations of CO or H_2 in the absence and presence of O_2 in the simulated exhaust gases, respectively. In contrast to DFI in the absence of O_2, the NO_x slip during the lean phase and the NO_x excursion during rich phase increase with successive cycles, regardless of the type and concentration of the reductant. Consequently the average NO_x conversion in 10 cycles decreases significantly in the presence of O_2 in the regeneration phase. The results suggest that some of the reductant is consumed by directly reacting with oxygen, and thus less is available to participate in the reduction reactions. The exothermic oxidation reaction results in an increase of 53^oC in the catalyst

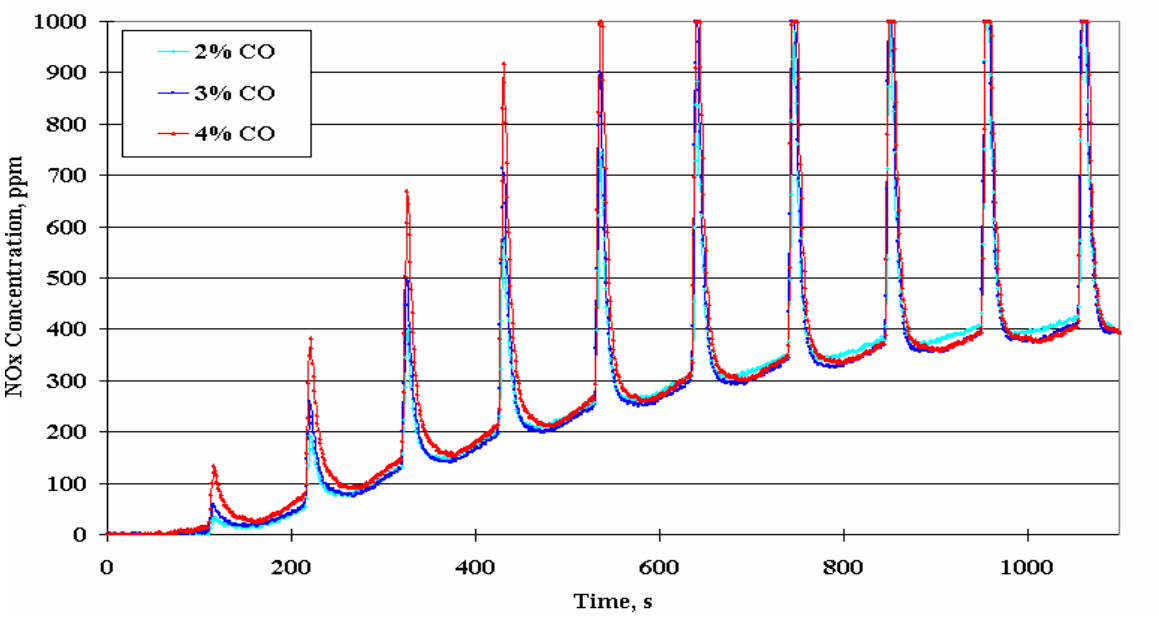

Figure 4.39 NO_x conversion versus time for various CO injections using DFI in presence of O_2 with 500ppm of NO_x inlet concentration (100 s lean and 5 s rich, T=350^{o}C, GHSV=50,000 hr^{-1})

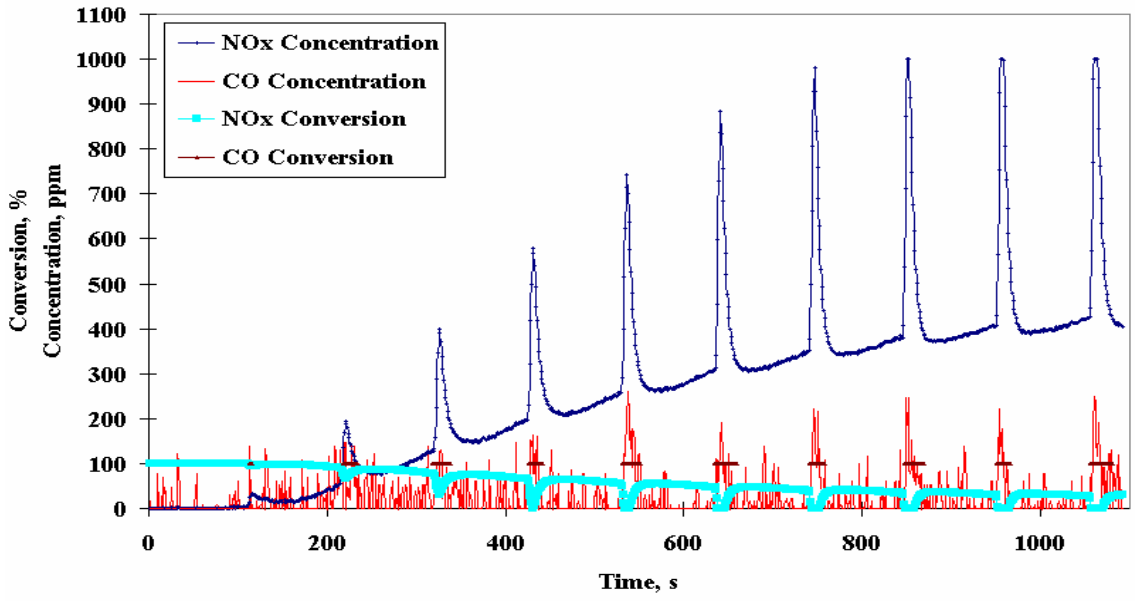

Figure 4.40 NO_x conversion and concentration histories for 2% CO injections using DFI in presence of O_2 with 500ppm of NO_x inlet concentration (100 s lean and s 5 rich, T=350^{o}C, GHSV=50,000 hr^{-1})

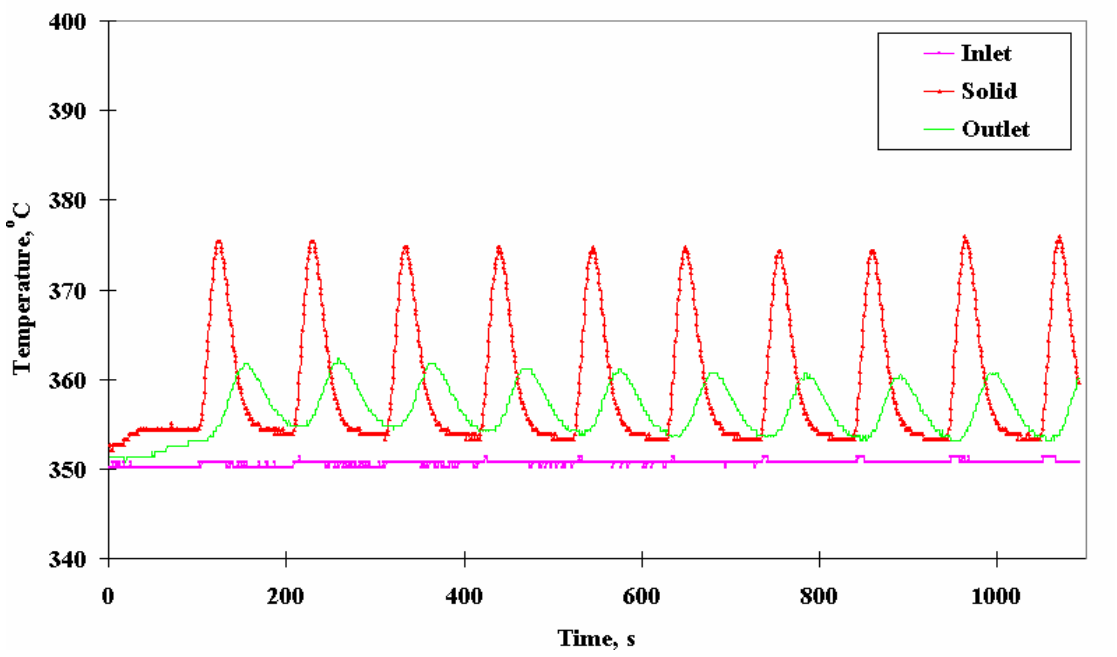

Figure 4.41 Temperature histories for 2% CO injections using DFI in presence of O_2 with 500ppm of NO_x inlet concentration (100 s lean and 5 s rich, T=350°C, GHSV=50,000 hr^{-1})

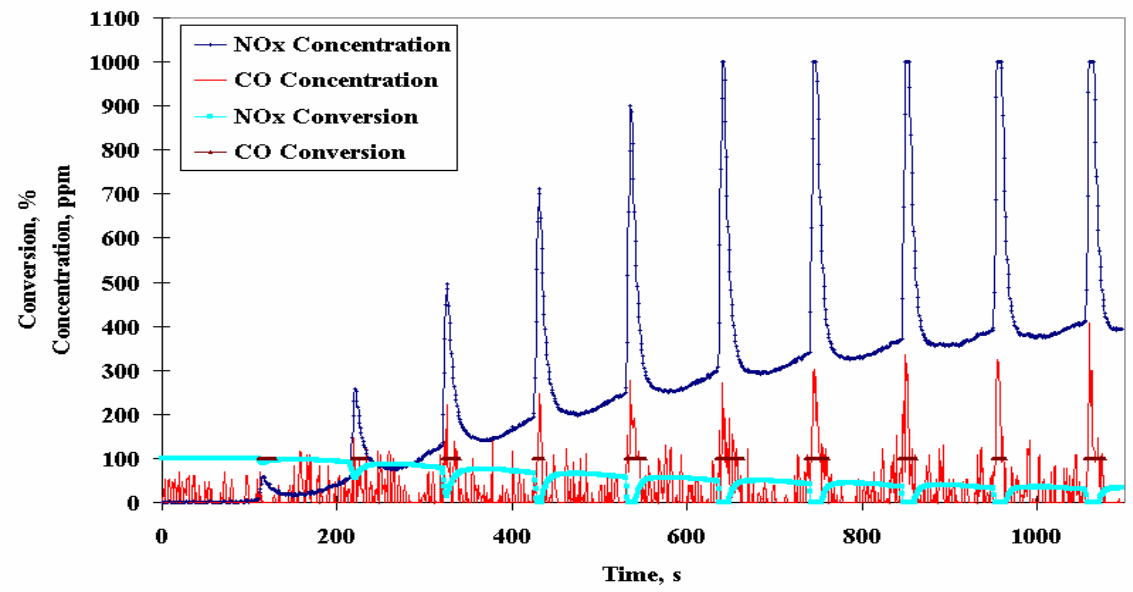

Figure 4.42 NO_x conversion and concentration histories for 3% CO injections using DFI in presence of O_2 with 500ppm of NO_x inlet concentration (100 s lean and 5 s rich, T=350°C, GHSV=50,000 hr^{-1})

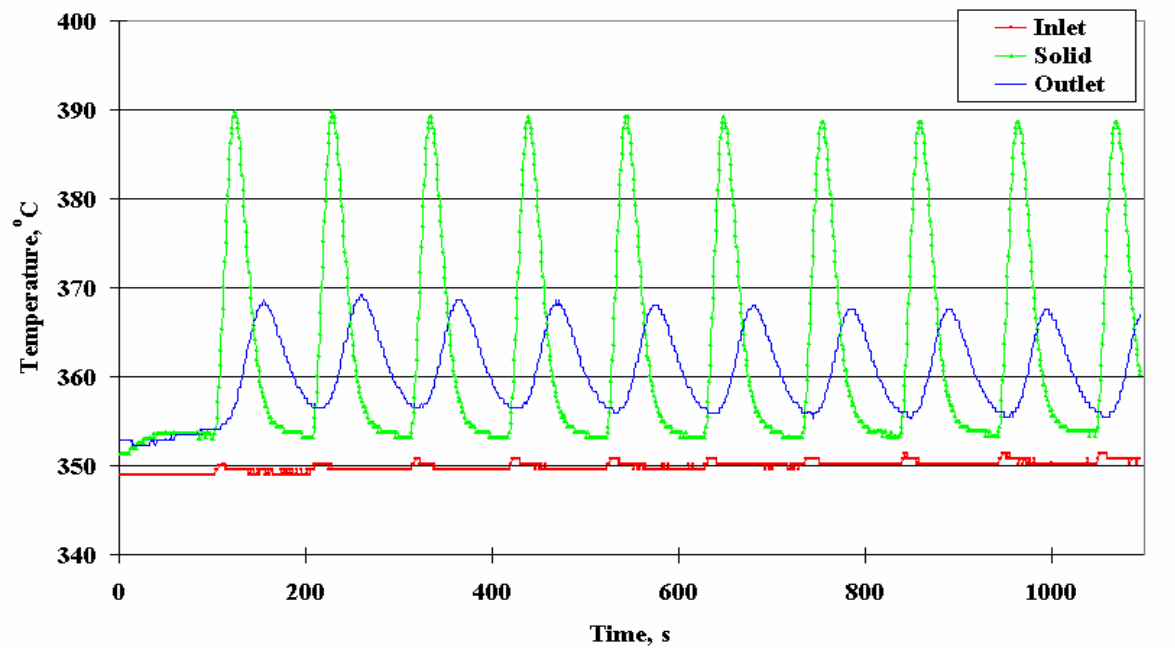

Figure 4.43 Temperature histories for 3% CO injections using DFI in presence of O_2 with 500ppm of NO_x inlet concentration (100 s lean and 5 s rich, T=350°C, GHSV=50,000 hr^{-1})

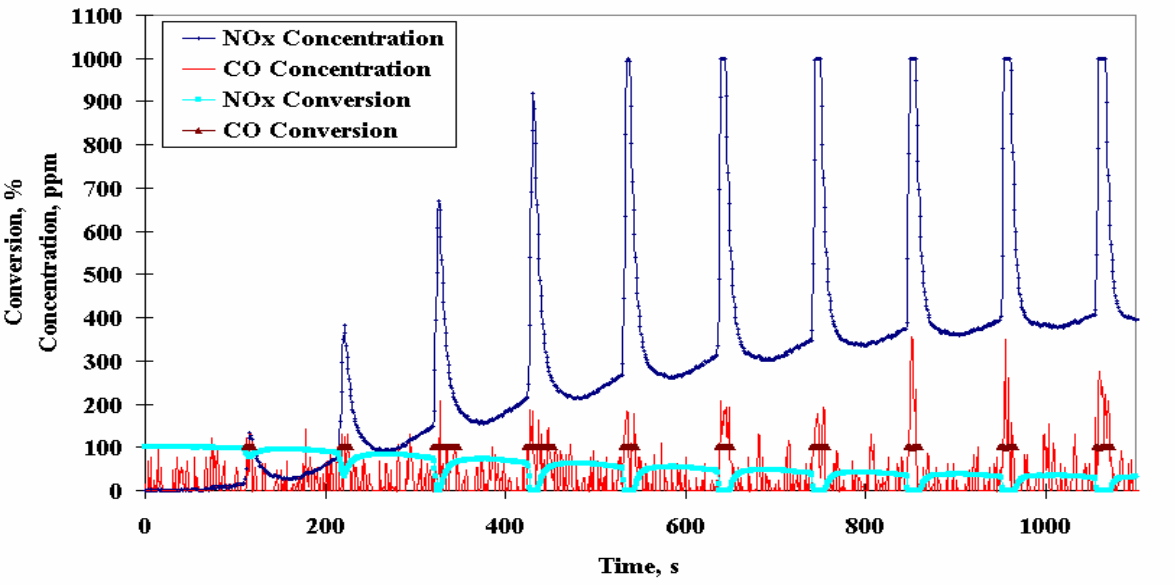

Figure 4.44 NO_x conversion and concentration histories for 4% CO injections using DFI in presence of O_2 with 500ppm of NO_x inlet concentration (100 s lean and 5s rich, T=350°C, GHSV=50,000 hr^{-1})

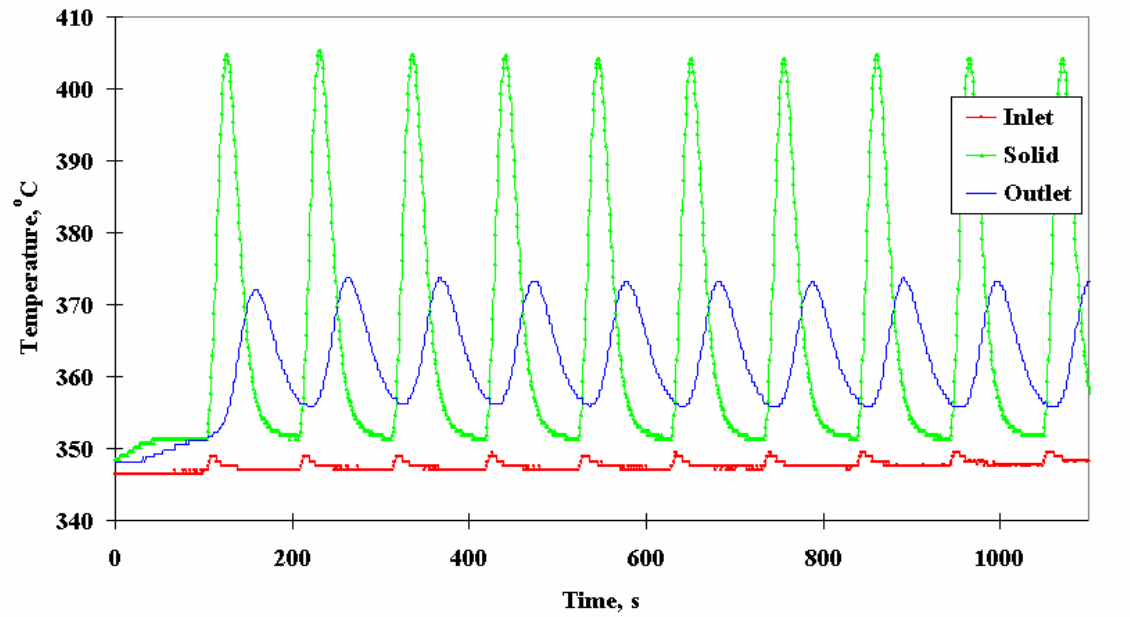

Figure 4.45 Temperature histories for 4% CO injections using DFI in presence of O_2 with 500ppm of NO_x inlet concentration (100 s lean and 5 s rich, T=350°C, GHSV=50,000 hr^{-1})

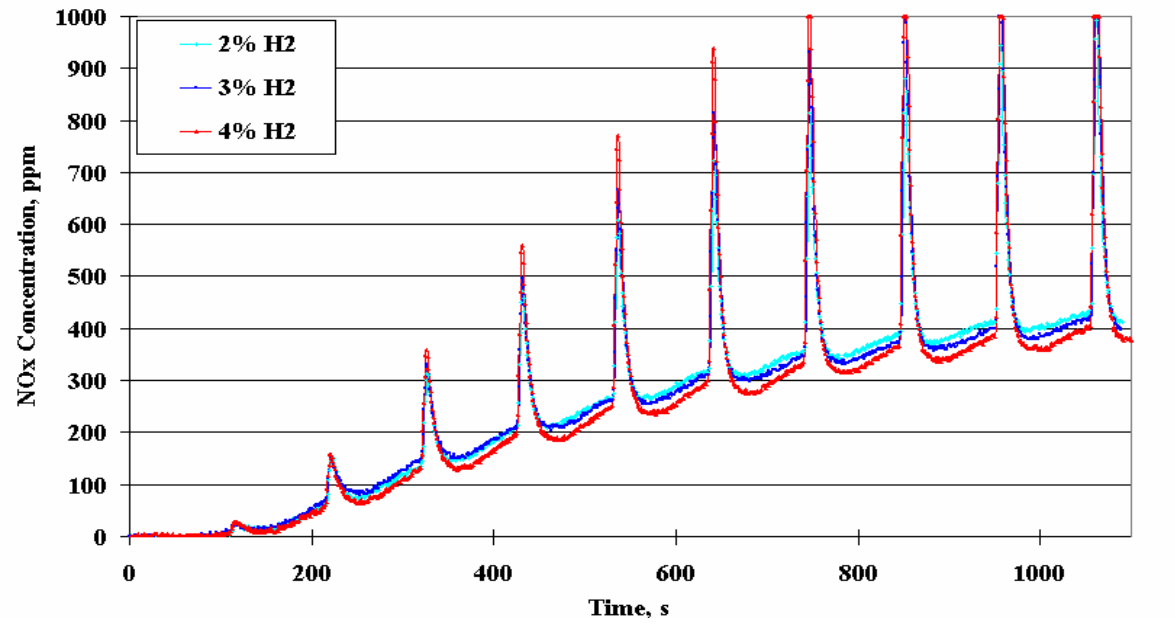

Figure 4.46 NO_x Conversion versus time for various H_2 injections using DFI in presence of O_2 with 500ppm of NO_x inlet concentration (100 s lean and 5 s rich, T=350°C, GHSV=50,000 hr^{-1})

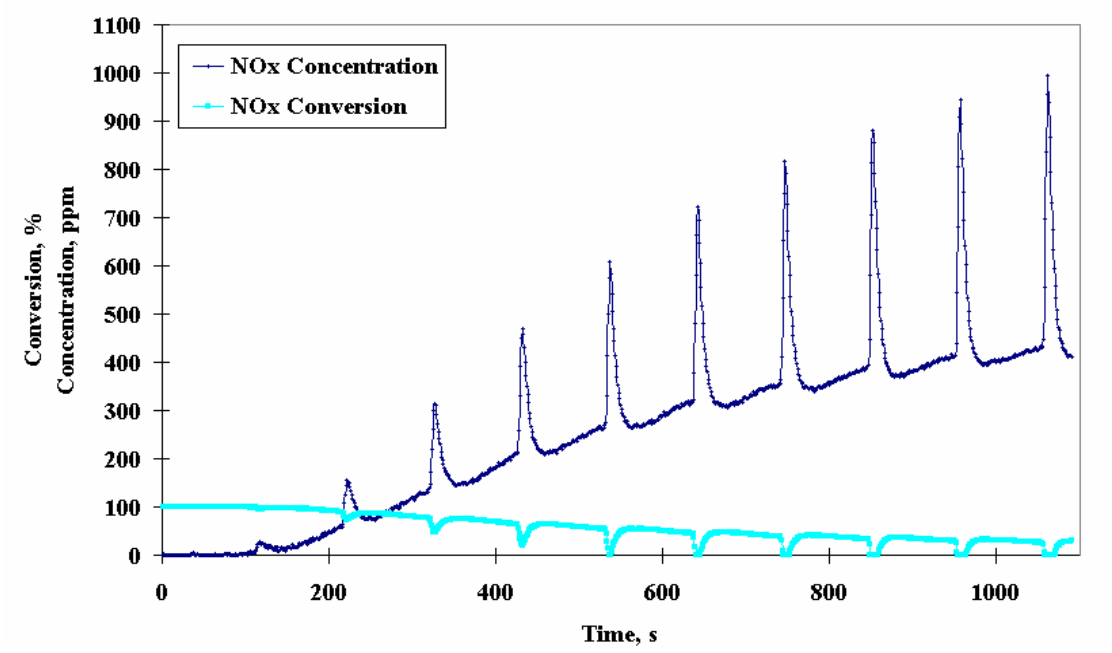

Figure 4.47 NO_x conversion and concentration histories for 2% H_2 injections using DFI in presence of O_2 with 500ppm of NO_x inlet concentration (100 s lean and 5 s rich, T=350°C, GHSV=50,000 hr^{-1})

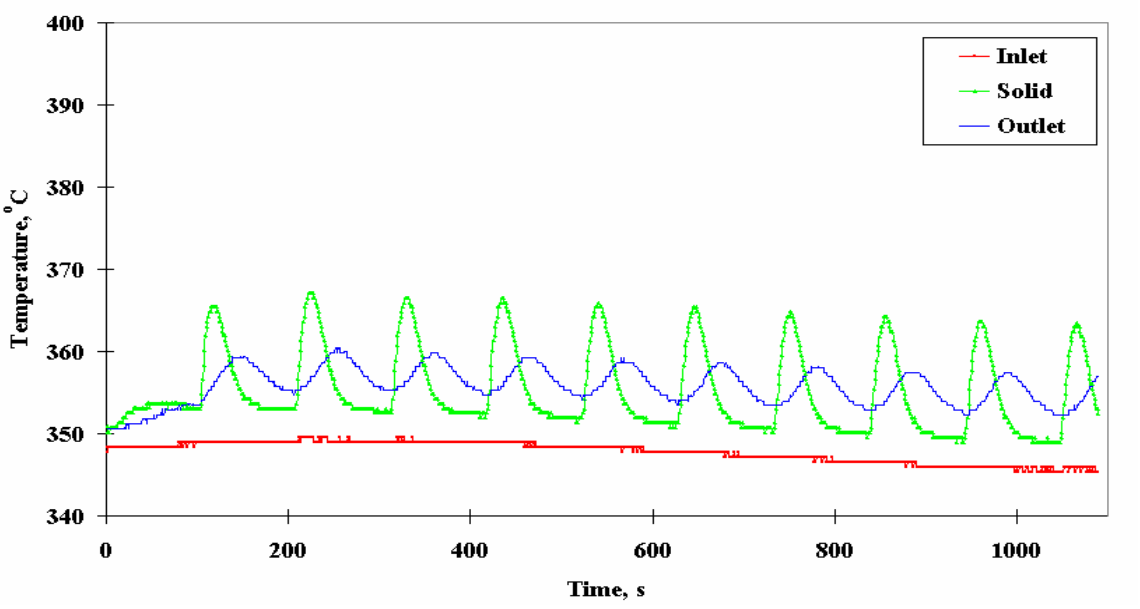

Figure 4.48 Temperature histories for 2% H_2 injections using DFI in presence of O_2 with 500ppm of NO_x inlet concentration (100 s lean and 5 s rich, T=350°C, GHSV=50,000 hr^{-1})

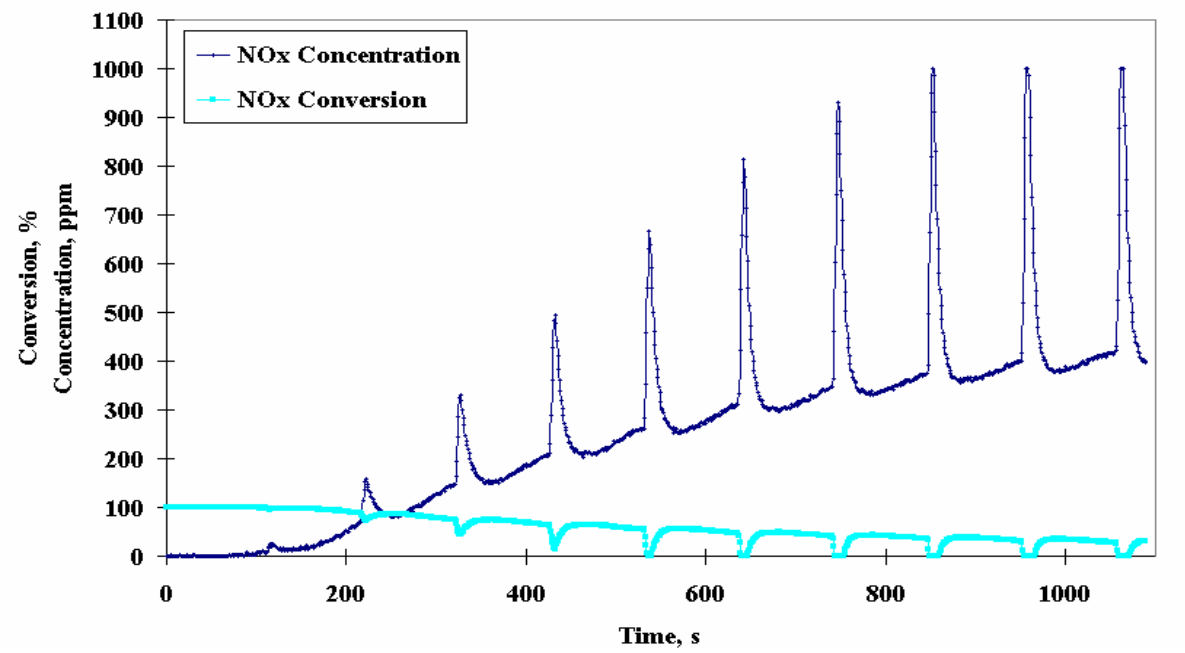

Figure 4.49 NO_x conversion and concentration histories for 3% H_2 injections using DFI in presence of O_2 with 500ppm of NO_x inlet concentration (100 s lean and 5 s rich, T=350°C, GHSV=50,000 hr^{-1})

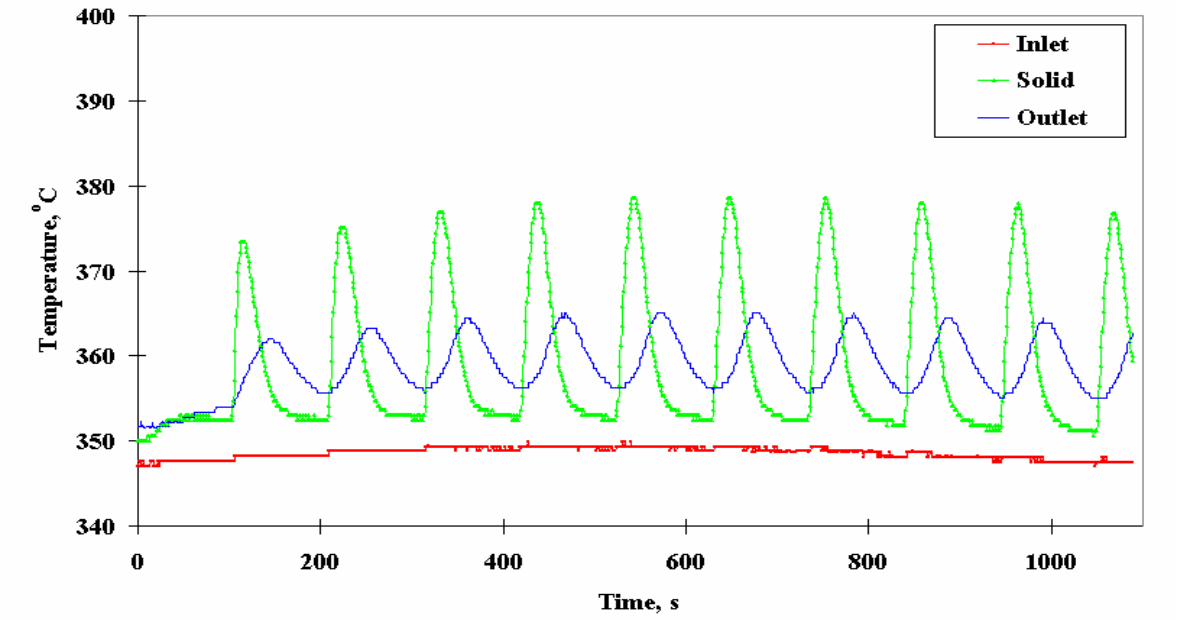

Figure 4.50 Temperature histories for 3% H_2 injections using DFI in presence of O_2 with 500ppm of NO_x inlet concentration (100 s lean and 5 s rich, T=350°C, GHSV=50,000 hr^{-1})

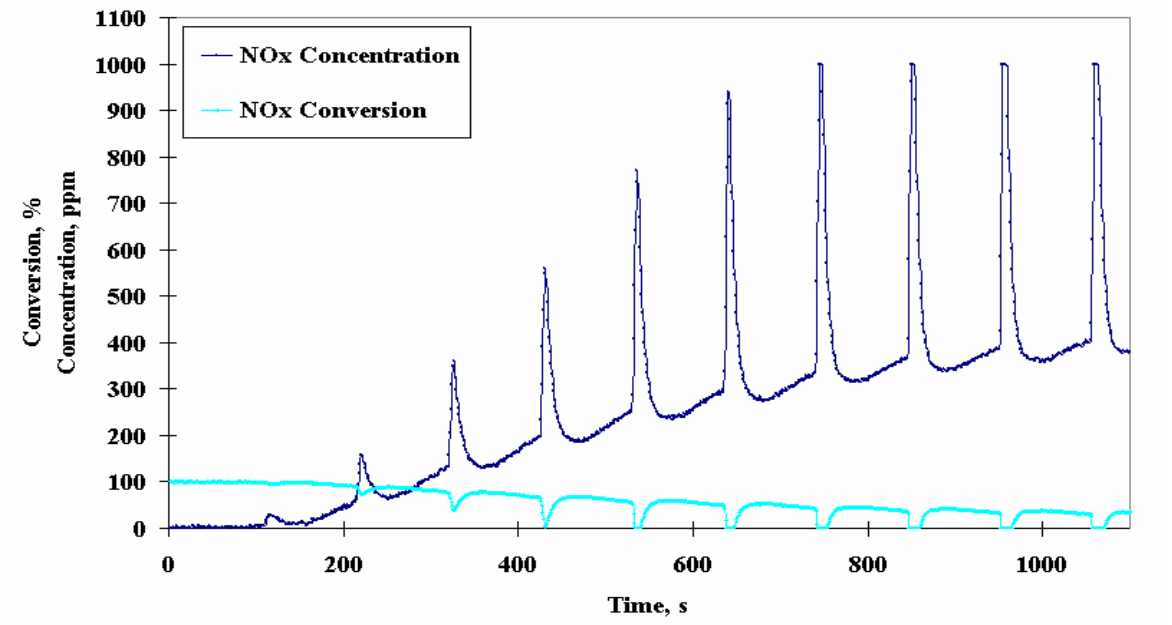

Figure 4.51 NO_x conversion and concentration histories for 4% H_2 injections using DFI in presence of O_2 with 500ppm of NO_x inlet concentration (100 s lean and 5 s rich, T=350°C, GHSV=50,000 hr^{-1})

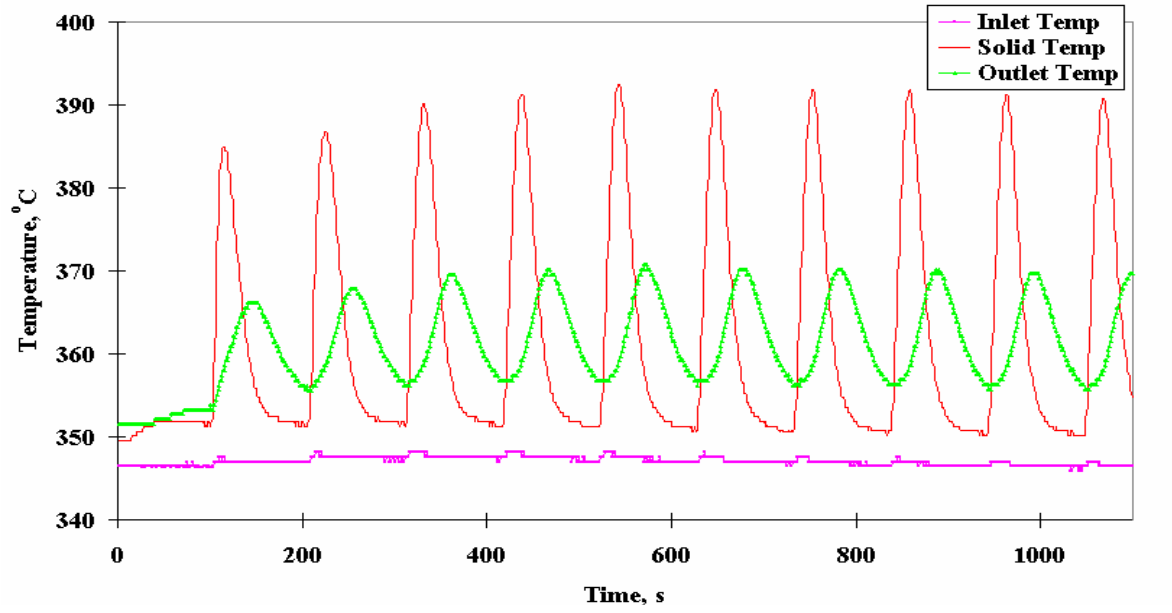

Figure 4.52 Temperature histories for 4% H_2 injections using DFI in presence of O_2 with 500ppm of NO_x inlet concentration (100 s lean and 5 s rich, T=350°C, GHSV=50,000 hr^{-1})

Table 4.10 Result from direct fuel injection with O_2 (5 s rich and 100 s lean, T=350°C, GHSV=50,000 hr^{-1})

Reductant	NO_x Conversion, %	CO Conversion, %	LNT Temperature Increase, °C
2% CO injection with O_2	56.0	99.6	23
3% CO injection with O_2	56.4	99.7	36
4% CO injection with O_2	53.3	99.8	53
2% H2 injection with O_2	56.2	-	14
3% H2 injection with O_2	56.7	-	26
4% H2 injection with O_2	58.1	-	40

temperature (4% CO injection with O_2). Further observation of the results indicates that the NO_x conversion efficiency when injecting 4% CO in the absence of oxygen is less than in cycling experiment at the same concentration. However, the NO_x conversion efficiency was found to be similar for both direct injection and cycling experiment with 4% H_2. As in the case of cycling H_2 appears to be slightly better than CO in the regeneration of LNTs.

Chapter 5

CONCLUSIONS

The effects of temperature and gas hourly space velocity on the performance of EmeraChem LNT are investigated in the present study, from which the NO_x storage capacity and the breakthrough can be obtained. These two performance parameters are necessary in determining the optimum operating temperature and the time at which the regeneration of the LNT is initiated. The maximum NO_x storage capacity occurs at 350^oC and below 350^oC is limited by chemical kinetics. The NO_x storage capacity at temperatures above 350^oC is suppressed due to equilibrium-limited. Moreover the NO_x storage capacity decreases with increasing GHSV because the resident time of NO_x molecules to be stored decreases as the GHSV increases. The maximum NO_2/NO final ratio and breakthrough time occur at 400^oC, and the difference between temperatures for the maximum NO_x storage capacity and NO oxidation must be possibly due to the instability of nitrite or nitrate compounds above 400^oC.

The desorption experiments are conducted at 350 and 500^oC and a GHSV of 25,000 hr^{-1}, in which the flow of O_2 and NO_x was shut off at the end of the NO_x absorption period. Since the trapping of NO_x is driven by chemical equilibrium, the net reducing environment provides a driving force for the decomposition of nitrate species with subsequent release of NO_x from the LNT surface. In addition, the NO_x release is greater at 500 than 350^oC since the rate of nitrite decomposition rate increases with increasing temperature.

The effects of lean and rich duration and reductant concentration on the regeneration of the LNT catalyst were investigated at a temperature of 350^{o}C and a space velocity of 50,000 hr^{-1}. The optimum lean/rich cycle of EmeraChem LNT was found to be 100 s lean and 5 s rich, with which a higher NO_x conversion efficiency with the lowest fuel penalty is obtained. Of the two reductants investigated in the present study, H_2 is found to be a slightly better reductant in reducing NO_x than CO.

Two different DFI experiments were performed at a temperature of 350^{o}C and a GHSV of 50,000 hr^{-1}, in which after every 100 s of the lean pulses, a 5-second pulse of either H_2 or CO was injected directly into the LNT: direct fuel injection in the presence oxygen and without oxygen in the main stream. The NO_x conversion efficiency with either pure H_2 or CO as reductant is found to be similar for both DFI in the absence of O_2 and lean/rich cycling experiment. In the presence of O_2 during fuel injection, part of the reductant was consumed by directly reacting with oxygen rather than by the reduction reactions, thus the NO_x conversion decreases to 57 %.

REFERENCES

1. “Nitrogen Oxides (NOx) and Power Plants,” Environmental Defense, 2006, New York, NY.

2. “Public Health and Environmental Damage Caused By Power Plant Pollution,” Clean the Air, 2005, Washington, DC.

3.“National Air Quality and Emissions Trends Report 2003,” U.S. Environmental Protection Agency.

4. New Jersey Institute of Technology, Newark, NJ 07102, March 2006, http://www.bengu- pc2.njit.edu/trp-chem/paint_html/source.htm.

5. BIO 3002 Environmental Life, Eastern Illinois University, Chaleston, Illinois, March 2006, http://www.ux1.eiu.edu/~cfruf/bio3002/greenhouse_effect.htm.

6. Matsumodo, S., “Catalytic Reaction of Nitrogen Oxide,” Cattek, vol. 4, 2000.

7. Helden, R., Verbeek, R., Aken, M., Genderen, M., Patchett, J., Straten, T., Kruithof, J., and Saluneaux, C., “Engine Dynamometer and Vehicle Performance of a Urea SCR-Systme for Heavy-Duty Truck Engine,” SAE, 2002-01-0286.

8. Schmieg, Steven J., Cho, Byong K., Oh, Se H., “Hydrocarbon Reactivity on a Plasma Catalyst System: Thermal Versus Plasma-Assisted Lean NO_x Reduction”, SAE, 2001-01-3565.

9. Brogan, M.S., Clark, A.D., and Brisley, R.J., 1998, “Recent Progress in NO_x Trap Echnology,” International Congress and Exposition, Detroit, Michigan, 1998

10. Larsson, M., Andersson, L., Fast, O., Litorell, M., and Mukuie, R., “NO_x Trap Control by Physically Based Model,” Society of Auto motive Engineers, Inc., 1999.

11. Olsson, L., Fridell, E., Skoglundh, M., and Andersson, B., "Mean field modeling of NO_x storage on $Pt/BaO/Al_2O_3$," Catalysis Today, Vol. 73, 2002, pp.263-270.

12. Kim, Y., Sun, J., Kolmanovsky L., and Koncsol, J., "A Phenomenological Control Oriented Lean NO_x Trap Model," SAE International, Detroit, Michigan, 2003.

13. Laurent, F., Pope, C.J., Mahzoul, H., Delfosse, L., and Gilot, P., "Modelling of NO_x Adsorption over NO_x Adsorbers," Laboratoire de Gestion des Risques et Environnement, Universite de Haute Alsace, Muljouse, France, 2002.

14. Mahzoul, H., and Brilhac, P.G., "Experimental and Mechanistic Study of NOx Absorption over NOx Trap Catalysts," Laboratoire Gestion des Risques et Environnement Universite de Hayte Alsace, Mulhouse, France, 1998.

15. Fridell, E., Persson, H., Westerberg, B., Olsson, L., and Skoglundh, M., "The Mechanism for NO_x Storage," Competence Centre for Catalysis Chalmers Universit of Technology, Goteborg, Sweden, 2000.

16. Lietti, L., Forzatti, P., Nova, I., and Tronconi, E., "NO_x Storage Reduction over Pt-Ba/γ-Al_2O_3 Catalyst," Dipartimento di Chimica Industriale e Ingegneria Chimica "Giulio Natta" del Politecnico, Milano, Italy, 2001.

17. Nova, I., Castoldi, L., Lietti, L., Tronconi, E., and Forzatti, P., "On the dynamic behavior of NO_x-storage/reduction $Pt-Ba/AL_2O_3$ catalyst," Catalysis Today, vol. 75, 2002, pp.431-437.

18. Castoldi, L., Nova, I., Lietti, L., and Forzatti, P., "Study of the effect of Ba loading for catalystic activity," Catalysis Today, vol. 96, 2004, pp. 43-52.

19. Epling, W.S., Parks, J.E., Campbell, G..C., Yezerets, A., Currier, N. W., and Campbell, L. E., "Further evidence of multiple NO_x sorption sites on NO_x storage/reduction catalysts," Catalysis Today, vol. 96, 2004, pp.21-30.

20. Broqvist, P., Gronbeck, H., Fridell, E., and Panas, I., "NO_x storage on BaO: theory and experiment," Catalysis Today, vol. 96, 2004, pp.71-78.

21. Cant, N.W., and Patterson, M.J., "The storage of nitrogen oxides on aluminal-supported barium oxide," Catalysis Today, vol. 73, 2002, pp.271-278.

22. Naktsuji, T., Yasukawa, R., Tabata, K., Sugaya, T., Ueda, K., and Niwa, M., "Highly Durable NO_x Reduction System and Catalysts for NO_x Storage Reduction System," International Congress and Exposition, Detroit, Michigan, 1998.

23. Wagner, G.J., Ph.D., "Advanced Reciprocating Engine Systems Bench Flow Reactor Testing of NO_x Absorber Catalyst for Lean- Burn Natural Gas Engine: Efficiency of Regeneration Process Utilizing Methane Oxidation and Reforming Catalysts," Research Report for Oak Ridge National Lab., EmeraChem LLC., Knoxville, 2003.

24. Kabin, K.S., Muncrief, R.L., and Harold M.P., "NO_x storage and reduction on a Pt/BaO/alumina monolithic storage catalyst," Catalysis Today, vol. 96, 2004, pp.79-89.

25. Su, Y., and Amiridis, M.D., "In situ FTIR studies of the mechanism of NO_x storage and reduction on $Pt/Ba/Al_2O_3$ catalysts," Catalysis Today, vol. 96, 2004, pp.31-41.

26. Poulston, S., and Rajaram, R.R., "Regeneration of NO_x trap catalysts," Catalysis Today, vol. 81, 2003, pp.603-610.

27. Lizuka, H., Kaneeds, M., Higashiyama, K., Kuroda, O., Shinotsuka, N., and Watanabe, H., "Improvement of Heat Resistance for Lean NO_x Catalyst," SAE International, Detroit, Michigan, 2004.

28. Dou, D., and Balland, J., "Impact of Alkali Metals on the Performance and Mechanical Properties of NO_x Adsorber Catalysts," SAE International, Detroit, Michigan, 2002.

29. Iwachido,K., Tanada, H., Watanave, T., Yamada, N., Nakayama, O., and Ando, H., "Development of the NO_x Adsorber Catalyst for Use with High-Temperature Condition," SAE International, Detroit, Michigan, 2001.

30. Kanneeda, M., Lizuka, H., Higashiyama, K., Kuroda, O., Hiratusuka, T., Shinotsuka, N., Ohno, H., Takanohashi, T., and Satoh, N., "Improvement of Thermal Resistance for Lean NO_x Catalyst," SAE International, Detroit, Michigan, 2003.

31. Chakravarthy, K., Daw, C.S., and Lenox, K.E., "Key characteristics of the sorption process in lean NO_x traps," SAE International, Detroit, Michigan, 2003.

32. Papadakis, K., Odenbrand, C.U.I., Creaser, D., "Stationary NO_x Storage and Reduction Experiments on a Heavy-Duty Diesel Engine Rig Using a Bypass System," SAE Japan, Yokohama, Japan, 2003

33. Epling W.S., Campbell, L.E., Yezerets, A., Currier, N.W., and ParksII J.E., "Overview of the Fundamental Reactions and Degradation Mechanisms of NO_x Storage / Reduction Catalysts," Catalysis Reviews, vol. 46, 2004, pp.163-245.

34. Ohtsuka, H., and Tabata, T., Appl. Catal. B: Environ., vol.29, 2001, pp.177.

35. Ohtsuka, H., Appl. Catal. B: Environ., vol. 33, 2001, pp.325

36. Amberntsson, A., Fridell, E., and Skoglundh, M., Appl. Catal. B: Environ. vol.11, 2003, pp.429.

37. Salasc, S., Koglundh, M., and Fridell, E., Appl. Catal. B: Environ. vol.36, 2002, pp. 145.

38. Olsson, L., Westerberg, B., Persson, H., Fridell, E., Skoglundh, M., and Andersson, B.J., Phy. Chem. B, vol. 103, 1999, 10433.

39. Toops, T., Smith, D., Partridge, W., Epling, W., and Parks, J., Proceeding of the Third Joint Meeting of the U.S. Sections of the Combustion Institute, 2003.

40. Epling, W., Campbell, G., and Parks, J., Catal. Lett., vol. 90, 2003, pp. 45.

41. Rodrigues, F., Juste, L., Potvin, C., Tempere, J.F., Blanchard, G., and Djega-Mariadassou, G., Catal. Lett., vol. 72, 2001, pp. 59.

42. Epling, W., Campbell, G., Parks, J., Currier, N., and Yezerets, A., 18the North American Meeting of the North American Catalysis Society, Cancun, Mexico, June 2003.

43. Fridell, E., Skoglundg, M., Westerberg, B., Johansson, S., and Smedler, G..J., Catal., vol.183, 1999, pp.196.

44. Narula, C., Nakouzi, S., Wu, R., Goralski, C., and Allard, L., AIChE J., vol. 47, 2001, pp.744.

45. Li, Y., Roth, S., Dettling, J., and Beutel, T., Topics Catal., vol. 16/17, pp.139.

46. Li, X, Meng, M. Lin, P., Fu, Y., Hu, T., Xie, Y., and Zhang, J., Topics Catal., vol. 22, 2003, pp.111

47. Prinetto, F., Chiotti, G., Nova, I., Lietti, L., Tronconi, E., and Forzatti, P.J., Phys. Chem. B, vol.105, 105, 12732

48. Kobayashi, T., Yamada, T., and Kayano, K., SAE Technical Paper Series 970745.

49. Kikuyama, S., Matsukuma, I., Kikuchi, R., Sasaki, K., and Eguchi, K., Appl. Catal. A: Gen., vol. 226, 2002, pp. 23.

50. Nova, I., Scotti, A., Tronconi, E., Lietti, L., and Forzatti, P., 18th North American Meeting of the North American Catalysis Society, Cancun, Mexico, June 2003.

51. Schmitz, P., and Baird, R.J., Phys. Chem. B, vol. 106, 2002, 4172.

52. Paterson, A., Rosenberg, D., and Anderson, J., Stud. Surf. Sci. Catal., vol. 138, 2001, pp.429.

53. Nova, I., Castoldi, L., Lietti, L., Tronconi, E., Forzatti, P., Prinetto, F., and Ghiotti, G..J., Catal., vol. 222, 2004, pp.377.

54. Takahashi, N., Shinjoh, H., Iijima, T., Suzuki, T., Yamazaki, K., Yokota, K., Suzuki, G., Miyoshi, N., Matsumoto, S., Tanizawa, T., Tanaka, T., Tateishi, S., and Kasahara, K., Catal. Today, vol. 27, 1996, pp. 63.

55. Westerberg, B., and Fridell, E.J., Mol. Catal. A:Chem., vol. 165, 2001, pp. 249.

56. Adbulhamid, G., Fridell, E., and Skoglundh, M., Topics Catal., vol. 30/31, 2004, pp. 161.

57. Mahzoul, H, Gilot, P., Brilhac., J.F., and Stanmore, B., Topics Catal., vol. 16/17, 2001, pp.293.

58. Farrauto, R.J., and Bartholomew, C.H., Fundamentals of Industrial Catalytic Processes, 1st ed., Blackie Academic & Professional, New York, NY, 1997.

59. Satterfield, C.N., Heterogeneous Catalysis in Industrial Practice, 2nd ed., Krieger Publishing Company, Malabar, FL, 1996

60. Li, J., Theis, J., Chun, W., Goralski, C., Kudla, R., Watkins, W., and Hurley, R., SAE Techinical Paper Series 2001-01-2503.

61. Soon, J.S., Miller, T., Epling, W., Huff, S., Chakravarthy, K., Lenox, K., Partridge, W., and Daw, S., 4th Department of Energy National Laboratory Catalysis Conference, Oak Ridge, TN, 2003.

62. Limousy, L., Mahzoul, H., Brilhac, J.F., Garin, F., Maire, G., and Gilot, P., Appl. Catal. B: Environ., vol. 42, 2002, pp.237.

63. Theis, J., Li, J., Ura, J., and Hurley, R., SAE Technical Paper Series, 2002-01-0733.

64. Muncrief, R., Coym, K., Harold, M., 18th North American Meeting of the North American Catalysis Society, Cancun, Mexico, June 2003.

65. Balcon, S., Potvin, C., Salin, L., Tempere, J.F., Djega-Mariadassou, G., Catal. Lett., vol. 60, 1999, pp.39.

66. Uy, D.,O' Neill, A., Weber, W., Appl. Catal. B; Environ., vol 35, 2002, pp.219.

67. Amberbtsson, A., Persson, H.; Engstrom, P., Kasemo, B., Appl. Catal. B: Environ., vol. 31, 2001, pp.27.

68. Liu, Z., Anderson, J.J., Catal., vol.224, 2004, pp.18.

69. Burch, R., Breen, J., Meunier, F., Appl. Catal. B, Environ., vol.39, pp.283.

70. Obuchi, A., Ohi, A., Nakamura, M., Ogata, A., Mizuno, K., Ohuchi, H., Appl. Catal. B: Environ., vol.2, pp.71.

71. Guth, E.D., Campbell, L.E., "REGENERATION OF CATALYST/ABSORBER," United States Patent 5599758, 1997.

APPENDIX

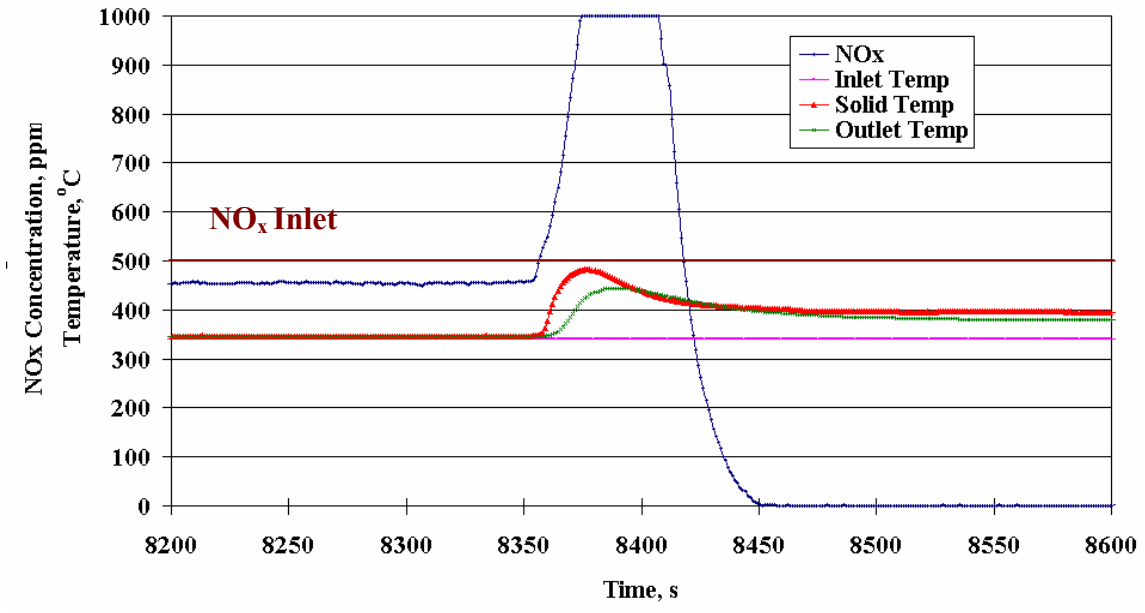

Figure A.1 Outlet NO_x concentration and temperature profile during regeneration performed at 350°C and a GHSV=25,000hr^{-1} with 500ppm of inlet NO_x concentration

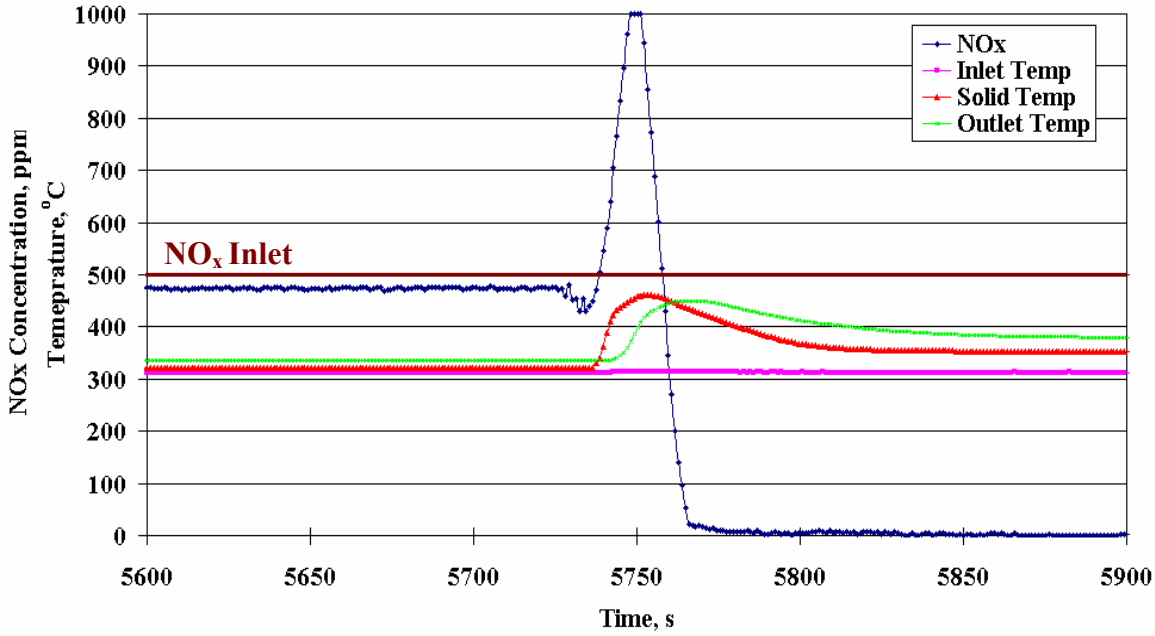

Figure A.2 Outlet NO_x concentration and temperature profile during regeneration performed at 350°C and a GHSV=50,000hr^{-1} with 500ppm of inlet NO_x concentration

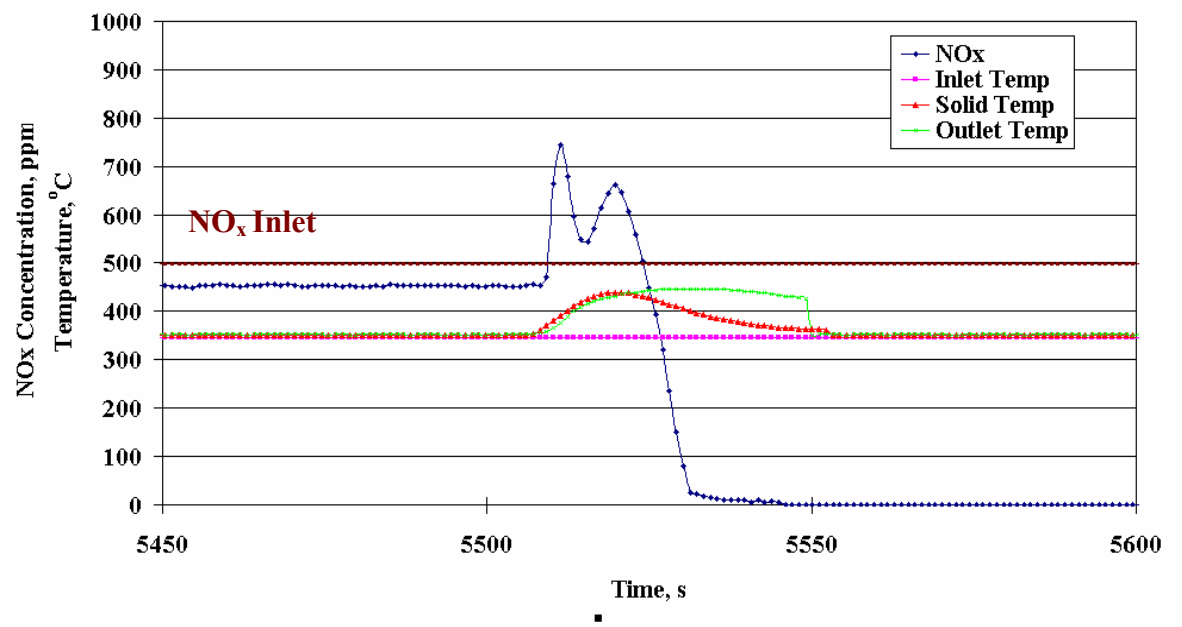

Figure A.3 Outlet NO_x concentration and temperature profile during regeneration performed at 350°C and a GHSV=75,000hr^{-1} with 500ppm of inlet NO_x concentration

VITA

Hakyong Kim was born in Seoul, South Korea on May 23, 1973. After completing high school in 1992, he attended Kong-Ju National University 2 years. At the end of his second year in college he decided to join the South Korean army to fulfill his military obligation. He served in an air-defense artillery battalion from 1994 to 1996. Upon being honorably discharged from the Korean army he decided to continue his college education in the U.S. He entered the University of Tennessee's Aerospace Engineering Program in 1998 and graduated with a Bachelor of Science degree in Aerospace Engineering in 2003. He enrolled in the graduate program at the University of Tennessee in Fall 2003 and received his Master of Science degree in Mechanical Engineering from the University of Tennessee in August 2006.